

THESIS

ENTRAINMENT EFFECTS OF OVERSHOOTING THERMALS ON LAND-
ATMOSPHERE INTERACTIONS

Submitted by

Erica L. McGrath-Spangler

Department of Atmospheric Science

In partial fulfillment of the requirements

For the Degree of Master of Science

Colorado State University

Fort Collins, Colorado

Summer 2008

COLORADO STATE UNIVERSITY

June 13, 2008

WE HEREBY RECOMMEND THAT THE THESIS PREPARED UNDER OUR SUPERVISION BY ERICA L. MCGRATH-SPANGLER ENTITLED ENTRAINMENT EFFECTS OF OVERSHOOTING THERMALS ON LAND-ATMOSPHERE INTERACTIONS BE ACCEPTED AS FULFILLING IN PART REQUIREMENTS FOR THE DEGREE OF MASTER OF SCIENCE.

Committee on Graduate Work

David A. Krueger

Jeffrey L. Collett, Jr.

Adviser: A. Scott Denning

Department Head: Richard H. Johnson

ABSTRACT OF THESIS

ENTRAINMENT EFFECTS OF OVERSHOOTING THERMALS ON LAND- ATMOSPHERE INTERACTIONS

The response of planetary boundary layer (PBL) carbon dioxide (CO_2) concentration to surface carbon fluxes is inversely proportional to the depth of that layer. The PBL, extending from the surface, interacts strongly with the biosphere and mixes fluxes of carbon, water, energy, and momentum throughout its depth by turbulent eddies. Its diurnal cycle matches that of surface heating and reaches its maximum depth in the early afternoon when photosynthetic uptake is also at a maximum, diluting the effects of carbon flux out of the atmosphere. Overshooting thermals entrain free tropospheric air down into the boundary layer producing negative fluxes of mass and heat at the top of the layer. This process acts to grow the PBL and change the atmospheric response to carbon uptake by the surface vegetation. The scale of overshooting thermals is generally smaller than that resolved by mesoscale models and so the effects produced by this process are not determined in the models. This results in the exclusion of the enhanced entrainment associated with overshooting thermals at the PBL top and ultimately leads to the underestimation of PBL depth.

A parameterization of boundary layer top entrainment was developed in the ecosystem-atmosphere model SiB-RAMS based on the assumption that the heat flux at the top of the boundary layer is negatively proportional to the heat flux at the surface. Two experiments were performed, one idealized and the other simulating real conditions,

that show that a deeper, warmer, and drier boundary layer with a weaker capping inversion results from the additional entrainment. Compared with hourly observations by a radar sounding system, the monthly mean diurnal cycle of PBL depth at a site in northern Wisconsin is more accurately reproduced by simulations including the entrainment parameterization. As the proportionality constant within the parameterization increases, the warming, drying, and deepening effects of the PBL are also increased.

Overshooting thermals warm and dry the boundary layer by entraining free tropospheric air. The warmer boundary layer and cooler overlying inversion encourage boundary layer growth by reducing the stratification at the PBL top. The drier conditions also induce a closing of the surface vegetation's stomata in an evolved response to limit water loss while assimilating carbon. This limits transpiration, reducing latent heat flux in favor of sensible heat flux and thus altering the Bowen ratio and warming, drying, and deepening the boundary layer further in a positive feedback loop. In addition, the closing of the stomata reduces carbon assimilation and net ecosystem exchange. The combination of these interconnected processes leads to a modification of the free troposphere through the boundary layer top mixing and altered radiative budget generating adjusted cloud cover, precipitation, and large-scale weather which is then able to amend the boundary layer.

Erica L. McGrath-Spangler
Atmospheric Science Department
Colorado State University
Fort Collins, CO 80523
Summer 2008

ACKNOWLEDGMENTS

I would like to thank my advisor, Dr. Scott Denning, for his understanding and enthusiasm. His constant reminders to enjoy the journey and never accept the first attempt have made me a better scientist and hopefully a better person. I would also like to thank my committee members, Drs. Jeff Collett and David Krueger for taking the time to read and review this thesis.

Thank you to all of the Denning group members. Thank you to Amy Dykstra and Connie Hale for always making sure my questions were answered. Thank you to Anna Harper, my officemate, for ensuring that I left my desk every once in awhile and Nick Parazoo, on whom I can always count for a laugh. Kathy Corbin, Ian Baker, and Ravindra Lokupitiya have been constant sources of information, encouragement, and friendship. I never would have finished this thesis without their help and understanding.

I am forever grateful to my husband Tim. He has been my best friend through all the ups and downs of graduate school while his trust in me and loving support have allowed me to succeed where I never thought it possible.

The data providers were invaluable in this research. I wish to thank Ken Davis at The Pennsylvania State University, Steven Wofsy and J. (Bill) Munger at Harvard University, David Hollinger with the USDA Forest Service, Hans Peter Schmid at the Institute of Meteorology and Climate Research, Peter Curtis at The Ohio State University, and the AmeriFlux network for their hard work and dedication to providing

observational records. Thank you also to Oak Ridge National Laboratory for providing public access to these data.

This research was supported by National Aeronautics and Space Administration grant NNG05GD15G.

TABLE OF CONTENTS

1. Introduction	1
References	8
2. Idealized Case Study	13
Abstract	13
2.1 Introduction	13
2.2 Model setup	18
2.3 Entrainment parameterization and implementation	22
2.4 Results	25
2.4.1 Physical effects	25
2.4.2 Physiological effects	35
2.4.3 Parameterization effects	40
2.5 Conclusions and future work	42
References	44
3. Real Case Study	49
Abstract	49
3.1 Introduction	50
3.2 Methods	52
3.2.1 Model description	52

3.2.2 Model input	53
3.2.3 Entrainment parameterization	55
3.3 Observations	56
3.4 Monthly climate overview	59
3.4.1 July 1999	59
3.4.2 August 1999	60
3.4.3 September 1999	60
3.5 Results	61
3.5.1 WLEF results	61
3.5.2 Tower results	67
3.5.3 National results	71
3.6 Conclusions	81
References	83
4. Conclusions and Future Work	89
4.1 Conclusions	89
4.2 Future work	91
References	92

LIST OF FIGURES

FIG 2.1 Temporal evolution of the boundary layer height for the entraining and control cases.....	26
FIG 2.2 Profile of potential temperature for both the entraining and control cases on 20 August 2004 at 12 pm LT.....	27
FIG 2.3 Profile of water vapor mixing ratio for both the entraining and control cases on 20 August 2004 at 12 pm LT.....	28
FIG 2.4 Profile of virtual potential temperature for both the entraining and control cases on 20 August 2004 at 12 pm LT.....	30
FIG 2.5 Temporal evolution of potential temperature in the lowest atmospheric model level for the entraining and control cases.....	31
FIG 2.6 Temporal evolution of the zonal (a) and meridional (b) winds in the lowest atmospheric model level for the entraining and control cases.....	32
FIG 2.7 Temporal evolution of the sensible (a) and latent (b) heat fluxes in the lowest atmospheric model level for the entraining and control cases.....	33
FIG 2.8 Temporal evolution of vegetative stress factors for the entraining and control cases. (a) Humidity stress (b) Temperature stress.....	36
FIG 2.9 Temporal evolution of conductance for both the entraining and control cases..	37

FIG 2.10 Temporal evolution of NEE (a), ground respiration (b), and canopy net assimilation (c) for the entraining and control cases.....	38
FIG 2.11 Temporal evolution of carbon dioxide concentration in the lowest atmospheric model level for the entraining and control cases.....	39
FIG 2.12 Sensitivity of potential temperature (a), water vapor mixing ratio (b), PBL depth (c), and CO ₂ concentration (d) in the lowest model level to α . Values taken from 1200 LT on the second day of simulation.....	41
FIG 3.1 Monthly mean diurnal cycle of PBL depth (m) in (a) July, (b) August, and (c) September. Model estimates are averaged over non-precipitating hours only. Error bars are the standard deviation of daily values at each hour.....	62
FIG 3.2 Monthly mean diurnal cycle at WLEF of water vapor mixing ratio (g kg ⁻¹) during (a) July, (b) August, and (c) September and of temperature (K) during (d) July, (e) August, and (f) September at 30 m.....	63
FIG 3.3 Monthly mean diurnal cycle at WLEF of net ecosystem exchange ($\mu\text{mol m}^{-2} \text{s}^{-1}$) during (a) July, (b) August, and (c) September and of CO ₂ concentration perturbations (ppmv) during (d) July, (e) August, and (f) September at 30 m	65
FIG 3.4 Monthly mean diurnal cycle at WLEF of sensible heat flux (W m^{-2}) during (a) July, (b) August, and (c) September and of latent heat flux (W m^{-2}) during (d) July, (e) August, and (f) September at 30 m.....	66
FIG 3.5 Monthly mean diurnal cycle at Howland Forest of sensible heat flux (W m^{-2}) during (a) July, (b) August, and (c) September and of latent heat flux (W m^{-2}) during (d) July, (e) August, and (f) September.....	67

FIG 3.6 Monthly mean diurnal cycle at Harvard Forest of sensible heat flux (W m^{-2}) during (a) July, (b) August, and (c) September and of latent heat flux (W m^{-2}) during (d) July, (e) August, and (f) September.....68

FIG 3.7 Monthly mean diurnal cycle at Morgan-Monroe of sensible heat flux (W m^{-2}) during (a) July, (b) August, and (c) September and of latent heat flux (W m^{-2}) during (d) July, (e) August, and (f) September.....69

FIG 3.8 Monthly mean diurnal cycle at University of Michigan Biological Station of sensible heat flux (W m^{-2}) during (a) July, (b) August, and (c) September and of latent heat flux (W m^{-2}) during (d) July, (e) August, and (f) September.....70

FIG 3.9 Effect of entrainment from overshooting thermals (entraining case minus control case) on PBL depth (m) in the time mean from July through September.....72

FIG 3.10 Effect of entrainment from overshooting thermals (entraining case minus control case) on (a) water vapor mixing ratio (g kg^{-1}) and (b) temperature (K) at 30 m in the time mean from July through September.....73

FIG 3.11 Effect of entrainment from overshooting thermals (entraining case minus control case) on (a) latent heat flux (W m^{-2}) and (b) sensible heat flux (W m^{-2}) in the time mean from July through September.....74

FIG 3.12 Effect of entrainment from overshooting thermals (entraining case minus control case) on (a) humidity stress and (b) temperature stress in the time mean from July through September.....76

FIG 3.13 Effect of entrainment from overshooting thermals (entraining case minus control case) on (a) net ecosystem exchange ($\mu\text{mol m}^{-2} \text{s}^{-1}$), (b) carbon

assimilation ($\mu\text{mol m}^{-2} \text{s}^{-1}$), and (c) soil respiration ($\mu\text{mol m}^{-2} \text{s}^{-1}$) in the time mean from July through September.....	77
FIG 3.14 Effect of entrainment from overshooting thermals (entraining case minus control case) on CO_2 concentration at 500 m in the time mean from July through September.....	79
FIG 3.15 Effect of entrainment from overshooting thermals (entraining case minus control case) on surface perturbation pressure (hPa) in the time mean from July through September.....	80

Chapter 1

Introduction

Carbon dioxide (CO₂) is the most important anthropogenic greenhouse gas and is the largest contributor to human-induced climate change (IPCC, 2007). CO₂ has multiple sources and sinks near the surface that alter its concentration in the atmosphere. Anthropogenic sources such as fossil fuel burning and land use changes (Houghton, 1999; Davis et al., 2003) account for the recent warming trend and the rate of CO₂ increase of 1-2 ppmv yr⁻¹ over the past half-century (Conway et al., 1994; Davis et al., 2003). These increases have led to warmer global temperatures, rising sea levels, and changing precipitation patterns (IPCC, 2007).

However, only about half of the carbon being released into the atmosphere by humans remains there (e.g. Schimel et al., 1994; Denning et al., 1995; 2005). The remainder is taken up by the oceans and the terrestrial biosphere (e.g. Tans et al., 1990; Sarmiento et al., 1992; Sarmiento and Sundquist 1992; Schimel et al., 1994; Denning et al., 1995). In order to understand how CO₂ concentrations are going to change in the future, it is necessary to understand the processes that control the natural surface sources and sinks and how they will evolve in the future (e.g. Denning et al., 1996a; Gurney et al., 2003; Friedlingstein et al., 2006).

Coupled ecosystem-atmosphere models are used to simulate fluxes of CO₂ at the surface that then modify the concentration of CO₂ in the atmosphere (Denning et al.,

1996a; 2003). These fluxes are determined by parameterizations of plant photosynthetic assimilation and soil respiration (Wofsy et al., 1988; Baker et al., 2003) and estimates of the anthropogenic fluxes due to fossil fuel combustion and other sources (Andres et al., 1996; Marland et al., 2005; Wang et al., 2007; Corbin et al., 2008). Fluxes of carbon at the surface occur into and out of the planetary boundary layer (PBL) (Wofsy et al., 1988; Baker et al., 2003) and are mixed by turbulent eddies to produce a nearly homogeneous vertical profile of CO₂ concentration (Stull 1976; 1988). Understanding the processes that govern the PBL is thus important in determining the vertical and horizontal distribution of CO₂ concentrations (Wofsy et al., 1988; Denning et al., 1995; Yi et al., 2001; 2004; Chen et al., 2005).

The response of CO₂ concentration to fluxes is directly proportional to the depth of the PBL (Denning et al., 1995; Yi et al., 2001; 2004). The amount of carbon fluxed into or out of the PBL is diluted through the entire depth of the layer by turbulent mixing (Yi et al., 2004). If the surface takes up one unit of carbon, the net loss will be distributed throughout the PBL. That one unit of uptake will have a greater impact on PBL concentrations if the PBL depth is only one kilometer than if the PBL is 2 kilometers deep (Wofsy et al., 1988; Denning et al., 1995; Yi et al., 2001; 2004). Since the PBL is also responsible for mediating the exchange of carbon as well as heat, water, and momentum between the surface and the overlying atmosphere (Stull, 1976; 1988; Baker et al., 2003; Denning et al., 2008), accurately determining the depth of this layer is vital to carbon studies. An error in the depth of the PBL relates linearly to an error in the simulated CO₂ concentration (Denning et al., 1995; 1996b; 1999; 2008; Zhang, 2002; Gerbig et al., 2003). Most measurements of CO₂ concentration are made within the PBL

(Chen et al., 2005) using flasks and continuous towers and so observation to model comparisons will produce a mismatch when the PBL depth is not simulated correctly.

Although extremely important for simulating CO₂ concentrations, few models accurately determine the PBL depth and vertical turbulent mixing (Denning et al., 1995; 1996a; 2008; Gurney et al., 2003; Yi et al., 2004). The PBL is a vertically homogeneous layer capped by a temperature inversion. In order to resolve this capping inversion, many model levels are needed at a height that varies in both space and time (Denning et al., 2008). The high vertical resolution is required for proper representation of surface layer ventilation and turbulent entrainment, but is only required over a small fraction of the total column and is excessive over the rest of the boundary layer and free troposphere, generating unnecessary computational expense (Denning et al., 2008). In addition, many of the processes that control PBL development are small-scale and unresolved by the models (Ayotte et al., 1996; Gerbig et al., 2003). It is difficult to observe fluxes and processes at the top of the PBL because of its height, typically at several kilometers above the surface. Since these observations are scarce, parameterizations of entrainment are more primitive than models of surface exchange, resulting in entrainment being one of the weakest aspects of PBL models (Davis et al., 1997).

In addition to carbon budget studies, the PBL and the processes that govern its development are important to most meteorological phenomena. Examining the bulk aerodynamic formulae for sensible and latent heat fluxes, these fluxes are proportional to the average potential temperature and humidity within the boundary layer. Thus, the radiative budget is highly dependent upon processes in the boundary layer that determine temperature and water vapor concentrations. Processes that dry the PBL produce a

humidity stress on the vegetation, resulting in the closing of stomata and reducing transpiration and latent heat flux (Davis et al., 1997).

As warm air rises from the surface in thermals, if sufficient moisture is present, they might rise high enough to reach their lifting condensation level (LCL) and produce clouds (Stull, 1988). Clouds reflect solar radiation and absorb and emit upwelling longwave radiation, consequently modifying the surface radiation budget further. The decreased solar insolation reaching the ground reduces the sensible and latent heat fluxes, resulting in a slowing of the PBL heating. The decreased amount of light reaching the vegetation should decrease photosynthesis, but this is complicated by the increased efficiency of diffuse light in reaching lower canopy levels on partly cloudy days (Davis et al., 1997). If the thermals are lifted still further, they could reach their level of free convection (LFC) and produce convective precipitation. Thunderstorm and hurricane evolution are tied to the inflow of moist boundary layer air (Stull, 1988).

Air pollution can be trapped within the boundary layer. Pollutants are transported by eddies that cannot penetrate far into the stable layer capping the boundary layer. The stable layer, as a result, acts as a lid to surface-emitted pollutants producing high pollutant concentrations within the boundary layer, near the source, and lower concentrations in the free atmosphere above (Stull, 1988).

Entrainment at the top of the boundary layer, an important process governing PBL development, is a result of rising surface thermals that overshoot their neutral level and continue into the overlying inversion. During their subsequent descent, the thermals drag down free tropospheric air and grow the boundary layer through the insertion of energy and mass (Stull, 1988; Sullivan et al., 1998). The thermals also distort the boundary

separating the PBL and the free troposphere (Stull, 1976), directly incorporating the free troposphere into the boundary layer. The overshooting thermals play a crucial role in entrainment mechanics (Sayler and Breidenthal, 1998; Sullivan et al., 1998; Stevens and Bretherton, 1999), one of the most important processes of any model to represent (Ayotte et al., 1996).

Entrainment is difficult to quantify in regional-scale studies. Most mesoscale models are unable to resolve overshooting thermals because of coarse grid intervals (Ayotte et al., 1996; Gerbig et al., 2003). The horizontal grid increment necessary is on the scale of tens to hundreds of meters (Stull, 1988; Pielke, 1991) and much too computationally expensive for large domains and long temporal scales. Observations of entrainment are also challenging due to mesoscale variations, coupling between physical processes (Sullivan et al., 1998), and the 1-3 km height at which they are typically occurring (Davis et al., 1997). Although difficult to determine explicitly, a representation of entrainment is necessary to accurately simulate the depth of the PBL in meteorological models.

The focus of this study is to include an entrainment parameterization in a coupled ecosystem-atmosphere model. The coupling of the Simple Biosphere (SiB) model (Sellers et al., 1986; 1996; Denning et al., 1996a) and the Regional Atmospheric Modeling System (RAMS) (Pielke, 1974; Tripoli and Cotton, 1982; Pielke et al., 1992; Cotton et al., 2003) is called SiB-RAMS and has been developed at Colorado State University (Denning et al., 2003; Nicholls et al., 2004; Wang et al., 2007; Corbin et al., 2008). The parameterization is based on a closure assumption for the heat flux at the base of the capping inversion, stating that this heat flux is proportional to the heat flux at

the surface. Other studies have set this proportionality constant at values ranging from zero to one with the most common value being around 0.2 (e.g. Betts, 1973; Carson, 1973; Deardorff, 1974; Rayment and Readings, 1974; Willis and Deardorff, 1974; Stull, 1976; Davis et al., 1997; Sullivan et al., 1998; Yi et al., 2001).

The parameterization introduces a downward heat flux at the top of the PBL to simulate the effects of overshooting thermals that are neglected in most mesoscale models. The heat flux has consequences for the model concerning temperature, water vapor mixing ratio, vegetative response, and CO₂ concentration. These variables are measured at many locations and so these changes can be compared to observations. Evaluation of the parameterization will be performed at a very tall tower site in northern Wisconsin.

The WLEF tall tower in northern Wisconsin is a good candidate for evaluation purposes. Since 1994, continuous measurements of CO₂ concentrations have been made at 11, 30, 76, 122, 244, and 396 m by Li-COR 6251 CO₂ analyzers (Bakwin et al., 1998; Davis et al., 2003). Micrometeorological and eddy covariance flux measurements have been made at 30, 122, and 396 m heights since 1996 (Berger et al., 2001; Davis et al., 2003). In addition, during the time periods of March through November 1998 and 1999, a National Center for Atmospheric Research (NCAR) Integrated Sounding System (ISS), which includes a radar profiler and a Radio-Acoustic Sounding System (RASS), was deployed eight kilometers east of the tower (Angevine et al., 1998; Yi et al., 2001; 2004; Denning et al., 2008). The signal-to-noise ratio of the profiler can be used to measure the afternoon PBL depth near the tower (Angevine et al., 1994; Yi et al., 2001; 2004; Denning et al., 2008). Since the profiler is unable to detect features below 400 m,

shallow PBL depths, characteristic of the early morning, and the stable nocturnal boundary layer are determined from the vertical profile of CO₂ concentrations from the tower as described by Yi et al. (2001; 2004) and Denning et al. (2008).

The entrainment parameterization was evaluated in two steps. The first step involved a purely idealized case so that the effects of the parameterization could be assessed devoid of any outside influences. Cyclic boundary conditions, flat terrain, and a homogeneous land surface limited advection from outside the domain and spatial heterogeneity within the region. The second step was evaluating the effectiveness of the parameterization in the simulation of a real case. The model was allowed to spin up for four months from March through June of 1999 before results were analyzed during July, August, and September of that same year. Monthly mean diurnal cycles of PBL depth, temperature, and other variables were compared to observations at WLEF and four other towers within the AmeriFlux network.

REFERENCES

- Andres, R.J., G. Marland, I. Fung, and E. Matthews, 1996: A $1^{\circ} \times 1^{\circ}$ distribution of carbon dioxide emissions from fossil fuel consumption and cement manufacture, 1950-1990. *Global Biogeochem. Cycles*, **10**, 419-429.
- Angevine, W.M., A.B. White, and SK. Avery, 1994: Boundary-layer depth and entrainment zone characterization with a boundary-layer profiler. *Bound-Layer Meteor.*, **68**, 375-385.
- Angevine, W.M., P.S. Bakwin, and K.J. Davis, 1998: Wind profiler and RASS measurements compared with measurements from a 450-m tall tower. *J. Atmos. Sci.*, **31**, 674-701.
- Ayotte, K.W., P.P. Sullivan, A. Andr n, S.C. Doney, A.A.M. Holtslag, W.G. Large, J.C. McWilliams, C.-H. Moeng, M.J. Otte, J.J. Tribbia, and J.C. Wyngaard, 1996: An evaluation of neutral and convective planetary boundary layer parameterizations relative to large eddy simulation. *Bound. Layer Meteor.*, **79**, 131-175.
- Baker, I., A.S. Denning, N. Hanan, et al., 2003: Simulated and observed fluxes of sensible and latent heat and CO₂ at the WLEF-TV tower using SiB2.5. *Global Change Biology*, **9**, 1262-1277.
- Bakwin, P.S., P.P. Tans, D.F. Hurst, C. Zhao, 1998: Measurements of carbon dioxide on very tall towers: Results of the NOAA/CMDL program. *Tellus*, **50B**, 401-415.
- Berger, B.W., K.J. Davis, C. Yi, P.S. Bakwin, and C. Zhao, 2001: Long-term carbon dioxide fluxes from a very tall tower in a northern forest: Flux measurement methodology. *J. Ocean Atmos. Technol.*, **18**, 529-542.
- Betts, A.K., 1973: Non-precipitating cumulus convection and its parameterization. *Quart. J. Roy. Meteor. Soc.*, **99**, 178-196.
- Carson, D.J., 1973: The development of a dry inversion-capped convectively unstable boundary layer. *Quart. J. Roy. Meteor. Soc.*, **100**, 450-467.
- Chen, B., J.M. Chen, and D.E.J. Worthy, 2005: Interannual variability in the atmospheric CO₂ rectification over a boreal forest region. *J. Geophys. Res.*, **110**, D16301.
- Climate Change 2007. Fourth Assessment Report of the Intergovernmental Panel on Climate Change, ed. S. Solomon, D. Qin, M. Manning, Z. Chen, M. Marquis,

K.B. Averyt, M. Tignor, and H.L. Miller, Cambridge University Press, Cambridge, U.K. and New York, USA, 2007. (referred as IPCC, 2007)

- Conway, T.J. et al., 1995: Evidence for interannual variability of the carbon cycle from the National Oceanic and Atmospheric Administration/Climate Monitoring and Diagnostics Laboratory Global Air Sampling Network. *J. Geophys. Res.*, **99**, 22831-22855.
- Corbin, K.D., A.S. Denning, L. Lu, J.-W. Wang, I.T. Baker, 2008: Possible representation errors in inversions of satellite CO₂ retrieval. *J. Geophys. Res.*, **113**, D02301.
- Cotton, W.R., R.A. Pielke Sr., R.L. Walko, G.E. Liston, C.J. Tremback, H. Jiang, R.L. McAnelly, J.Y. Harrington, M.E. Nicholls, G.G. Carrio, and J.P. McFadden, 2003: RAMS 2001: Current status and future directions. *Meteor. and Atmos. Phys.* **82**, 5-29.
- Davis, K.J., P.S. Bakwin, C. Yi, B.W. Berger, C. Zhao, R.M. Teclaw, and J.G. Isebrands, 2003: The annual cycles of CO₂ and H₂O exchange over a northern mixed forest as observed from a very tall tower. *Global Change Biology*, **9**, 1278-1293.
- Davis, K.J., D.H. Lenschow, S.P. Oncley, C. Kiemle, G. Ehret, A. Giez, and J. Mann, 1997: Role of entrainment in surface-atmosphere interactions over the boreal forest. *J. Geophys. Res.*, **102**, D24.
- Deardorff, J.W., 1974: Three-dimensional numerical study of the height and mean structure of a heated planetary boundary layer. *Boundary-Layer Meteor.*, **7**, 81-106.
- Denning, A.S., I.Y. Fung, and D.A. Randall, 1995: Latitudinal gradient of atmospheric CO₂ due to seasonal exchange with land biota. *Nature*, **376**, 240-243.
- Denning, A.S., J.G. Collatz, C. Zhang, D.A. Randall, J.A. Berry, P.J. Sellers, G.D. Colello, and D.A. Dazlich, 1996a: Simulations of terrestrial carbon metabolism and atmospheric CO₂ in a general circulation model. Part 1: Surface carbon fluxes. *Tellus*, **48B**, 521-542.
- Denning, A.S., D.A. Randall, G.J. Collatz, and P.J. Sellers, 1996b: Simulations of terrestrial carbon metabolism and atmospheric CO₂ in a general circulation model. Part 2: Spatial and temporal variations of atmospheric CO₂. *Tellus*, **48B**, 543-567.
- Denning, A.S., T. Takahashi, and P. Friedlingstein, 1999: Can a strong atmospheric CO₂ rectifier effect be reconciled with a "reasonable carbon budget? *Tellus*, **51B**, 249-253.

- Denning, A.S., M. Nicholls, L. Prihodko, I. Baker, P.-L. Vidale, K. Davis, and P. Bakwin, 2003: Simulated variations in atmospheric CO₂ over a Wisconsin forest using a coupled ecosystem-atmosphere model. *Global Change Biology*, **9**, 1241-1250.
- Denning, A.S., et al., 2005: *Science Implementation Strategy for the North American Carbon Program*. Report of the NACP Implementation Strategy Group of the U.S. Carbon Cycle Interagency Working Group. Washington, DC: U.S. Carbon Cycle Science Program, 68pp.
- Denning, A.S., N. Zhang, C. Yi, M. Branson, K. Davis, J. Kleist, P. Bakwin, 2008: Evaluation of modeled atmospheric boundary layer depth at the WLEF tower. *Agric. and Forest Meteorol.*, **148**, 206-215.
- Friedlingstein, P., et al., 2006: Climate-carbon cycle feedback analysis: Results from the C⁴MIP model intercomparison. *J. Climate*, **19**, 3337-3353.
- Gerbig, C., J.C. Lin, S.C. Wofsy, B.C. Daube, A.E. Andrews, B.B. Stephens, P.S. Bakwin, and C.A. Grainger, 2003: Toward constraining regional-scale fluxes of CO₂ with atmospheric observations over a continent: 1. Observed spatial variability from airborne platforms. *J. Geophys. Res.*, **108**, D00301.
- Gurney, K.R. et al., 2003: TransCom 3 CO₂ inversion intercomparison: 1. Annual mean control results and sensitivity to transport and prior flux information. *Tellus*, **55B**, 555-579.
- Houghton, R.A. 1999: The annual net flux of carbon to the atmosphere from changes in land use 1850-1990. *Tellus*, **51B**, 298-313.
- Marland, G., T.A. Boden, and R.J. Andres, 2005: Global, regional, and national CO₂ emissions, in *Trends: A Compendium of Data on Global Change*, Carbon Dioxide Inf. Anal. Cent., Oak Ridge Natl. Lab., U.S. Dep. of Energy, Oak Ridge, Tenn. (Available at http://cdiac.ornl.gov/trends/emis/em_cont.htm).
- Nicholls, M.E., A.S. Denning, L. Prihodko, P.-L. Vidale, I. Baker, K. Davis, and P. Bakwin, 2004: A multiple-scale simulation of variations in atmospheric carbon dioxide using a coupled-biosphere-atmospheric model. *J. Geophys. Res.*, **109**, D18117.
- Pielke, R.A., 1974: A three-dimensional numerical model of the sea breezes over south Florida. *Mon. Wea. Rev.*, **102**, 115-139.
- Pielke, R.A., 1991: Overlooked scientific issues in assessing hypothesized greenhouse gas warming. *Environ. Software*, **6**, 100-107.

- Pielke, R.A., W.R. Cotton, R.L. Walko, C.J. Tremback, W.A. Lyons, L.D. Grasso, M.E. Nicholls, M.D. Moran, D.A. Wesley, T.J. Lee, and J.H. Copeland, 1992: A comprehensive meteorological modeling system RAMS. *Meteor. Atmos. Phys.*, **49**, 69-91.
- Rayment, R. and C.J. Readings, 1974: A case study of the structure and energetics of an inversion. *Quart. J. Roy. Meteor. Soc.*, **100**, 221-233.
- Sarmiento, J.L., J.C. Orr, and U. Siegenthaler, 1992: A perturbation simulation of CO₂ uptake in an ocean general circulation model. *J. Geophys. Res.*, **97**, 3621-3645.
- Sarmiento, J.L. and E.T. Sundquist, 1992: Revised budget for the oceanic uptake of anthropogenic carbon dioxide. *Nature*, **356**, 589-593.
- Sayler, B.J. and R.E. Breidenthal, 1998: Laboratory simulations of radiatively induced entrainment in stratiform clouds. *J. Geophys. Res.*, **103**, 8827-8837.
- Schimel, D. et al, 1994: Radiative forcing of climate change and an evaluation of the IPCC IS92 emission scenarios. In *Climate Change 1994*, ed. Houghton, J.T. et al., Cambridge University Press, Cambridge, U.K., 39-71.
- Sellers, P.J., Y. Mintz, Y.C. Sud, and A. Dalcher, 1986: A simple biosphere model (SiB) for use within general circulation models. *J. Atmos. Sci.*, **43**, 505-531.
- Sellers, P.J., D.A. Randall, G.J. Collatz, J.A. Berry, C.B. Field, D.A. Dazlich, C. Zhang, G.D. Collelo, L. Bounoua, 1996: A revised land surface parameterization (SiB2) for atmospheric GCMs, Part 1: Model formulation. *J. Climate*, **9**, 676-705.
- Stevens, D.E. and C.S. Bretherton, 1999: Effects of resolution on the simulation of stratocumulus entrainment. *Quart. J. Roy. Meteor. Soc.*, **125**, 425-439.
- Stull, R.B., 1976: The energetics of entrainment across a density interface. *J. Atmos. Sci.*, **33**, 1260-1267.
- Stull, R.B., 1988: *An introduction to boundary layer meteorology*. Kluwer Academic Publishers, Norwell, MA. 666 pp.
- Sullivan, P.P., C.-H. Moeng, B. Stevens, D.H. Lenschow, and S.D. Mayer, 1998: Structure of the entrainment zone capping the convective atmospheric boundary layer. *J. Atmos. Sci.*, **55**, 3042-3064.
- Tans, P.P., I.Y. Fung, T. Takahashi, 1990: Observational constraints on the global atmospheric CO₂ budget. *Science*, **247**, 1431-1438.
- Tripoli, G.J. and W.R. Cotton, 1982: The Colorado State University three-dimensional cloud/mesoscale model – 1982. Part I: General theoretical framework and sensitivity experiments. *J. de Rech. Atmos.*, **16**, 185-220.

- Wang, J.-W., A.S. Denning, L. Lu, I.T. Baker, K.D. Corbin, and K.J. Davis, 2007: Observations and simulations of synoptic, regional, and local variations in atmospheric CO₂. *J. Geophys. Res.*, **112**, D04108.
- Willis, G.E. and J.W. Deardorff, 1974: A laboratory model of the unstable planetary boundary layer. *J. Atmos. Sci.*, **31**, 1297-1307.
- Wofsy, S.C., R.C. Harriss, and W.A. Kaplan, 1988: Carbon dioxide in the atmosphere over the Amazon basin. *J. Geophys. Res.*, **93**, 1377-1387.
- Yi, C., K.J. Davis, B.W. Berger, and P.S. Bakwin, 2001: Long-term observations of the dynamics of the continental planetary boundary layer. *J. Atmos. Sci.*, **58**, 1288-1299.
- Yi, C., K.J. Davis, P.S. Bakwin, A.S. Denning, N. Zhang, A. Desai, J.C. Lin, and C. Gerbig, 2004: Observed covariance between ecosystem carbon exchange and atmospheric boundary layer dynamics at a site in northern Wisconsin. *J. Geophys. Res.*, **109**, D08302.
- Zhang, N., 2002: Observations and simulations of the planetary boundary layer at a tall tower in northern Wisconsin. Master's thesis, Colorado State University, Department of Atmospheric Science, Fort Collins, CO 80523, 71 pp.

Chapter 2

Idealized Case Study

Abstract

The response of atmospheric carbon dioxide to a given amount of surface flux is inversely proportional to the depth of the boundary layer. Overshooting thermals that entrain free tropospheric air down into the boundary layer modify the characteristics and depth of the lower layer through the insertion of energy and mass. This alters the surface energy budget by changing the Bowen ratio and thereby altering the vegetative response and the surface boundary conditions. Although overshooting thermals are important in the physical world, their effects are unresolved in most regional models. A parameterization to include the effects of boundary layer entrainment was introduced into a coupled ecosystem-atmosphere model (SiB-RAMS). The parameterization is based on a downward heat flux at the top of the boundary layer that is proportional to the heat flux at the surface. Results with the parameterization show that the boundary layer simulated is deeper, warmer, and drier than when the parameterization is turned off. These results alter the vegetative stress factors thereby changing the carbon flux from the surface. The combination of this and the deeper boundary layer change the concentration of carbon dioxide in the boundary layer.

2.1) Introduction

The planetary boundary layer (PBL) is the layer of the atmosphere that is closest to the Earth's surface. It feels the effects of the surface through turbulent motions within the boundary layer, which work to mix the entire layer so that the characteristics of the PBL, such as the potential temperature, mixing ratio, wind speed, concentrations of trace gases, etc., are relatively homogeneous. The depth of the PBL (Z_i) is thus important for determining the concentrations of trace gases within the layer and the exchange of the variables energy, water, momentum, and trace gases between the surface and the free atmosphere, making it a significant factor in studies of pollution, heat island effects, the general circulation and many other problems of meteorology (Stull, 1976).

In particular, the planetary boundary layer depth is important for carbon budget studies. Carbon dioxide (CO_2) is released and absorbed by land ecosystems on a daily and seasonal basis. The amount of uptake and release of carbon by plants is diluted through the volume of the boundary layer so that the concentration of carbon dioxide within the boundary layer is dependent upon the PBL height.

Atmospheric inversions are a useful method for estimating surface sources and sinks of CO_2 (e.g. Gurney et al., 2002; Gerbig et al., 2003a; Zupanski et al., 2007). Downstream tracer concentrations are compared to observations and used to optimize prior upstream sources and sinks (Gerbig et al., 2003b; Zupanski et al., 2007). In this manner, model fluxes of CO_2 are corrected with observations. The sensitivity of tracer concentrations to surface fluxes is inversely proportional to the depth of the boundary layer, so errors in Z_i translate linearly to errors in retrieved fluxes (Denning et al., 1995;

1996b; 1999; 2008; Zhang, 2002; Gerbig et al., 2003a). These errors can lead to the inaccurate estimation of carbon sources and sinks.

During the daytime, in the clear atmosphere, the surface heats up through absorption of solar radiation producing a statically unstable temperature profile. This warm surface air is positively buoyant and rises through the mixed layer in warm air plumes or thermals. Due to their momentum, rising thermals overshoot their neutral level and continue into the overlying inversion layer, becoming negatively buoyant. These thermals fall back down into the mixed layer, bringing with them warm, dry free tropospheric air that is then entrained into the boundary layer by turbulent eddies (Stull, 1976; 1988; Sullivan et al., 1998).

Entrainment causes the boundary layer to grow through the insertion of energy through heat transport and mass from the free troposphere (Sullivan et al., 1998). Through the same process, turbulent kinetic energy (TKE, defined as $\frac{1}{2}(\overline{u'^2} + \overline{v'^2} + \overline{w'^2})$ where u , v , and w are the horizontal and vertical components of the wind and overbars and primes indicate the mean and departures from that mean respectively) is exported into the overlying inversion, making it turbulent and thus directly a part of the planetary boundary layer. The mixing process of boundary and inversion layers also blends characteristics of the free troposphere and boundary layer, modifying such variables as wind speed and concentrations of trace gases like CO₂ (Stull, 1976).

The boundary layer is the volume through which surface CO₂ exchange occurs. As this layer deepens, the effect of carbon assimilation is diluted through a greater volume. This means that for equal rates of assimilation, a deeper boundary layer exhibits a smaller decrease in the concentration of carbon. The temperature and humidity

conditions of the boundary layer not only affect the energy budget of the layer, but also the physiological state of the vegetation. As temperatures increase and humidity decreases, the plants can begin to show signs of stress. This decreases the assimilation of carbon and higher soil temperatures increase heterotrophic respiration. All of these effects combine to modify CO₂ concentrations near the surface. The importance of including the effects of overshooting thermals in modeling studies thus becomes apparent if the concentration of carbon in the boundary layer or the behavior of the surface vegetation is vital to the study.

Mesoscale meteorological modeling usually uses a resolution too coarse to resolve the overshooting thermals and thus does not capture the entrainment process at the top of the boundary layer (Ayotte et al., 1996; Gerbig et al., 2003a); consequently, these models cannot accurately describe the convective boundary layer (André et al., 1978). The horizontal scale of boundary layer thermals is about $1.5 * Z_i$ or on the scale of 100 meters to two kilometers (Stull, 1988). According to Pielke (1991), at least four grid increments are required to represent an atmospheric feature reasonably. This means that, at best, the horizontal grid increment of the mesoscale model would need to be 500 meters and sometimes as fine as twenty-five meters. Currently, model simulations with this resolution are too computationally expensive for large model domains and over long periods of time and cannot be done to fully resolve boundary layer thermals.

Since one of the most important roles of any model is to represent entrainment (Ayotte et al., 1996), several attempts have been made to understand entrainment better through large eddy simulations (LES) (Sullivan et al., 1998; Stevens and Bretherton, 1999) and through laboratory experiments (Sayler and Breidenthal, 1998). These studies

conclude that overshooting thermals play a crucial role in entrainment mechanics and that the strength of entrainment varies with atmospheric conditions. Unfortunately, atmospheric observations of entrainment rates are difficult because of mesoscale variations and coupling between physical processes (Sullivan et al., 1998).

In the current formulation of the Brazilian version of the Regional Atmospheric Modeling System (BRAMS) version 2.0, there is no parameterization to account for entrainment at the top of the boundary layer (Freitas et al., 2006). The boundary layer depth is diagnosed from the virtual potential temperature profile by finding the lowest layer where the virtual potential temperature profile increases by a specified amount (0.5 K in these simulations), indicating the capping inversion.

In RAMS, the vertical eddy diffusivities for momentum, heat, and TKE are inversely proportional to the vertical gradient of potential temperature through an equation for the turbulent length scale for stable conditions by André et al. (1978). They admit that this parameterization is crude and not elaborate enough to describe the turbulence in a strongly thermally stratified environment. As the stratification increases, the turbulent length scale and the vertical eddy diffusivities decrease, increasing the TKE eddy dissipation term, and can do so enough to prevent vertical mixing. The temperature inversion at the top of the boundary layer can then act similar to a material surface and retard the exchange of energy and mass that occurs in the physical world. If the simulated boundary layer is too cold and too moist with a shallow boundary layer when compared to observations, an entrainment parameterization to include the effects of overshooting thermals will produce better results.

This paper discusses the implementation of an entrainment parameterization into BRAMS based on a closure assumption for the heat flux at the base of the capping inversion that warms, dries, and increases the depth of the boundary layer. The parameterization includes a tunable coefficient that is allowed to vary in the different simulations, and comparisons are presented that show the effects of changing this coefficient. Section 2 is a description of the model setup. Section 3 discusses the parameterization itself and its implementation into RAMS. Results of model simulations using the parameterization are given in section 4. A conclusion and direction for future work is presented in section 5.

2.2) Model Setup

The parameterization has been implemented in a modified form of RAMS version 5.04 called BRAMS version 2.0. The major differences between RAMS and BRAMS are the implementation of the Grell convection scheme and the shallow convection scheme (Walko et al., 2002). The surface model used is the third version of the Simple Biosphere Model (SiB3), initially developed by Sellers et al. (1986). The coupling of the surface model and atmospheric model is called SiB-RAMS (Denning et al., 2003; Nicholls et al., 2004; Wang et al., 2007; Corbin et al., 2008).

RAMS was initially developed at Colorado State University as a non-hydrostatic three-dimensional model in order to study mesoscale and cloud-scale phenomena (Pielke, 1974; Tripoli and Cotton, 1982; Pielke et al., 1992; Cotton et al., 2003). It includes time-dependent equations for velocity, ice-liquid water potential temperature, total water mixing ratio and diagnostic formulations of potential temperature and vapor mixing ratio (Denning, et al., 2003) on either a terrain-following σ_z coordinate system or the Adaptive

Aperature (ADAP) coordinate system. The ADAP coordinate is a fully Cartesian grid in which the grid cells are allowed to intersect the topography and allows partial grid cells along the topography (Walko et al., 2002). The terrain-following coordinate system is used in the simulations discussed in this paper, but the implemented parameterization accommodates both systems.

The lowest vertical level of RAMS, called the reference level, provides temperature, vapor pressure, wind velocity, pressure, precipitation, and CO₂ concentrations as upper boundary conditions to SiB3. The RAMS model also provides the direct and diffuse components of short wave and near infrared radiation incident at the surface through its radiation scheme (Harrington 1997). These input variables to SiB3 are updated every model timestep. In return, SiB3 produces surface latent and sensible heat fluxes ($\overline{w'\theta_v}'|_s$ and $\overline{w'r_v}'|_s$ where θ_v and r_v are the virtual potential temperature and mixing ratio respectively and s represents the surface), vertical fluxes of carbon dioxide at the surface ($\overline{w'C}'|_s$ where C is the CO₂ concentration), momentum fluxes ($\overline{u'w}'|_s$), and upward long- and short-wave radiation. These variables are then inputs to RAMS at the reference level (Denning, et al., 2003) and serve as a lower boundary condition.

The turbulence closure option used during these simulations was the Mellor and Yamada (1982) scheme for vertical diffusion. Mellor and Yamada is a local option that employs a prognostic turbulent kinetic energy. The Smagorinsky (1963) scheme uses a deformation-based mixing coefficient and was used for horizontal diffusion. This option can be used for mesoscale simulations when turbulent boundary layer eddies cannot be resolved (Nicholls, et al., 2004).

Plant and plant photosynthesis are parameterized in the SiB model in an attempt to mimic the real world. SiB is a land-surface parameterization used to compute biophysical exchanges in climate models (Sellers et al., 1986), but also includes ecosystem metabolism (Sellers et al., 1996; Denning et al., 1996a). The photosynthesis parameterization was originally developed by Farquhar et al. (1980).

The parameterization assumes the leaf assimilation rate is the minimum of three limiting rates (Collatz et al., 1991; 1992). These are: (1) efficiency of the photosynthetic enzyme system (Rubisco limited), (2) amount of photosynthetically active radiation (PAR) captured by leaf chlorophyll (light limited), and (3) capacity of the leaf to export or utilize the products of photosynthesis (for C3 plants) and PEP-Carboxylase limitation (for C4 plants). The first and third limiting rates are functions of the canopy temperature and root zone soil wetness. Photosynthesis also depends upon the CO₂ concentration within the leaf and the relative humidity at the leaf surface through the leaf conductance. The leaf conductance is directly proportional to the relative humidity and inversely proportional to the CO₂ concentration and can be thought of as how open are the stomata. The larger the leaf conductance is allowed to become, the more carbon is assimilated by the leaf and the greater the rate of photosynthesis (Sellers et al., 1996). This parameterization of plant photosynthesis in the model controls how the surface characteristics are altered by the entrainment parameterization that is the topic of this paper.

A single grid was used on a domain of 200 km x 200 km with 25 individual grid cells (5x5) with a size of 40 km x 40 km each, centered at 45°N and 90°W. This grid spacing allows the resolution of mesoscale features, but is much too coarse to resolve the

individual thermals that entrain free atmospheric air into the boundary layer. Forty-two vertical grid levels were used with the lowest level at about 30 m and extending up to a domain top of 4 km with a vertical grid stretch ratio of roughly 1.1. Additional levels were included between 1500 m and 2200 m to produce an average layer depth of about 70 m. This was done to increase vertical resolution near a common boundary layer depth in order to resolve variations in the effects of the parameterization due to varying values of the tunable parameter.

Cyclic boundary conditions were used to isolate local processes that control PBL depth. Since the domain was periodic, large-scale advective influences were not included. The domain characteristics were horizontally homogeneous so that there were no influences from surface heterogeneity and no weather systems were allowed to advect into the domain. The only acting forces were those associated with the diurnal cycle and the parameterization itself. This setup also allowed the runs to be computationally inexpensive and quick to run. The simulation was allowed to run for 72 hours. The emphasis of this setup was to produce a simplified and idealized case in order to isolate the effects of the entrainment parameterization. It therefore does not resemble any particular event and model responses should be considered in this context.

The vertical profiles of pressure, temperature, humidity, and wind velocity were initialized horizontally homogeneously from a relatively cool August sounding, typical of Green Bay, Wisconsin at 44.48°N and 88.13°W with winds predominately out of the west and northwest. The topography was defined as flat and at sea level everywhere in the domain, removing any effects of terrain on boundary layer depth or growth. Similarly, the vegetation, soil textural class, fraction of photosynthetically active radiation (FPAR),

and leaf area index (LAI) were all prescribed as horizontally homogeneous. The vegetation type was C3 tall broadleaf and needleleaf trees while the soil type was loam. The default FPAR and LAI used were 0.93 and 6.2, respectively. In order to isolate the effects of dry convection, all water present in the model had to remain as water vapor, even if supersaturation occurred, in order to prevent the formation of clouds and precipitation. Clouds would have inhibited convective growth of the boundary layer.

2.3) Entrainment parameterization and implementation

The temperature profile in the well-mixed boundary layer can be assumed constant in time [$\frac{\partial}{\partial t}(\frac{\partial \theta_v}{\partial z})=0$ where t is time and z is the vertical direction] as the boundary layer warms because of the turbulent mixing throughout that layer, assuming radiative heating is independent of height. This implies that the heat flux throughout the boundary layer is linear with height, otherwise part of the layer would change temperature at a different rate from another part, and the temperature profile would not be constant in time and the layer would no longer be well-mixed. At the inversion interface, overshooting thermals inject cool, moist, CO₂-depleted turbulent boundary layer air into the overlying inversion and entrain warm, CO₂-rich free tropospheric air downward creating negative heat and carbon fluxes in the region of overshoot. Since the mixed layer is heated both from the surface due to solar heating and from the top of the boundary layer by entrainment, the profile of heat flux throughout the boundary layer is linear (Stull, 1976). Above the inversion, the perturbation vertical velocity is assumed zero, implying the heat flux is also zero.

This implies that the negative heat flux at the base of the capping inversion ($\overline{w'\theta'}|_z$) is linearly proportional to the heat flux at the surface, leading to the closure assumption for the heat flux at the top of the boundary layer:

$$\overline{w'\theta'}|_z = -\alpha \overline{w'\theta'}|_s \quad (1)$$

where α is the proportionality constant (Stull, 1988). Estimates of α from experimentation and theory range anywhere from zero to one with most published values being between 0.1 and 0.3 (e.g. Betts, 1973; Carson, 1973; Deardorff, 1974; Rayment and Readings, 1974; Willis and Deardorff, 1974; Stull, 1976; Davis et al., 1997; Sullivan et al., 1998; Yi et al., 2001).

This assumption was used to include a heat flux and a flux of other variables such as wind velocity and carbon dioxide concentration from overshooting thermals to alter the temperature, water vapor mixing ratio, winds, and CO₂ mixing ratios of the boundary layer and the lowest layer of the inversion. The heat flux can be used to define a time rate of change of potential temperature for the layers just above and just below the base of the inversion:

$$\frac{\partial\theta}{\partial t} = \frac{\alpha \overline{w'\theta'}|_s}{\Delta z} \quad (2)$$

where Δz is the thickness of the layer. Through this heating at the top of the boundary layer, the whole mixed layer warms through turbulent mixing whereas the inversion layer cools. This process weakens the capping inversion and makes it easier for the boundary layer to grow.

The heat flux across the capping inversion can be used to define a mass flux representative of the amount of mixing between the layers surrounding the interface

between the boundary layer and the capping inversion required to produce these temperature changes. This mass flux is given by:

$$M = \frac{\rho \alpha \overline{w' \theta_v'} |_s}{\Delta \theta_v} \quad (3)$$

where ρ is the density of the air and is computed from the total Exner function and ice-liquid potential temperature prognosed by RAMS (Medvigy et al., 2005). This gives the mass flux the units of $\text{kg m}^{-2} \text{s}^{-1}$. When multiplied by the specific humidity of the layer, q_v , this becomes a mass flux of water vapor. This can be used to find a time rate of change of the mixing ratio for the layers above and below the interface given by:

$$\frac{\partial r_v}{\partial t} = - \frac{\alpha q_v \overline{w' \theta_v'} |_s}{\Delta \theta_v \rho_{\text{dry}} \Delta z} \quad (4)$$

where ρ_{dry} is the density of the dry air. This induces a drying of the whole boundary layer through turbulent mixing and a moistening of the capping inversion.

This same mass flux can be used to define time rates of change of the different components of the wind vector, TKE, and CO_2 concentration given in the equations below.

$$\frac{\partial u_i}{\partial t} = \frac{u_i \alpha \overline{w' \theta_v'} |_s}{\Delta \theta_v \Delta z} \quad (5)$$

$$\frac{\partial w}{\partial t} = - \frac{w \alpha \overline{w' \theta_v'} |_s}{\Delta \theta_v \Delta z} \quad (6)$$

$$\frac{\partial TKE}{\partial t} = - \frac{TKE \alpha \overline{w' \theta_v'} |_s}{\Delta \theta_v \Delta z} \quad (7)$$

$$\frac{\partial C}{\partial t} = \frac{C \alpha \overline{w' \theta_v'} |_s}{\Delta \theta_v \Delta z} \quad (8)$$

In these equations, u_i represents the two components of the horizontal wind vector. These equations represent the mixing across the overlying capping inversion and introduce negative fluxes of horizontal momentum and CO₂ concentration and positive vertical fluxes of vertical velocity and TKE.

Equations (2), (4), (5), (6), (7), and (8) are included in a parameterization within the shallow cumulus convection parameterization unique to BRAMS (Walko et al., 2002; Freitas et al., 2006). The boundary layer height is diagnosed from the virtual potential temperature profile as the height where the temperature increases by 0.5 K, defining the capping inversion. After the PBL height is determined by this method, the temperature, mixing ratio, wind velocity, TKE, and carbon dioxide concentration tendencies for the layers above and below Z_i are altered by the above equations. Before the end of the timestep, the seven variables are updated by their respective tendency arrays.

2.4) Results

2.4.1) Physical effects

Inclusion of a parameterization for boundary layer entrainment due to overshooting thermals results in a deeper boundary layer as is evident in Figure 2.1. The greater depth is a product of the input of heat energy from the overlying inversion and the upward transport of turbulent kinetic energy, physically incorporating the lowest levels of the inversion into the boundary layer. The modeled boundary layer is allowed to grow as long as the surface sensible heat flux is positive. Once it becomes negative, an inversion is formed and the boundary layer collapses. The discretized nature of the model does not allow the boundary layer to grow in a smooth way as it would in the physical world. Z_i is

limited by the predetermined model levels and can only change when enough energy is present to move from one level to the next.

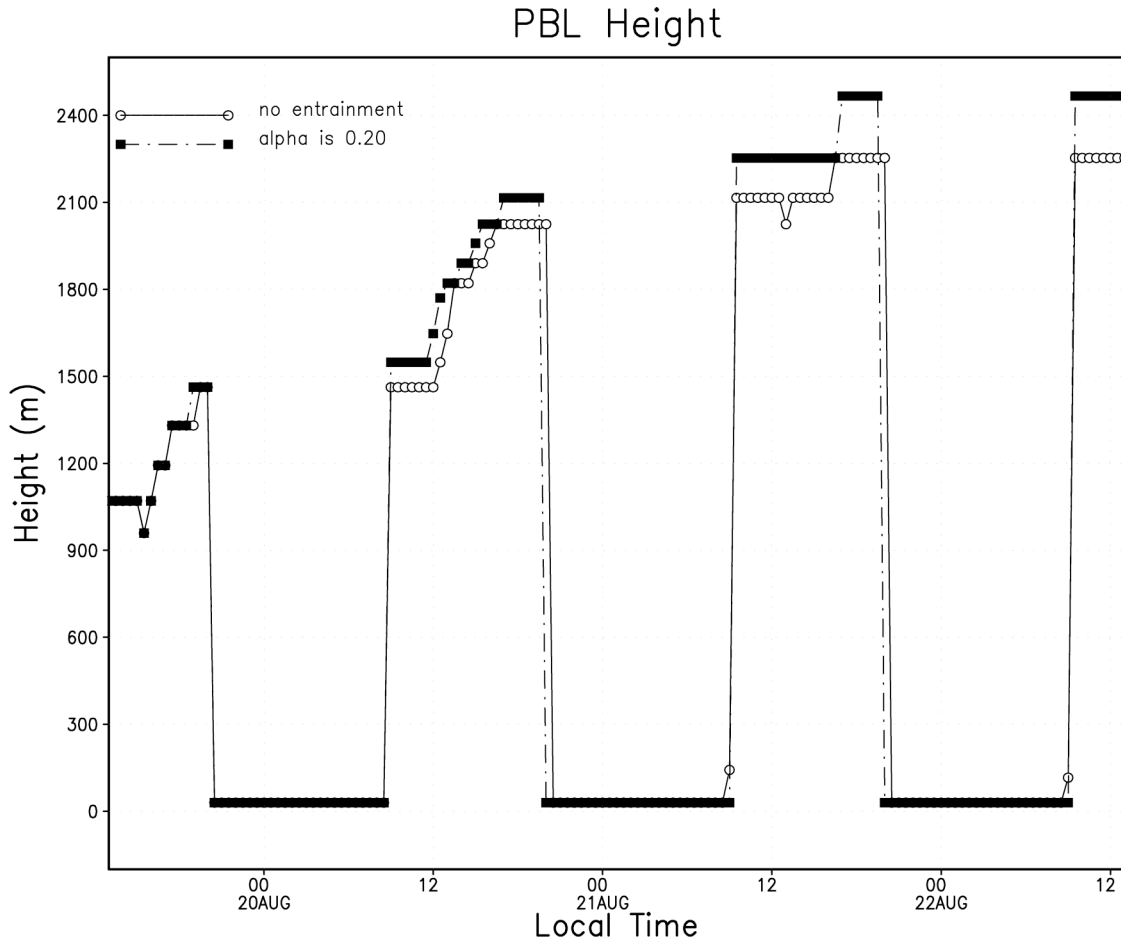


Figure 2.1 Temporal evolution of the boundary layer height for the entraining and control cases.

Figure 2.2 shows the vertical profile of potential temperature at 1700 UTC (1200 LT) on the first day of simulation. Throughout the depth of the boundary layer, the entraining case is warmer than the control case by a few degrees. In the middle of the layer, the entraining case is 3.5 K warmer for an increase of just over 1%. However, the inversion is slightly cooler in the entraining case, almost 0.3% (0.84 K) cooler. The combination of a warmer mixed layer and a weaker capping inversion means that it is easier for overshooting thermals to break through the inversion and grow the boundary

layer through entrainment. In addition, since the boundary layer is warmer, less surface heating is required to erode the inversion and grow the boundary layer. Turbulent mixing within the boundary layer distributes this warming throughout its depth.

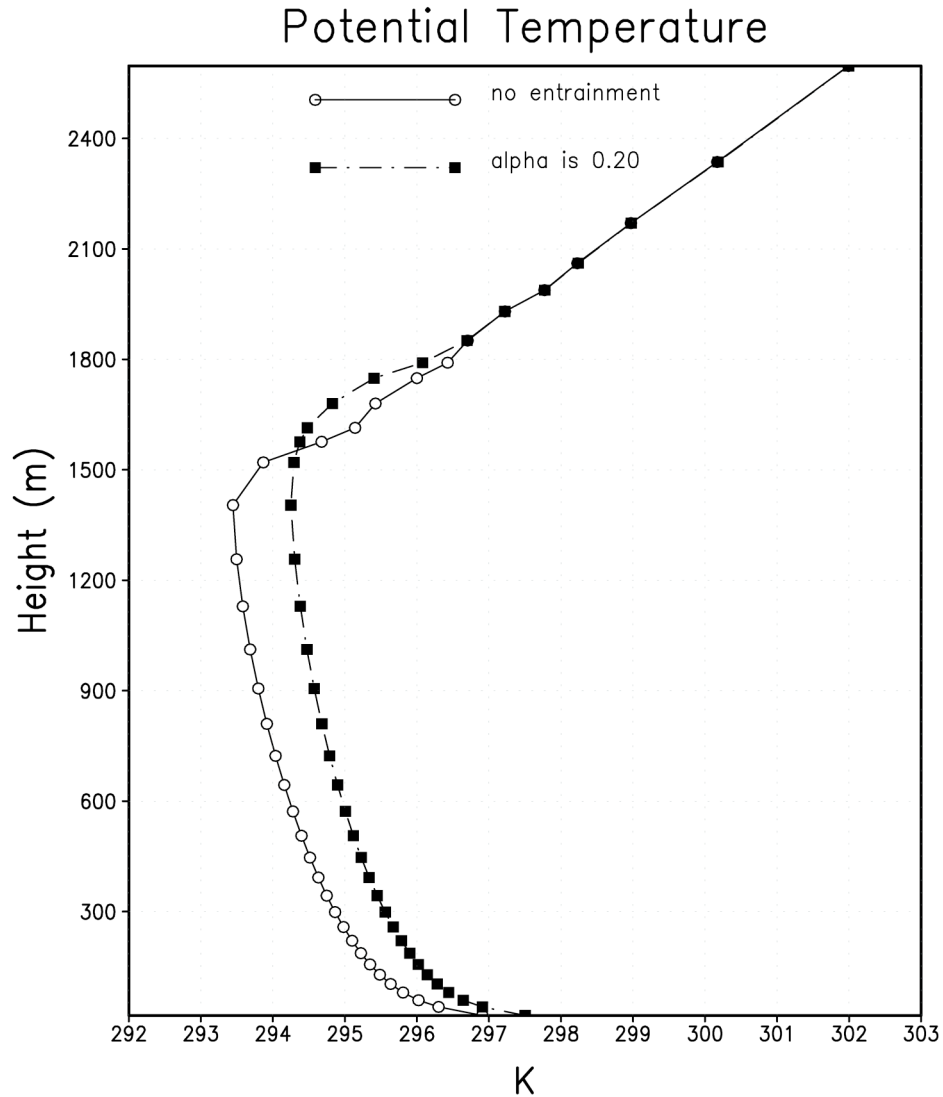


Figure 2.2 Profile of potential temperature for both the entraining and control cases on 20 August 2004 at 12 pm LT.

The stronger TKE in the entraining case produces a better-mixed, closer to adiabatic thermal profile. Overall, the impact of the parameterization on the potential temperature increases the depth of the boundary layer.

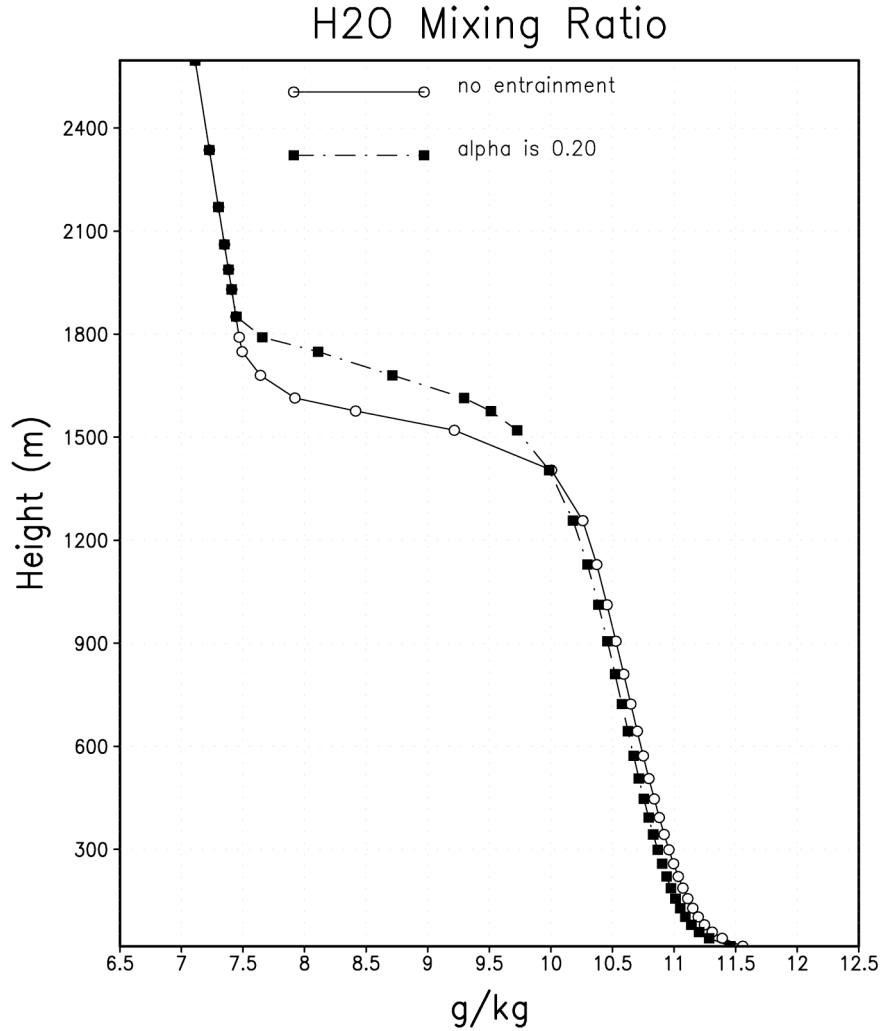


Figure 2.3 Profile of water vapor mixing ratio for both the entraining and control cases on 20 August 2004 at 12 pm LT.

The water vapor mixing ratio profile is also modified by the parameterization (Figure 2.3). In both the entraining and control cases, the highest mixing ratios are located at the surface, a result of the source of water from evaporation and transpiration being located at the surface, and gradually decrease to the top of the boundary layer where there is a sharp gradient transitioning into the much drier overlying air. The upward transport of moisture, carried by the overshooting thermals, results in a drier boundary layer and a moister inversion layer in the entraining case. The change in water

vapor mixing ratio in the middle of the boundary layer is about 0.66% (0.07 g kg^{-1}) decrease in the entraining case, but the greater moisture content in the overlying inversion is slightly over 17% (1.4 g kg^{-1}) due to the low water content and shallow depth of the inversion layer. Since water vapor present in an air mass decreases the density of that air mass, the overall effect of upward advection of water vapor is to decrease the ability of thermals to penetrate the inversion and make it harder for the well-mixed layer to erode the inversion. This inhibits boundary layer growth through a reduction in the positive buoyancy of thermals originating at the surface and favors a shallower boundary layer.

The effects of the parameterization on the potential temperature and the water vapor mixing ratio act in opposite directions. In order to understand the combined effect, the profile of the virtual potential temperature must be examined. Virtual potential temperature can be related to potential temperature and water vapor mixing ratio through the equation:

$$\theta_v = \theta(1 + 0.61r_v). \quad (9)$$

As r_v and θ increase, so does the virtual potential temperature. Since the virtual potential temperature is used to determine the top of the boundary layer and includes the effects of both potential temperature and water vapor mixing ratio, it is a direct way of determining which effect dominates.

Figure 2.4 shows the profile of the virtual potential temperature. The boundary layer is warmer in the entraining case and the middle of the layer is warmer by about a quarter of a percent (0.77 K). In the inversion layer, the entraining case is still cooler than the control case by about 0.14% (0.4 K). Although the effects of vertical moisture advection oppose those of temperature, the temperature effects dominate and the overall

result is a vertical potential temperature profile that is less inhibitive to boundary layer growth after the influence of overshooting thermals is considered.

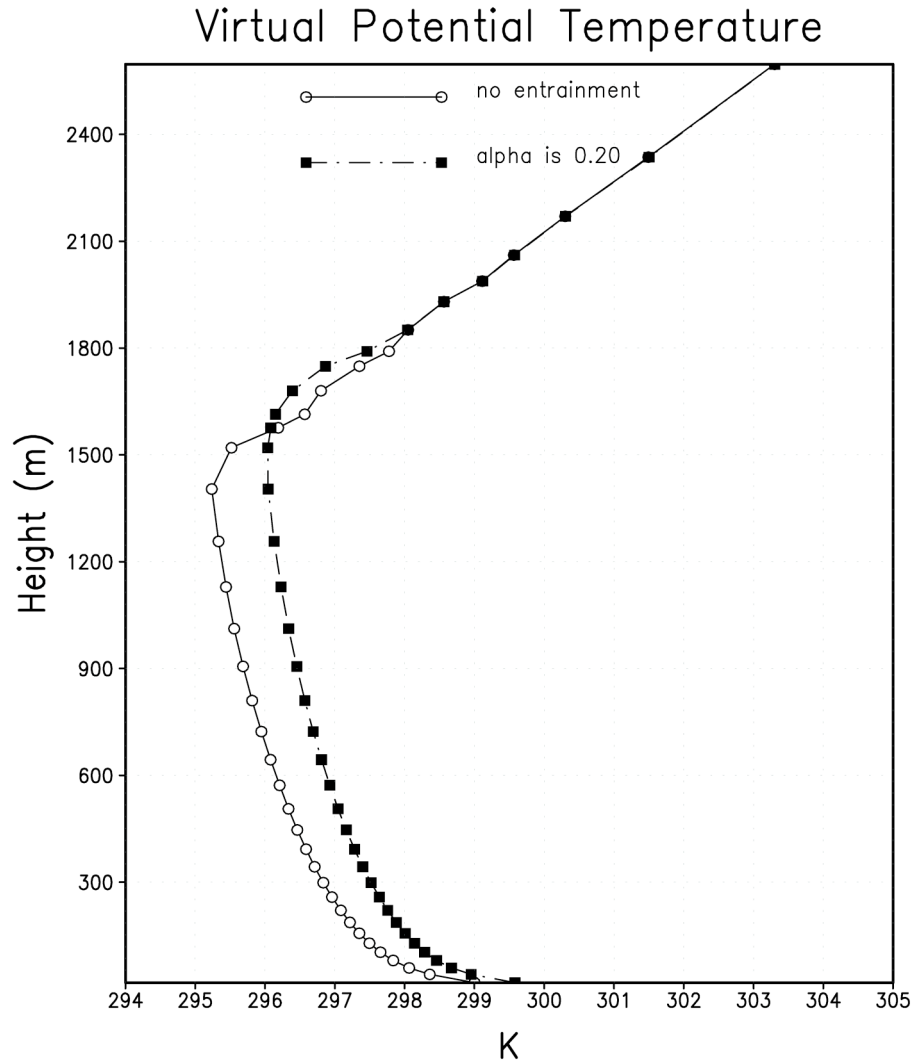


Figure 2.4 Profile of virtual potential temperature for both the entraining and control cases on 20 August 2004 at 12 pm LT.

Surface variables are also affected by overshooting thermals through the mixing of boundary layer characteristics throughout the depth of the boundary layer by eddies and their associated TKE. Modification of surface variables is important when comparing the model results to observations. Figure 2.5 shows the temporal evolution of potential temperature in the lowest atmospheric model level. The entraining case has

warmer temperatures than the control case throughout the simulation. The differences increase with time such that on the third day of simulation, the daytime entraining case's potential temperature is 1.5 K warmer than the control case.

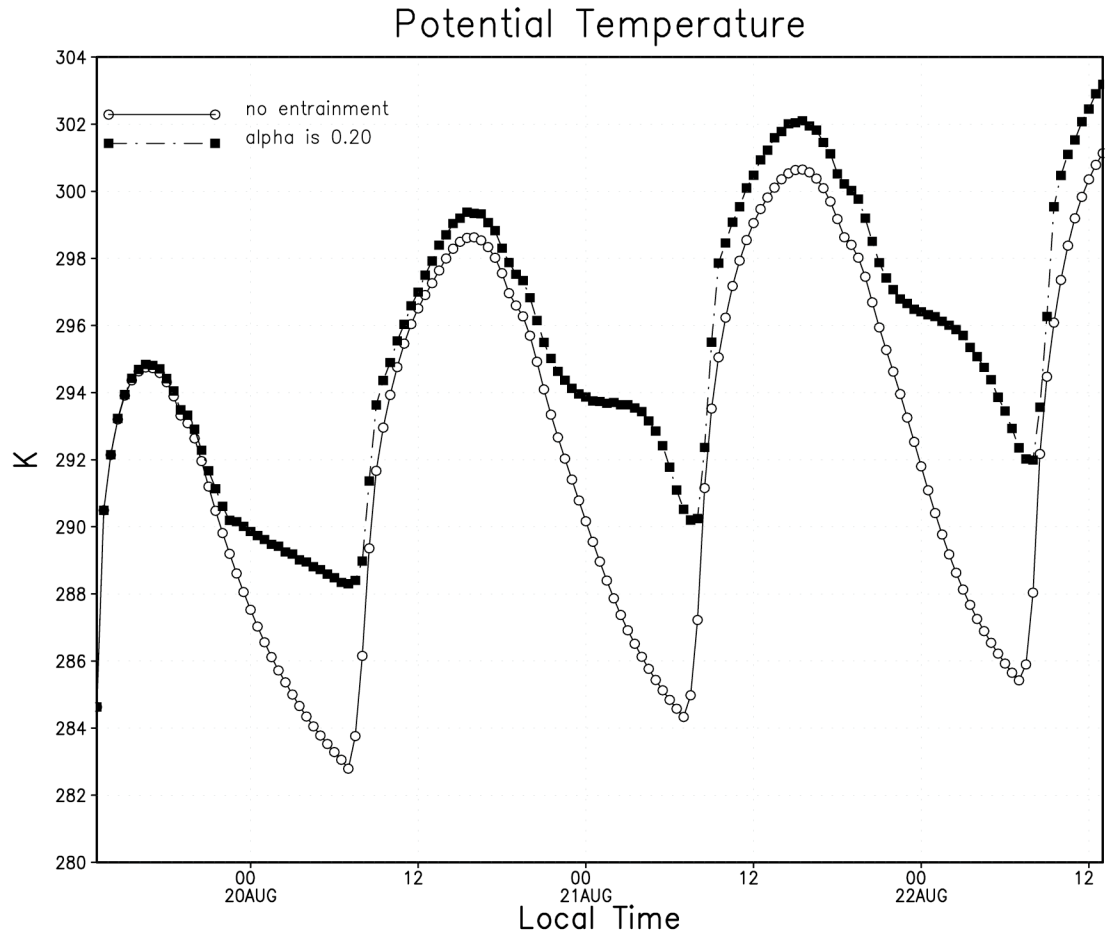


Figure 2.5 Temporal evolution of potential temperature in the lowest atmospheric model level for the entraining and control cases.

At night, the entraining case is much warmer than the control case, by as much as 6 K toward the end of the simulation. This is due, in part, to the heat capacity of the atmosphere. The daytime temperature is warmer in the entraining case and so it does not cool off as quickly resulting in a warmer nighttime temperature. A more significant cause of the warm nighttime temperatures is that the nocturnal inversion is not as strong in the entraining case. The nighttime TKE is stronger near the surface (not shown)

producing a weaker nocturnal capping inversion. The weaker capping inversion allows more mixing between the surface air and the overlying residual layer. The consequence of increased mixing is that the radiatively cooled surface air is mixed with warmer overlying air and thus remains warmer.

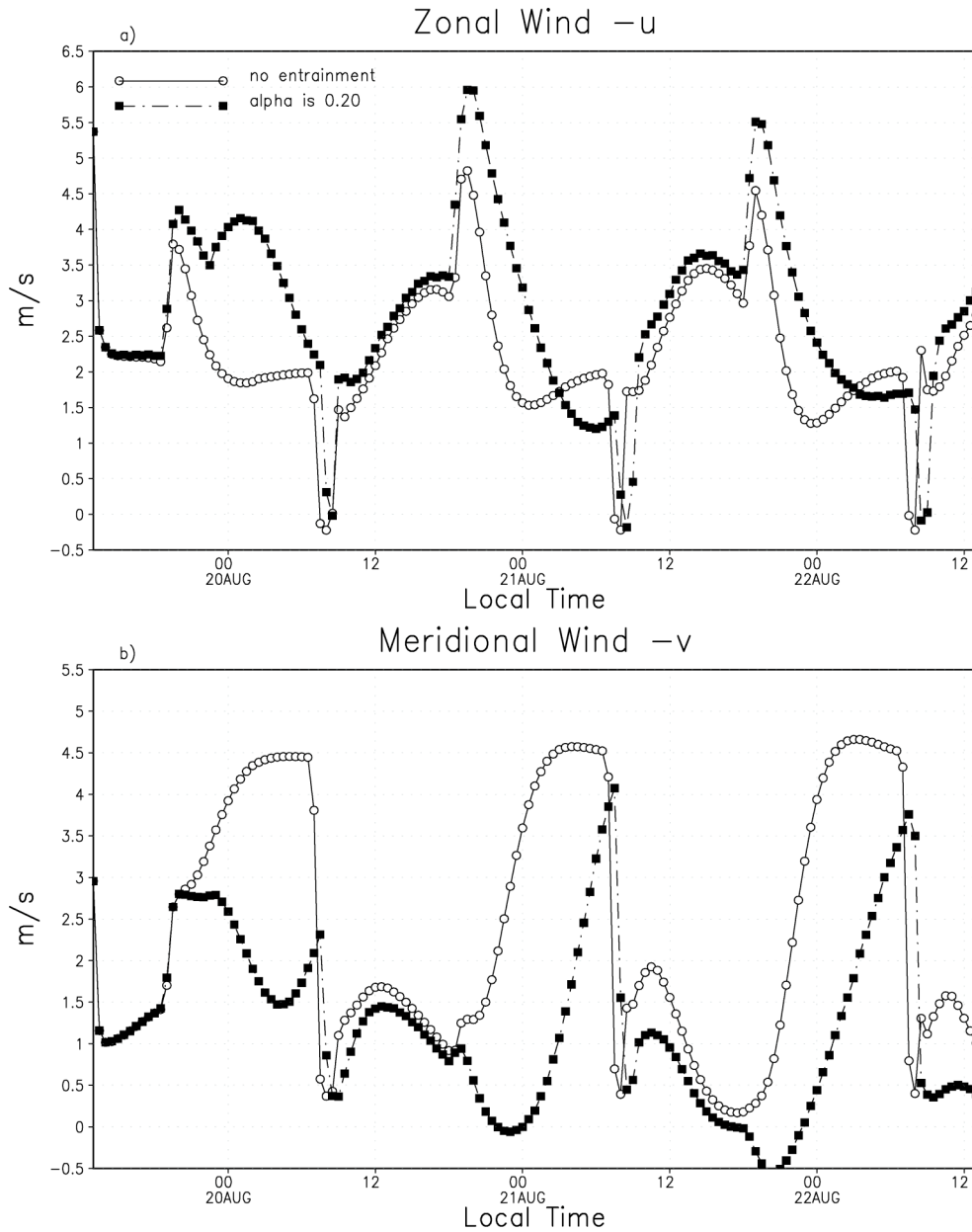


Figure 2.6 Temporal evolution of the zonal (a) and meridional (b) winds in the lowest atmospheric model level for the entraining and control cases.

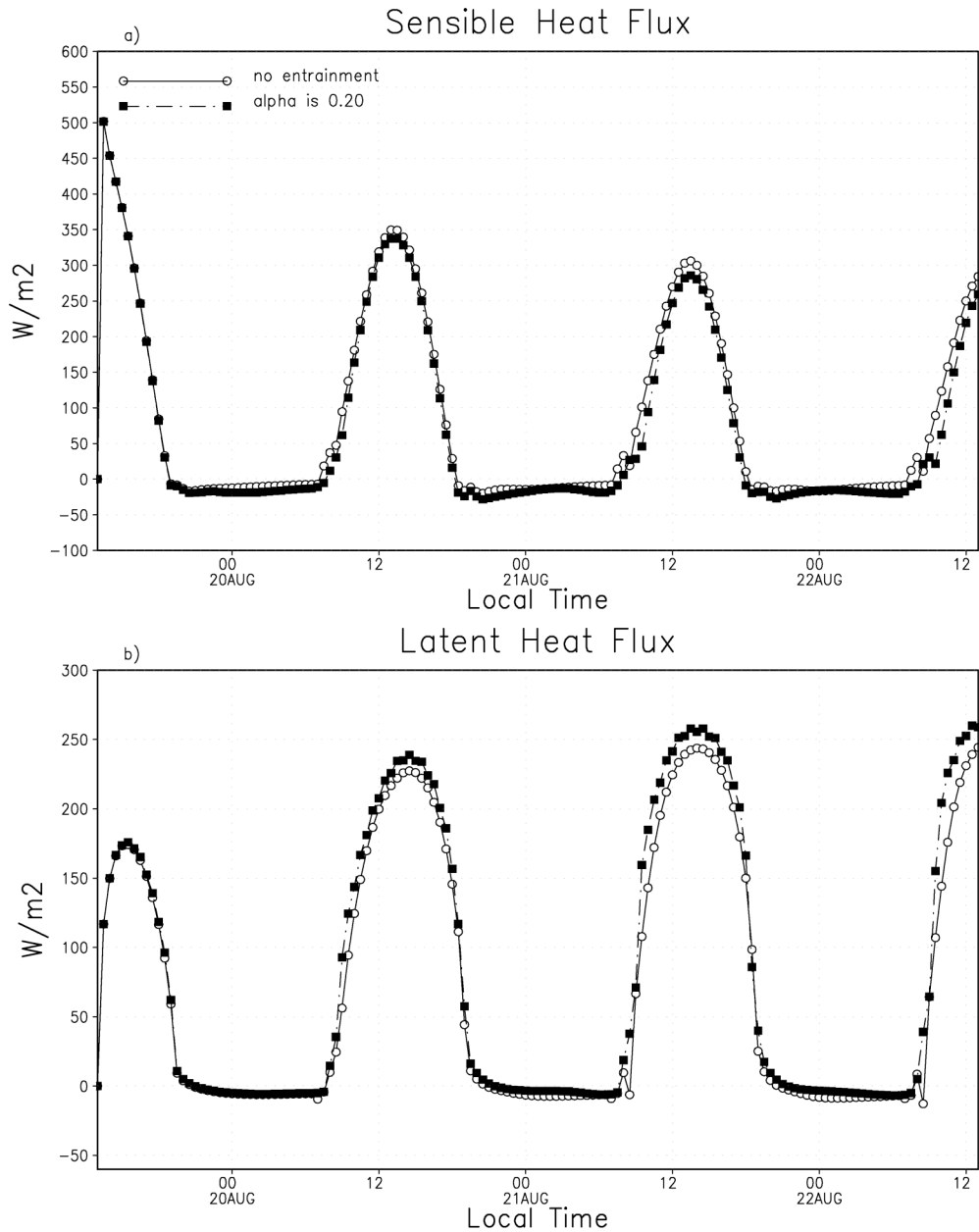


Figure 2.7 Temporal evolution of the sensible (a) and latent (b) heat fluxes in the lowest atmospheric model level for the entraining and control cases.

Figure 2.6 shows the effects of overshooting thermals on the horizontal wind velocity near the surface. Momentum from the free troposphere is mixed downward by the overshooting thermals. The TKE in the boundary layer mixes that momentum throughout the depth of the boundary layer and therefore adjusts the profile of the wind. The wind profile directly above the boundary layer is northwesterly and so when it is

advected downward, it turns the boundary layer wind in that direction. In the lowest atmospheric model level, this results in the zonal wind in Figure 2.6a becoming stronger and more positive and the meridional wind in Figure 2.6b becoming weaker and less positive.

The temporal evolution of sensible and latent heat fluxes from the canopy air space (CAS) into the boundary layer is shown in Figures 2.7a and 2.7b respectively. The daytime sensible heat flux is smaller in the entraining case because the boundary layer is warmer in this case. Sensible heat flux is proportional to the gradient in temperature between the CAS and the boundary layer so if that gradient is weakened through warming of the boundary layer, the heat flux is lessened. On the third day of simulation, the sensible heat flux of the control case is 20 W m^{-2} stronger. This produces a change of about 7% in the sensible heat flux resulting from the entrainment parameterization. Since the parameterization is proportional to the surface heat flux, reducing this flux reduces the effects of the thermals. Conversely, the sensible heat flux at night is more strongly negative in the entraining case. The surface cools off, but the atmosphere remains warm so that the gradient in temperature is greater in the entraining case. Because the sensible heat flux is more strongly negative at night, more solar heating is required during the day to produce a positive sensible heat flux.

As was the case for potential temperature and water vapor mixing ratio, the response of sensible and latent heat fluxes to entrainment is opposed. The drier boundary layer means that the gradient in water vapor mixing ratio between the boundary layer and the CAS is stronger in the entraining case. The drier boundary layer persists throughout the diurnal cycle inducing a larger positive latent heat flux during the day and a smaller

negative flux at night. As temperatures increase in the model atmosphere, the relative humidity decreases and the relative humidity gradient between the boundary layer and the CAS becomes even larger inducing an even stronger latent heat flux. A larger latent heat flux contributes to a larger total heat flux. The larger heat flux then contributes to a larger impact of the parameterization on the heat flux at the top of the boundary layer. At the peak of latent heat flux on the third day of simulation, the entraining case's latent heat flux is 15 W m^{-2} greater for a change of about 6%. The additional moisture from the surface source is then mixed upward by turbulent eddies to moisten the depth of the boundary layer. Although the sensible and latent heat fluxes oppose each other, the total buoyancy heat flux (not shown) is smaller in the entraining case than the control case.

2.4.2) Physiological effects

The physical modifications to the boundary layer directly impact the vegetation at the surface. The energy budget of the vegetated land surface partitions net downward radiation into turbulent fluxes of heat and moisture that warm and moisten the atmosphere, plus a smaller heat flux into the soil. The Bowen ratio of sensible to latent heat fluxes is determined by the conductance of plant stomata, which is actively controlled as an evolved response by plants to maximize CO_2 uptake by photosynthesis while minimizing water loss (Bonan et al., 2002; Ball et al., 1987; Collatz et al., 1991). Stomatal conductance (and hence transpiration) is generally greatest when photosynthetic carbon uptake is greatest, the air is nearly saturated with respect to water vapor, and the temperature moderate. The drying influence of entrainment can produce a humidity stress on the plants so that they close their stomata, causing a response in transpiration, the surface energy budget, and photosynthetic rates (Davis et al., 1997).

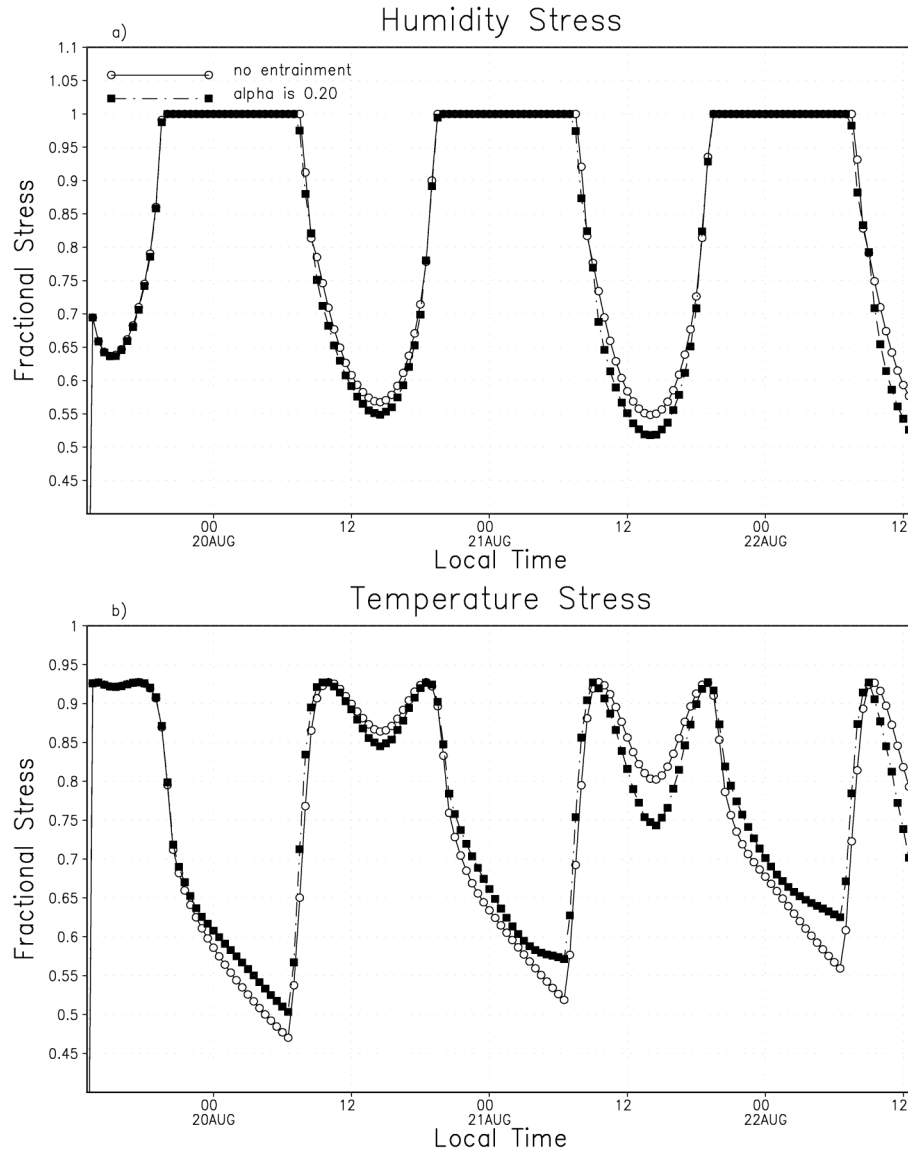


Figure 2.8 Temporal evolution of vegetative stress factors for the entraining and control cases. (a) Humidity stress (b) Temperature stress.

Stomatal conductance and photosynthesis were calculated iteratively according to enzyme kinetics, diffusion of CO_2 and water vapor, and the Ball-Berry equation (Collatz et al, 1991). Stomatal conductance is directly proportional to the relative humidity at the leaf surface (inside the laminar boundary layer surrounding the leaf), and is adjusted downward by multiplying by nondimensional “stress factors” to account for non-optimal temperatures or insufficient soil moisture (Sellers et al, 1996) (Figure 2.8).

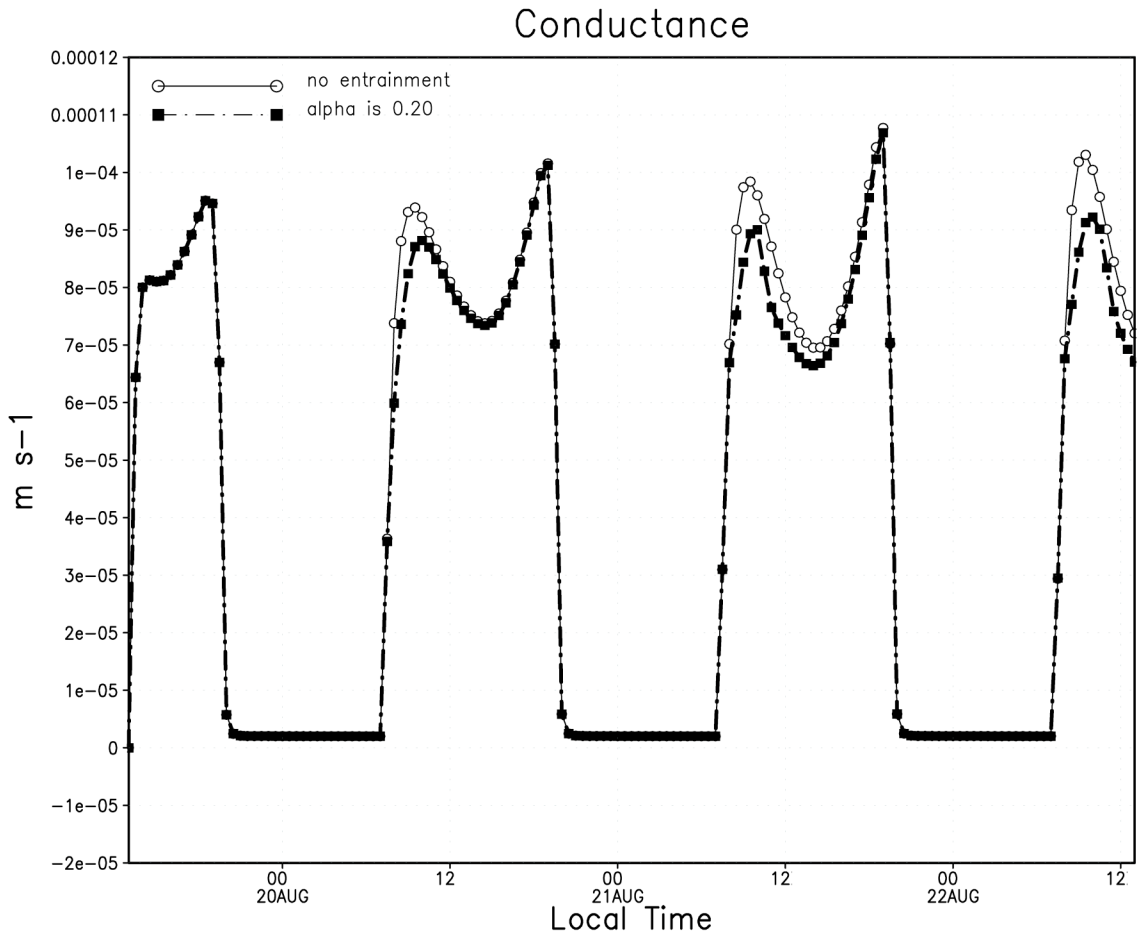


Figure 2.9 Temporal evolution of conductance for both the entraining and control cases.

Simulated stomatal conductance (Figure 2.9) was reduced during the hottest part of each day due to a combination of slightly reduced humidity and high-temperature stress. Entrainment of dry air into the boundary layer by overshooting thermals is communicated through turbulent mixing, leading to a slightly warmer and drier stomatal microenvironment, and therefore reduced stomatal conductance. Note that despite the slight reduction in stomatal conductance the simulated sensible heat flux was suppressed and latent heat flux was enhanced in the entraining case due to stronger gradients in the surface layer (Figure 2.7).

Figure 2.10 shows the impact of the vegetative stress on the net ecosystem exchange (NEE) of CO₂ and its components. In the morning, warmer temperatures cause the entraining case to have very slightly enhanced uptake of carbon. High-temperature stress and low humidity at mid-day produces less uptake, taking up $1.3 \mu\text{mol m}^{-2} \text{s}^{-1}$ less carbon by the third day. The NEE at night is very similar between the entraining and control cases with slightly greater respiration in the entraining case due to the warmer

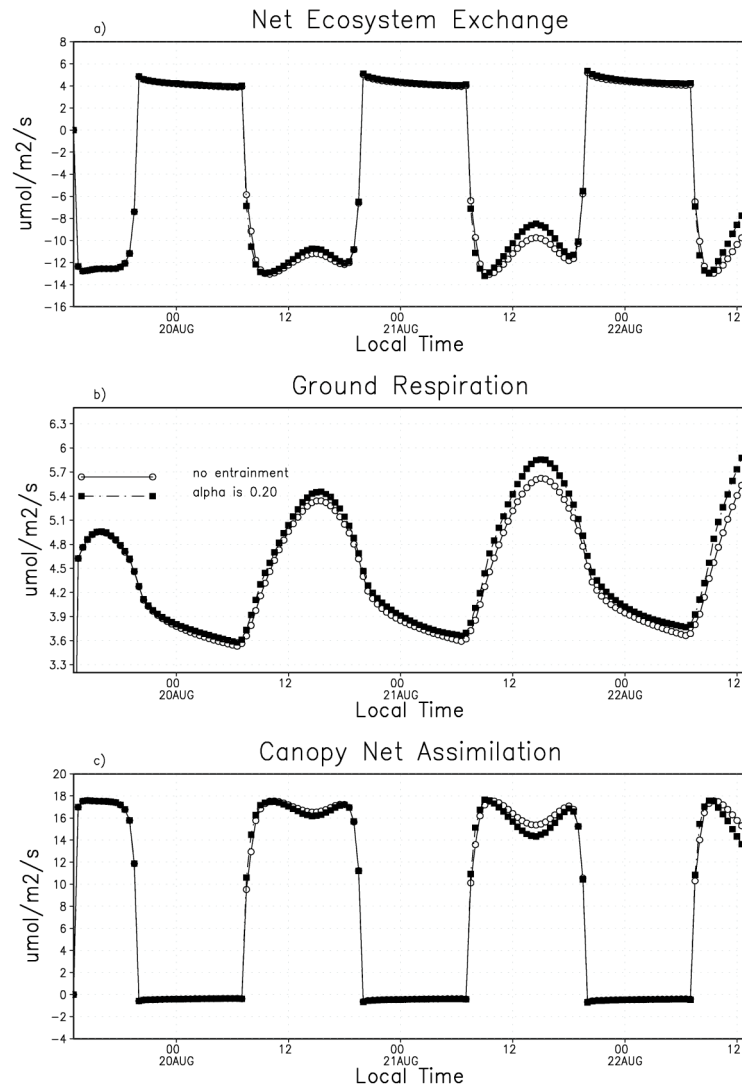


Figure 2.10 Temporal evolution of NEE (a), ground respiration (b), and canopy net assimilation (c) for the entraining and control cases.

surface temperature. Ground respiration is a function of the surface soil temperature and varies with the diurnal cycle of temperature (Fig 2.10b). Since the entraining case is warmer throughout the simulation, the ground respiration is larger and more carbon is released into the atmosphere from soil decomposition. Warmer and drier air at mid-day suppresses photosynthetic assimilation (Fig 2.10c). The entraining thermals in the simulation thus act indirectly on both components of the net CO₂ exchange to suppress the drawdown of CO₂ from the PBL through their effects on temperature and moisture.

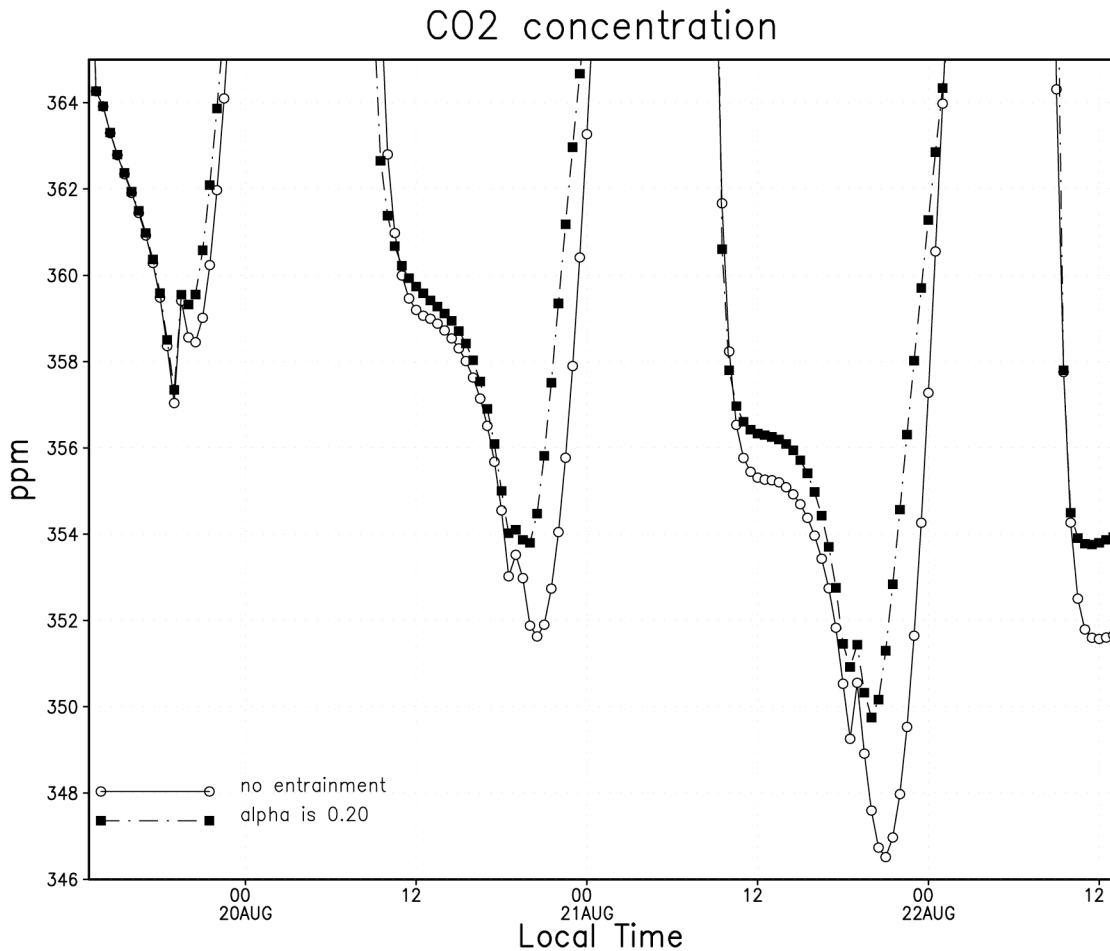


Figure 2.11 Temporal evolution of carbon dioxide concentration in the lowest atmospheric model level for the entraining and control cases.

The overall impact of simulated entrainment on CO₂ in the PBL reflects the modified NEE as well as dilution through the deeper mixed layer and enhanced mixing

through the PBL top. Figure 2.11 shows only the daytime concentration of CO₂ since this study is not concerned with nighttime values. During the day, negative NEE draws down the CO₂ concentration. The daily minimum in CO₂ concentration occurs near sunset, just as the vegetation stops removing carbon from the atmosphere.

CO₂ concentrations in the entraining case are higher than the control due to both the reduced assimilation and the depth of the boundary layer. As the boundary layer grows, a greater volume of the atmosphere is in contact with the surface. Removal of a given amount of carbon reduces the CO₂ concentration less when the carbon is removed from the greater volume. A deeper boundary layer consequently results in higher carbon dioxide concentrations within the boundary layer.

2.4.3) *Parameterization effects*

The previous results were obtained by setting the tunable parameter, α , to 0.20, indicating that the entrainment heat flux at the top of the boundary layer was assumed to be 20% of the surface heat flux. The following discussion determines the sensitivity of the system to varying strengths of the parameterization by using values of α between 0.0 and 0.5.

Figure 2.12 illustrates how mid-day potential temperature (Figure 2.12a), water vapor mixing ratio (Figure 2.12b), Z_i (Figure 2.12c), and CO₂ concentration (Figure 2.12d) in the lowest atmospheric model level on the second day of simulation vary as functions of α . The potential temperature linearly increases with α , with a correlation coefficient of 0.9944. Neglecting entrainment can result in boundary layer temperature errors that can also affect the assimilation of carbon by plants.

The water vapor mixing ratio linearly decreases for α greater than 0.10. As α increases, overshooting thermals remove water from the boundary layer and transfer it to the overlying inversion. The water vapor flux has a minimum at $\alpha = 0.05$ and increases up to $\alpha = 0.10$. As the boundary layer dries, the moisture gradient between the CAS and the boundary layer increases, producing a greater latent heat flux. The latent heat flux moistens the boundary layer, acting contrary to the overshooting thermals. A contributing factor to this process is that the simulation is idealized and no new air is allowed to advect into the domain to reduce the amount of latent heat flux at the surface. The correlation coefficient between α and the water vapor mixing ratio is -0.59 and is significant at the 95% level for the range of α shown.

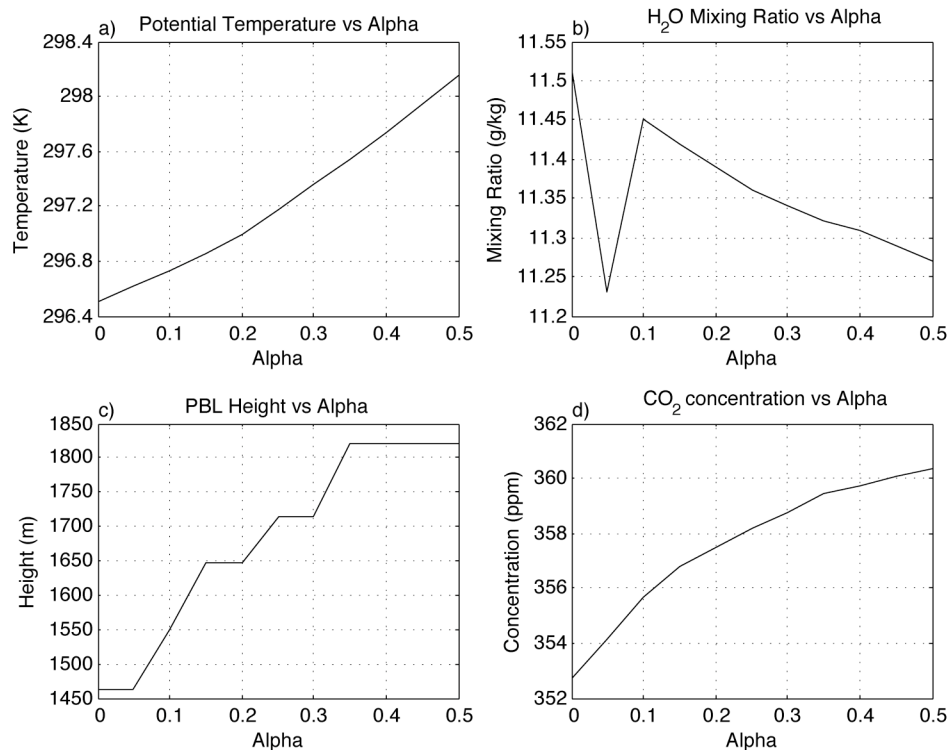


Figure 2.12 Sensitivity of potential temperature (a), water vapor mixing ratio (b), PBL depth (c), and CO₂ concentration (d) in the lowest model level to α . Values taken from 1200 LT on the second day of simulation.

The boundary layer height is dependent upon the vertical grid spacing. Energy is needed for Z_i to jump from one level to the next, and greater vertical resolution requires less energy to make a jump, but each jump is smaller. Z_i monotonically increases with α and does so with a correlation coefficient of 0.96. The boundary layer depth at this time behaves linearly with the strength of the entrainment heat flux.

Figure 2.12d shows how CO_2 concentration varies as a function of α . As α increases, so also does the concentration of CO_2 in the lowest model level. This can be attributed to deeper boundary layers diluting the effect of photosynthetic uptake and increased vegetative stress associated with the warmer and drier conditions of an entrainment heat flux. The correlation coefficient between CO_2 concentration and α is near unity and the increasing trend exceeds the 99.99% confidence level. With a regression coefficient of near 14.6, the amount of variability of CO_2 concentration with α is alarming for inversion studies that depend upon accurate modeled surface concentrations. Between $\alpha = 0.0$ and $\alpha = 0.20$, the concentration of carbon dioxide increases nearly 5 ppmv for a change of 1.35%.

2.5) Conclusions and Future Work

The effects of overshooting thermals are essential to studies of the carbon budget using modeling. This experiment seeks to parameterize these effects that are too fine for the grid spacing of mesoscale meteorological models to resolve. These thermals warm and dry the boundary layer through entrainment of free tropospheric air and mix wind velocities, TKE, and CO_2 concentrations. The addition of mass to the boundary layer also allows it to grow. This process weakens the capping inversion and reduces the

amount of energy needed within the boundary layer for it to grow further. The increased PBL depth means that the remaining uptake of carbon is diluted through a deeper layer, increasing carbon concentrations. The mass and heat fluxes associated with overshooting thermals affect the atmospheric conditions to which the underlying vegetation respond. The altered response, in turn, affects the photosynthetic uptake of carbon thereby increasing the daytime CO₂ concentration even further. Since most observations are performed within the boundary layer, neglect of this process produces a model-observation mismatch and introduces errors into the assumed distribution of sources and sinks.

With this end in mind, the parameterization added to SiB-RAMS introduces a negative sensible heat flux and a positive water vapor flux at the top of the boundary layer and mixes the other variables. This parameterization includes a tunable parameter, α , that is equal to the negative of the ratio of the entrainment heat flux at the top of the boundary layer to the surface heat flux. The parameterization does induce a warmer, drier boundary layer that affects such characteristics as sensible and latent heat fluxes, wind velocity, and carbon dioxide concentration.

Future work will focus on evaluation of the entrainment parameterization for real cases, estimation of the entrainment parameter α , and application to CO₂ source/sink estimation.

REFERENCES

- André, J.C., G. De Moor, P. Lacarrère, G. Therry, and R. Du Vachat, 1978: Modeling the 24-hour evolution of the mean and turbulent structures of the planetary boundary layer. *J. Atmos. Sci.*, **35**, 1861-1883.
- Ayotte, K.W., P.P. Sullivan, A. Andrén, S.C. Doney, A.A.M. Holtslag, W.G. Large, J.C. McWilliams, C.-H. Moeng, M.J. Otte, J.J. Tribbia, and J.C. Wyngaard, 1996: An evaluation of neutral and convective planetary boundary layer parameterizations relative to large eddy simulation. *Bound. Layer Meteor.*, **79**, 131-175.
- Ball, J.T., I.E. Woodrow, and J.A. Berry, 1987: A model predicting stomatal conductance and its contribution to the control of photosynthesis under different environmental conditions. *Progress in Photosynthesis Research*, ed. J. Biggens, 221-224.
- Betts, A.K., 1973: Non-precipitating cumulus convection and its parameterization. *Quart. J. Roy. Meteor. Soc.*, **99**, 178-196.
- Bonan, G.B., S. Lewis, L. Kergoat, and K.W. Oleson, 2002: Landscapes as patches of plant functional types: An integrating concept for climate and ecosystem models. *Global Biogeochemical Cycles*, **16**, 5.1-5.23.
- Carson, D.J., 1973: The development of a dry inversion-capped convectively unstable boundary layer. *Quart. J. Roy. Meteor. Soc.*, **100**, 450-467.
- Collatz, G.J., J.T. Ball, C. Grivet, and J.A. Berry, 1991: Physiological and environmental regulation of stomatal conductance, photosynthesis and transpiration: A model that includes a laminar boundary layer. *Agric. For. Meteor.*, **54**, 107-136.
- Collatz, G.J., M. Ribas-Carbo, and J.A. Berry, 1992: Coupled photosynthesis-stomatal conductance model for leaves of c-4 plants. *Aust. J. Plant Physiol.*, **19**, 519-538.
- Corbin, K.D., A.S. Denning, L. Lu, J.-W. Wang, I.T. Baker, 2008: Possible representation errors in inversions of satellite CO₂ retrieval. *J. Geophys. Res.*, **113**, D02301.
- Cotton, W.R., R.A. Pielke Sr., R.L. Walko, G.E. Liston, C.J. Tremback, H. Jiang, R.L. McAnelly, J.Y. Harrington, M.E. Nicholls, G.G. Carrio, and J.P. McFadden, 2003: RAMS 2001: Current status and future directions. *Meteor. and Atmos. Phys.* **82**, 5-29.

- Davis, K.J., D.H. Lenschow, S.P. Oncley, C. Kiemle, G. Ehret, A. Giez, and J. Mann, 1997: Role of entrainment in surface-atmosphere interactions over the boreal forest. *J. Geophys. Res.*, **102**, D24.
- Deardorff, J.W., 1974: Three-dimensional numerical study of the height and mean structure of a heated planetary boundary layer. *Boundary-Layer Meteor.*, **7**, 81-106.
- Denning, A.S., J.G. Collatz, C. Zhang, D.A. Randall, J.A. Berry, P.J. Sellers, G.D. Colello, and D.A. Dazlich, 1996a: Simulations of terrestrial carbon metabolism and atmospheric CO₂ in a general circulation model. Part 1: Surface carbon fluxes. *Tellus*, **48B**, 521-542.
- Denning, A.S., I.Y. Fung, and D.A. Randall, 1995: Latitudinal gradient of atmospheric CO₂ due to seasonal exchange with land biota. *Nature*, **376**, 240-243.
- Denning, A.S., M. Nicholls, L. Prihodko, I. Baker, P.-L. Vidale, K. Davis, and P. Bakwin, 2003: Simulated variations in atmospheric CO₂ over a Wisconsin forest using a coupled ecosystem-atmosphere model. *Global Change Biology*, **9**, 1241-1250.
- Denning, A.S., D.A. Randall, G.J. Collatz, and P.J. Sellers, 1996b: Simulations of terrestrial carbon metabolism and atmospheric CO₂ in a general circulation model. Part 2: Spatial and temporal variations of atmospheric CO₂. *Tellus*, **48B**, 543-567.
- Denning, A.S., T. Takahashi, and P. Friedlingstein, 1999: Can a strong atmospheric CO₂ rectifier effect be reconciled with a "reasonable carbon budget? *Tellus*, **51B**, 249-253.
- Denning, A.S., N. Zhang, C. Yi, M. Branson, K. Davis, J. Kleist, and P. Bakwin, 2008: Evaluation of modeled atmospheric boundary layer depth at the WLEF tower. *Agric. And Forest Meteorol.*, **148**, 206-215.
- Farquhar, G.D., S.V. Caemmerer, and J.A. Berry, 1980: A biochemical-model of photosynthetic CO₂ assimilation in leaves of C-3 species. *Planta*, **149**, 78-90.
- Freitas, S.R., K. Longo, M. Silva Dias, P. Silva Dias, R. Chatfield, Á. Fazenda, and L.F. Rorigues, 2006: The coupled aerosol and tracer transport model to the Brazilian developments on the Regional Atmospheric Modeling System: Validation using direct and remote sensing observations. International Conference on Southern Hemisphere Meteorology and Oceanography (ICSHMO), 8., 101-107. CD-ROM. ISBN 85-17-00023-4.
- Gerbig, C., J.C. Lin, S.C. Wofsy, B.C. Daube, A.E. Andrews, B.B. Stephens, P.S. Bakwin, and C.A. Grainger, 2003a: Toward constraining regional-scale fluxes of

- CO₂ with atmospheric observations over a continent: 1. Observed spatial variability from airborne platforms. *J. Geophys. Res.*, **108**, D00301.
- Gerbig, C., J.C. Lin, S.C. Wofsy, B.C. Daube, A.E. Andrews, B.B. Stephens, P.S. Bakwin, and C.A. Grainger, 2003b: Toward constraining regional-scale fluxes of CO₂ with atmospheric observations over a continent: 2. Analysis of COBRA data using a receptor-oriented framework. *J. Geophys. Res.*, **108**, D003770.
- Gurney, K.R., R.M. Law, A.S. Denning, P.J. Rayner, D. Baker, P. Bousquet, L. Bruhwiler, Y.-H. Chen, P. Ciais, S. Fan, I.Y. Fung, M. Gloor, M. Heimann, K. Higuchi, J. John, T. Maki, S. Maksyutov, K. Masarie, P. Peylin, M. Prather, B.C. Pak, J. Randerson, J. Sarmiento, S. Taguchi, T. Takahashi, and C.-W. Yuen, 2002: Towards robust regional estimates of CO₂ sources and sinks using atmospheric transport models. *Nature*, **415**, 626-630.
- Harrington J.Y., 1997: The effects of radiative and microphysical processes on simulated warm and transition season Arctic stratus. PhD Diss., Atmospheric Science Paper No 637, Colorado State University, Department of Atmospheric Science, Fort Collins, CO 80523, 289 pp.
- Medvigy, D., P.R. Moorcroft, R. Avissar, and R.L. Walko, 2005: Mass conservation and atmospheric dynamics in the Regional Atmospheric Modeling System (RAMS). *Environmental Fluid Mechanics*, **5**, 109-134.
- Mellor, G.L. and T. Yamada, 1982: Development of a turbulence closure model for geophysical fluid problems. *Rev. Geophys.*, **20**, 851-875.
- Nicholls, M.E., A.S. Denning, L. Prihodko, P.-L. Vidale, I. Baker, K. Davis, and P. Bakwin, 2004: A multiple-scale simulation of variations in atmospheric carbon dioxide using a coupled-biosphere-atmospheric model. *J. Geophys. Res.*, **109**, D18117.
- Pielke, R.A., 1974: A three-dimensional numerical model of the sea breezes over south Florida. *Mon. Wea. Rev.*, **102**, 115-139.
- Pielke, R.A., 1991: Overlooked scientific issues in assessing hypothesized greenhouse gas warming. *Environ. Software*, **6**, 100-107.
- Pielke, R.A., W.R. Cotton, R.L. Walko, C.J. Tremback, W.A. Lyons, L.D. Grasso, M.E. Nicholls, M.D. Moran, D.A. Wesley, T.J. Lee, and J.H. Copeland, 1992: A comprehensive meteorological modeling system RAMS. *Meteor. Atmos. Phys.*, **49**, 69-91.
- Rayment, R. and C.J. Readings, 1974: A case study of the structure and energetics of an inversion. *Quart. J. Roy. Meteor. Soc.*, **100**, 221-233.

- Saylor, B.J. and R.E. Breidenthal, 1998: Laboratory simulations of radiatively induced entrainment in stratiform clouds. *J. Geophys. Res.*, **103**, 8827-8837.
- Sellers, P.J., Y. Mintz, Y.C. Sud, and A. Dalcher, 1986: A simple biosphere model (SiB) for use within general circulation models. *J. Atmos. Sci.*, **43**, 505-531.
- Sellers, P.J., D.A. Randall, G.J. Collatz, J.A. Berry, C.B. Field, D.A. Dazlich, C. Zhang, G.D. Collelo, L. Bounoua, 1996: A revised land surface parameterization (SiB2) for atmospheric GCMs, Part 1: Model formulation. *J. Climate*, **9**, 676-705.
- Smagorinsky, J.S., 1963: General circulation experiments with the primitive equations. 1: The basic experiment. *Mon. Weather Rev.*, **91**, 99-164.
- Sullivan, P.P., C.-H. Moeng, B. Stevens, D.H. Lenschow, and S.D. Mayer, 1998: Structure of the entrainment zone capping the convective atmospheric boundary layer. *J. Atmos. Sci.*, **55**, 3042-3064.
- Stevens, D.E. and C.S. Bretherton, 1999: Effects of resolution on the simulation of stratocumulus entrainment. *Quart. J. Roy. Meteor. Soc.*, **125**, 425-439.
- Stull, R.B., 1976: The energetics of entrainment across a density interface. *J. Atmos. Sci.*, **33**, 1260-1267.
- Stull, R.B., 1988: *An introduction to boundary layer meteorology*. Kluwer Academic Publishers, Norwell, MA. 666 pp.
- Tripoli, G.J. and W.R. Cotton, 1982: The Colorado State University three-dimensional cloud/mesoscale model – 1982. Part I: General theoretical framework and sensitivity experiments. *J. de Rech. Atmos.*, **16**, 185-220.
- Walko, R.L., C.J. Tremback, J. Panetta, S. Freitas, and A.L. Fazenda, 2002: RAMS Regional Atmospheric Modeling System version 5.0 model input namelist parameters. 8 Dec 2006 <http://www.cptec.inpe.br/brams/input_namelist.shtml>
- Wang, J.-W., A.S. Denning, L. Lu, I.T. Baker, K.D. Corbin, and K.J. Davis, 2007: Observations and simulations of synoptic, regional, and local variations in atmospheric CO₂. *J. Geophys. Res.*, **112**, D04108.
- Willis, G.E. and J.W. Deardorff, 1974: A laboratory model of the unstable planetary boundary layer. *J. Atmos. Sci.*, **31**, 1297-1307.
- Yi, C., K.J. Davis, B.W. Berger, and P.S. Bakwin, 2001: Long-term observations of the dynamics of the continental planetary boundary layer. *J. Atmos. Sci.*, **58**, 1288-1299.

- Zhang, N., 2002: Observations and simulations of the planetary boundary layer at a tall tower in northern Wisconsin. Master's thesis, Colorado State University, Department of Atmospheric Science, Fort Collins, CO 80523, 71 pp.
- Zupanski, D., A.S. Denning, M. Uliasz, M. Zupanski, A.E. Schuh, P.J. Rayner, W. Peters, and K. Corbin, 2007: Carbon flux bias estimation employing Maximum Likelihood Ensemble Filter (MLEF). *J. Geophys. Res.*, **112**, D17107.
- Zupanski, M., 2005: Maximum likelihood ensemble filter: Theoretical aspects. *Mon. Weather Rev.*, **133**, 1710-1726.

Chapter 3

Real Case Study

Abstract

The depth of the planetary boundary layer (PBL) is important for carbon dioxide source/sink estimation because the response of atmospheric carbon dioxide concentration to a given amount of surface flux is inversely proportional to this depth. The PBL depth is affected by entrainment from overshooting thermals that is usually neglected in mesoscale meteorological models. An experiment using the Regional Atmospheric Modeling System (RAMS) was performed for the late summer of 1999 that includes a parameterization of entrainment that is based on a downward heat flux at the top of the PBL that is proportional to the heat flux at the surface. This parameterization produces a warmer, drier, and deeper boundary layer. Compared with observations, the monthly mean diurnal cycle of PBL depth at a location in northern Wisconsin is better simulated when this parameterization is included. The warmer and drier conditions of the boundary layer can cause the vegetation's stomata to close in an evolved response to limit water loss, thus reducing transpiration and shifting the Bowen ratio. The stomatal closing also reduces carbon assimilation, consequently altering horizontal and vertical carbon gradients. These changes in the PBL feed back into the free troposphere, modifying the large-scale weather.

3.1) Introduction

The response of carbon dioxide (CO_2) concentration to the surface fluxes of carbon is directly proportional to the depth of the planetary boundary layer (PBL) (Denning et al., 1995; Yi et al., 2001; 2004). However, vertical turbulent mixing and PBL depth are not often simulated correctly by models (Denning et al., 1995; 1996a; 2008; Gurney et al., 2003) and an error in the depth of the PBL relates directly to an error in the modeled concentration of CO_2 in the boundary layer (Denning et al., 1995; 1996b; 1999; 2008; Zhang, 2002; Gerbig et al., 2003). This introduces an error into estimates of carbon sources and sinks made by inversion studies. These studies compare simulated CO_2 concentrations to observations and then establish what combination of sources and sinks produced them (e.g. Gurney et al., 2002; Gerbig et al., 2003; Zupanski et al., 2007) thus determining a carbon budget that can be used to understand future climate change.

The PBL is a well-mixed layer in turbulent contact with the surface with weak gradients and is capped by a temperature inversion. The inversion contains large gradients in temperature, water vapor, and tracer concentrations. It varies in depth from about 100 meters to 3 kilometers depending on location and conditions (Stull, 1988). In order to resolve the PBL in models, high resolution is needed near the top, but a high concentration of model levels is excessive over the rest of the PBL. To complicate things further, since the depth of the PBL varies spatially and temporally, the level at which the added resolution is needed is also variable (Denning et al., 2008). The computational expense associated with including the number of model levels necessary to resolve the capping inversion for all of the different potential heights of the PBL is prohibitive.

Growth and development of the PBL are controlled by small-scale processes that are not resolved by mesoscale models (Ayotte et al., 1996; Gerbig et al., 2003). Entrainment at the top of the boundary layer is a result of rising thermals from the PBL overshooting their neutral level and pulling free tropospheric air into the PBL on their subsequent descent (Stull, 1988). Entrainment is a small-scale process that is generally not resolved by mesoscale models because its resolution requires a grid interval on the order of tens to hundreds of meters (Stull, 1988; Pielke, 1991).

An entrainment parameterization was introduced to the coupled ecosystem-atmosphere model SiB-RAMS (Denning et al., 2003; Nicholls et al., 2004; Wang et al., 2007; Corbin et al., 2008). The parameterization is based on the assumption that the downward heat flux at the top of the PBL is proportional to the heat flux at the surface (e.g. Betts, 1973; Carson, 1973; Deardorff, 1974; Rayment and Readings, 1974; Willis and Deardorff, 1974; Stull, 1976; Davis et al., 1997; Sullivan et al., 1998; Yi et al., 2001). It has been shown in idealized simulations that the introduction of this parameterization results in a warmer, drier, and deeper PBL with a higher daytime concentration of CO₂ (McGrath-Spangler et al., submitted to ACPD). The deeper PBL is a result of downward heat transport into the PBL and upward transport of turbulent kinetic energy (TKE), making the lowest part of the overlying inversion turbulent and thus a part of the boundary layer. The PBL depth, potential temperature, and CO₂ concentration increase nearly linearly with the proportionality constant of the parameterization while water vapor mixing ratio decreases. The higher concentration of CO₂ is a result of the dilution of photosynthetic uptake from a deeper PBL and, to a lesser degree, reduced carbon

assimilation resulting from stomatal closing as a response to the drier atmospheric conditions.

The primary objective of this study is to evaluate the performance of this parameterization in a real case. The WLEF very tall tower in northern Wisconsin is the principal location for evaluation because observations of the PBL height were made there in 1999 (Yi et al., 2001; 2004; Denning et al., 2008). The months of July, August, and September of that year have observations at nearly an hourly timescale and provide a good timeframe for comparison. In addition, micrometeorological and CO₂ concentration measurements are made at several levels along the tower height providing a vertical profile (Davis et al., 2003). Comparisons between the model and observations will also be made at several other tower locations in the continental United States.

Section 2 describes the SiB-RAMS model and the entrainment parameterization in more detail. Section 3 discusses the observations and how they are made. Section 4 is an overview of the monthly climate. Section 5 illustrates the results and the final section provides some conclusions.

3.2) Methods

3.2.1) Model description

The ecosystem model in the coupled SiB-RAMS model is the third version of the Simple Biosphere (SiB3) model developed by Sellers et al. (1986). SiB3 calculates the transfer of energy, mass, and momentum between the atmosphere and land surface (Sellers et al., 1996a,b; Corbin et al., 2008) and is coupled to the Brazilian version of the Regional Atmospheric Modeling System (BRAMS) (Freitas et al., 2006). Denning et al. (2003), Nicholls et al. (2004), and Wang et al. (2007) describe the coupled model in more

detail. The Mellor and Yamada (1982) scheme was used for vertical diffusion, the Smagorinsky (1963) scheme for horizontal diffusion, and the two-stream radiation scheme developed by Harrington (1997) for radiative transfer. The Klemp and Wilhelmson (1978) radiation condition was used at the lateral boundaries.

The simulations presented here were performed on a single grid centered on the WLEF tower in northern Wisconsin. The grid used a grid increment of 40 km and spanned the continental United States and southern Canada. The Grell convective cumulus scheme (Grell, 1993; Grell and Devenyi, 2002) was used to parameterize convection.

3.2.2) Model input

Several data sets were used as input to the model. Vegetation data was derived from the 1-km AVHRR land cover classification data set (Hansen et al., 2000). Biome classes were converted to the corresponding SiB classes for compatibility. The original soil data comes from a 5'x5' resolution map containing percents of sand, clay, and silt generated by the SoilData System developed by the Global SoilData Task Group of the International Geosphere-Biosphere Programme (IGBP) Data Information System. The data were converted to SiB classes using a triangulation program. Normalized Difference Vegetation Index (NDVI) data were derived from 1-km resolution SPOT 10-day composites from the VEGETATION instrument on board the SPOT-4 (Système Probatoire d'Observation de la Terre) polar orbiting satellite. The NDVI data were provided by the United States Department of Agriculture Foreign Agriculture Service (USDA/FAS) through collaboration with the Global Inventory Modeling and Mapping Studies (GIMMS) Group at the National Aeronautics and Space Administration Goddard

Space Flight Center (NASA/GSFC). Surface fluxes of carbon from anthropogenic sources are derived from 1995 CO₂ emission estimates from Andres et al. (1998) with a scale of 1.1055 to adjust for 1999 (Marland et al., 2005; Wang et al., 2007). Air-sea CO₂ fluxes are the monthly 1995 estimates from Takahashi et al. (2002) and are assumed to adequately represent the conditions present in 1999.

Meteorological fields are initialized by the National Center for Environmental Prediction (NCEP) mesoscale Eta-212 grid reanalysis with 40-km horizontal resolution (AWIPS 40-k). This data set was also used to nudge the lateral boundary conditions every 30 minutes. Soil respiration factors and soil moisture were initialized from an offline SiB3 simulation run for 10 years using NCEP/NCAR (National Center for Atmospheric Research) reanalysis driver data from 1989 to 1999. Initial CO₂ concentrations were specified by the Parameterized Chemistry Transport Model (PCTM) (Kawa et al., 2004).

PCTM consists of a semi-Lagrangian scheme developed by Lin and Rood (1996). Subgrid scale transport processes such as convection and boundary layer diffusion are included for transporting tracer gases like CO₂. PCTM was driven by weather data derived from Goddard's finite volume General Circulation Model (fvGCM) and spun up for 3 years. The simulation was at 2.5° longitude by 2° latitude horizontal resolution with 25 vertical levels and a timestep of 1 hour. Land surface fluxes are from offline SiB3 (spun up for 15 years) on a 1° x 1° Cartesian grid (Baker et al., 2007) and ocean fluxes from Takahashi et al. (2002). PCTM was also used to nudge CO₂ concentrations on the lateral boundaries on an hourly timescale.

3.2.3) *Entrainment parameterization*

The entrainment parameterization was discussed in an idealized case by McGrath-Spangler et al. (submitted to ACPD) and is based on the idea that the heat flux at the top of the PBL is negatively proportional to the heat flux at the surface (Stull, 1988). This assumption produces the equation:

$$\overline{w'\theta'}|_{z_i} = -\alpha \overline{w'\theta'}|_s. \quad (1)$$

In (1), $\overline{w'\theta'}$ is the turbulent heat flux at the top of the PBL (z_i) and at the surface (s) and α is the tunable proportionality constant. Estimates of α range from zero to one, but most published values are between 0.1 and 0.3 (e.g. Stull, 1988). A value of 0.2 is the most appropriate for free convection (Stull, 1988).

Equation (1) can be used to derive equations for the time rate of change of potential temperature, wind velocity, water vapor mixing ratio, turbulent kinetic energy (TKE), and CO₂ concentration across the interface separating the PBL from the overlying inversion in SiB-RAMS. These equations mix the properties of the boundary layer with those of the free troposphere as would be done by overshooting thermals in the physical world. The result is warmer, drier, less turbulent conditions being mixed into the top model layer of the PBL to be mixed downward by turbulent eddies and cooler, moister, turbulent air being mixed up into the lowest layer of the overlying inversion.

In idealized simulations, the parameterization resulted in an insertion of heat energy into the PBL and an upward transport of TKE into the lowest layer of the overlying inversion. Both processes produced a deeper PBL. The downward advection of heat and upward moisture transport induced a warmer and drier boundary layer and a cooler and moister inversion layer. The effects of temperature and water vapor change

opposed each other in terms of their effect on the air density of the two layers. Examining the virtual potential temperature, which relates moisture and temperature, reveals that the temperature advection dominates, making it easier for the PBL to grow further through heating at the surface and through PBL top entrainment.

The drying caused by the additional entrainment increases physiological stress thereby limiting carbon assimilation by plants. The guard cells along the sides of a leaf's stomata control the size of these openings. When conditions within the atmosphere in the immediate vicinity of the leaf become less than optimal, the guard cells close the stomata, limiting water loss and reducing carbon assimilation. This increases the Bowen ratio as latent heat flux is reduced in favor of sensible heat flux. The temperature change associated with increased sensible heat flux encourages further growth of the PBL and modifications to both the PBL and the overlying atmosphere through multiple processes including adjusted cloud cover and precipitation resulting from the altered humidity and Bowen ratio.

As the tunable parameter, α , increases, the water vapor mixing ratio within the PBL decreases at a significant rate. At the same time, potential temperature, PBL depth, and daytime CO₂ concentration increase nearly linearly. With a regression coefficient of 14.6, CO₂ concentration increases by 5 ppmv as α increases from zero, no entrainment, to 0.2, the generally accepted value for convective conditions (Stull, 1988).

3.3) Observations

The primary evaluation of the entrainment parameterization will use observations from the WLEF television tower located in the Park Falls Ranger District of the Chequamegon National Forest, about 15 km east of Park Falls, Wisconsin, USA at

45.95°N latitude, 90.27°W longitude. The tower is in a region of low relief with a typical elevation change of about 20 m with undulations in terrain over a few hundred meters (Davis et al., 2003). The heterogeneous landscape of saturated and unsaturated soils has a maximum canopy height of about 25 meters with sugar maple (*Acer saccharum*), balsam fir (*Abies balsamea*), cedar (*Cedrus*), black spruce (*Picea mariana*), and many other tree species (Davis et al., 2003).

Since 1996, micrometeorological and eddy covariance flux measurements have been made at 30 m, 122 m, and 396 m (Berger et al., 2001; Davis et al., 2003). High precision, high accuracy CO₂ concentrations have been made at six levels (11 m, 30 m, 76 m, 122 m, 244 m, and 396 m) since 1994. The CO₂ measurements are made using LI-COR 6251 infrared gas analyzers (IRGA) (Bakwin et al., 2001; Davis et al. 2003; Denning et al., 2008).

During 1998 and 1999, from March to November, an NCAR Integrated Sounding System (ISS) was deployed about 8 km east of the WLEF tower (Yi et al., 2001; 2004; Denning et al., 2008). The ISS included a radar profiler, a Radar and Radio-Acoustic Sounding System (RASS), and a radiosonde (Yi et al., 2001). The profiler is a sensitive 915 MHz Doppler radar designed to respond to fluctuations of the refractive index in clear air (Ecklund et al., 1988; White et al., 1991; Angevine et al., 1993; 1994a,c; Yi et al., 2001) and can be used to detect the height of the PBL. The PBL top can be measured with a time resolution of 30 minutes or less, a vertical sampling of 60-100m, a minimum height of 150 m, and a maximum height of 1500 – 3000 m, depending on conditions (Angevine et al., 1994c; Yi et al., 2001). The RASS is an attachment to the profiler that

can measure temperature profiles up to a height of 800 m above ground level (Angevine et al., 1994b; Yi et al., 2001).

The PBL depth can be derived from the signal-to-noise ratio (SNR) recorded by the profiler (Angevine et al., 1994c; Yi et al., 2001) using the method described by White et al. (1991), Angevine et al. (1994c), and Yi et al. (2001). Unfortunately, PBL height cannot be estimated from the profiler under precipitating or heavy cloud conditions because it is very sensitive to the large drop size (Yi et al., 2001; 2004; Denning et al., 2008).

Boundary layers shallower than 400 m, such as those that occur at night and in the early morning, are not well defined from the profiler SNR measurements (Yi et al., 2001; 2004; Denning et al., 2008). In these cases, the strong stratification present in the nocturnal boundary layer produces a gradient in the CO₂ concentration (Yi et al., 2001; 2004; Denning et al., 2008). The vertical profile of CO₂ measured along the depth of the tower can be used to determine the depth of the nocturnal boundary layer.

During the early morning (net radiation positive), the top of the PBL is defined as the depth above ground to which the CO₂ measurements from the tower is nearly constant, indicating the growing PBL (Yi et al., 2001; 2004). At night, the top of the stable boundary layer is the level at which there is no longer a strong gradient in CO₂ (Yi et al., 2001; 2004; Denning et al., 2008). The heights of the stable layer were assumed to be the midpoints between the observing levels (Yi et al., 2001; 2004; Denning et al., 2008).

Measurements from four AmeriFlux towers (Baldocchi et al., 2001) will be used for further evaluation of the PBL top entrainment. The tower located within the Morgan-

Monroe State Forest (MMO) is a 46 m meteorological tower in south-central Indiana, USA. The surrounding deciduous forest has a mean canopy height of approximately 25 – 27 m (Schmid et al., 2000). The University of Michigan Biological Station (UMI) has a 46 m tower located in a mixed hardwood forest in northern Lower Michigan. The surrounding canopy has a height of about 22 m. A third tower in Maine’s Howland Forest (HWD) is 29 m tall with a surrounding canopy height of roughly 20 m. Howland Forest is primarily red spruce (*Picea rubens*) and eastern hemlock (*Tsuga canadensis*) (Hollinger et al., 2004). The tower in Harvard Forest (HVD) in Massachusetts is 30 m tall with an average canopy height of 24 m (Wofsy et al., 1993). The northern hardwood forest is dominated by northern red oak (*Quercus rubra*) (Barford et al., 2001) over moderately hilly terrain (Wofsy et al., 1993). These towers measure such variables as CO₂ concentration, air temperature, relative humidity, wind velocity, and sensible and latent heat fluxes.

3.4) Monthly Climate Overview

3.4.1) July 1999

The month of July experienced two distinct synoptic phases. The first half of the month was dominated by progressive mid-latitude waves moving from west to east while the second half experienced a trough in the west and a stagnant ridge in the east. The latter pattern produced cooler than normal temperatures from the central Rockies westward and warmer than normal from the central Plains to the Atlantic coast. The average national temperature was above the long-term mean, ranking July 1999 as the 25th warmest July on record since 1895, as of summer 2007.

The precipitation averaged across the United States ranked well below the long-term mean due to a drought in the Northeast and the eastern half of the country. Drier conditions were also present in portions of the Northwest. However, the West, Southwest, and the western Great Lakes states, particularly Wisconsin and Michigan, experienced wetter than normal conditions. The nationally warm and dry conditions continued into August (NOAA/NCDC).

3.4.2) August 1999

The synoptic pattern in August consisted of an upper-level trough off the California coast and a ridge covering much of the rest of the country. On several occasions, a trough developed near the Great Lakes region. This pattern produced cooler than normal conditions for California and the Great Lakes region and warmer to much warmer than normal conditions for the Northwest, northern Rockies, South, and Southeast. National U.S. temperatures were above the long-term mean, ranking as the 25th warmest August in the 113 year record.

Precipitation in the United States was well below average with drought conditions in the eastern half of the U.S. and severe to extreme drought over huge areas of the eastern and southern parts of the country. Widespread dryness occurred in the southern Great Plains to the Great Lakes and eastward to the coast. The drought conditions contributed to August 1999 being ranked the 24th driest August, although the northern Plains to the southern Rockies were wetter than normal (NOAA/NCDC).

3.4.3) September 1999

The September climate was dominated by high-pressure systems over eastern Canada and the Northeastern U.S. and over the Pacific coast. Several cold fronts and

low-pressure areas developed from the northern Plains to central Rockies. The two big events were hurricanes Dennis and Floyd that moved along the east coast. The weather pattern produced well above normal temperatures in the Northeast and warm temperatures along the Pacific coast. Cooler temperatures were present from the northern and central Plains from the Rockies to the Mississippi River and southward to northern Texas.

Hurricanes Dennis and Floyd produced record rainfall along the eastern U.S. and the cold fronts and low-pressure areas brought rain to the northern Plains and the central Rockies. Drier than normal conditions existed from the Pacific coast south and eastward to the mid and lower Mississippi valley. Drought conditions continued from the Ohio valley to the southeast and southern Plains.

3.5) Results

3.5.1) WLEF results

Figure 3.1 compares the observed monthly mean diurnal cycle of PBL depth measured near the WLEF tower in northern Wisconsin to the SiB-RAMS model for both the control ($\alpha = 0$) and entraining cases ($\alpha = 0.2$). The observed PBL depths are found as described above in section 3 and then averaged from available observations by time of day. The error bars represent the standard deviation of daily values at each hour. The model daytime PBL depths are determined by finding the lowest layer through which the potential temperature increased by 0.6 K and then finding the middle of that layer. When the heat flux is less than zero, indicating nighttime conditions, the PBL depth is assumed to be the middle of the layer through which the vertical gradient in CO₂ concentration is less than 1.5 ppmv. This is similar to the way that the observed nocturnal boundary layer

is found. The monthly mean diurnal cycle was found by averaging non-precipitating hours.

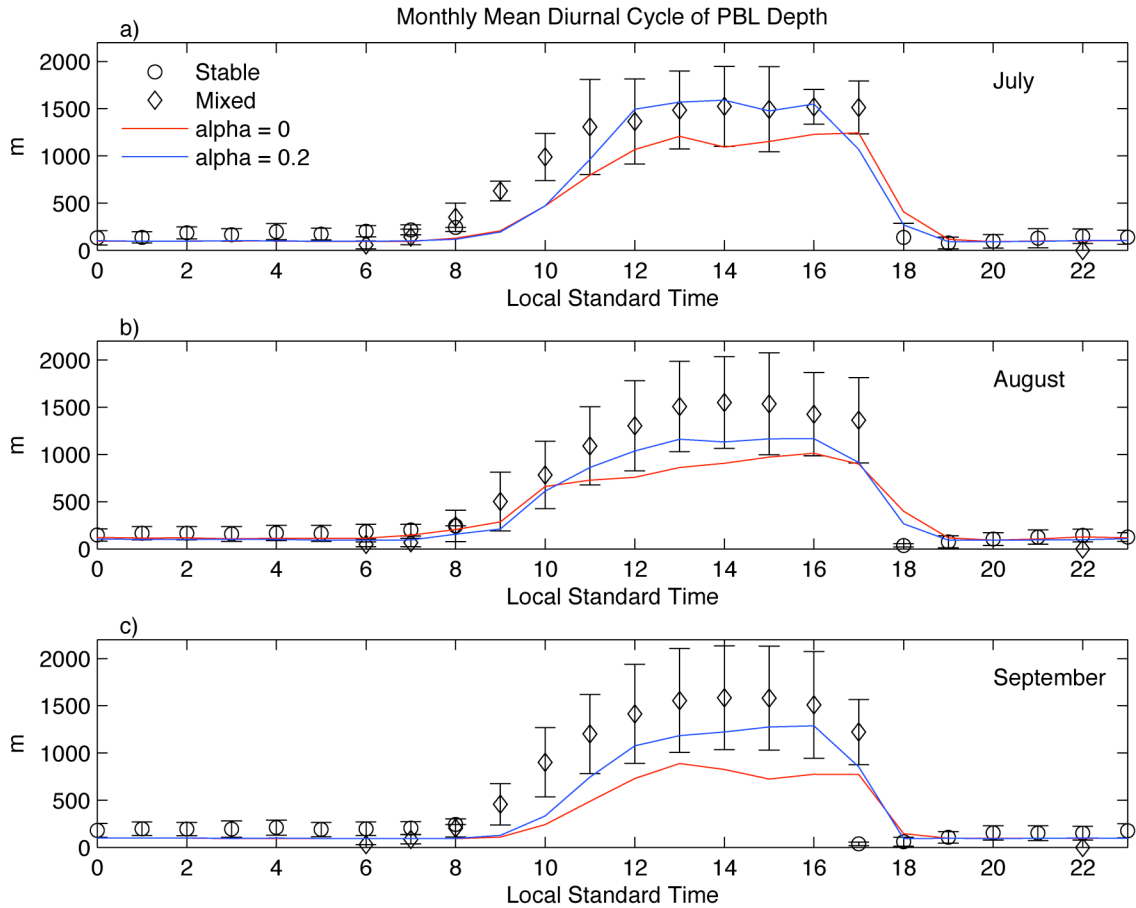


Figure 3.1 Monthly mean diurnal cycle of PBL depth (m) in (a) July, (b) August, and (c) September. Model estimates are averaged over non-precipitating hours only. Error bars are the standard deviation of daily values at each hour.

In July, from 10 a.m. local until 4 p.m., the entrained case was closer to the observations. Although the control case was within the standard deviation of the observations, the entraining case was much closer to the actual mean of the observations. In August, the control case was not within the standard deviation during the early afternoon and was about 500 m too shallow. The PBL in the entraining case, while still low, was deeper than the control PBL and was within the variability of the observations. The entraining case also had much steeper PBL growth during the late morning, better

coinciding with what was observed. In September, the situation was similar. The control case was too low when compared to the observations, starting around 8 in the morning and continuing throughout the day until about 6 p.m. The entraining case was again too low, but did fall within the standard deviation throughout the afternoon and provided a more realistic simulation of the midday PBL.

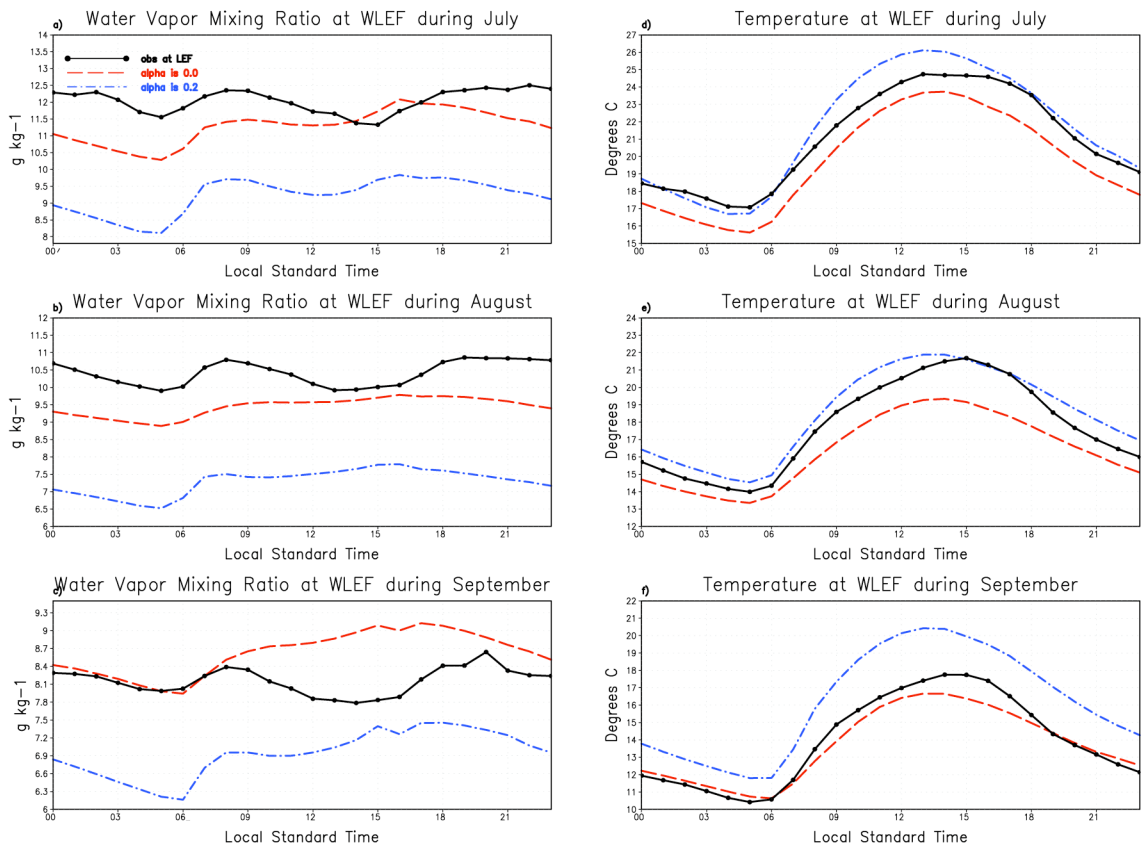


Figure 3.2 Monthly mean diurnal cycle at WLEF of water vapor mixing ratio (g kg^{-1}) during (a) July, (b) August, and (c) September and of temperature (K) during (d) July, (e) August, and (f) September at 30 m.

Differing PBL depths have large implications for CO_2 concentrations and gradients within the boundary layer. Deeper PBL depths dilute the assimilation of carbon and the warming and drying associated with entrainment alters the ability of the model vegetation to uptake carbon. Accurately simulating CO_2 concentration is important for

determining sources and sinks through atmospheric inversions and thus it is important to accurately simulate the PBL depth. Figure 3.1 shows that an entrainment parameterization can produce better estimates of PBL depth.

Figure 3.2 shows the differences in water vapor mixing ratio and temperature in July (a, d), August (b, e), and September (c, f) produced by the two model simulations compared to the observations. Water vapor was better simulated in the control run for all 3 months. The control water vapor mixing ratio was too moist only in the late morning and afternoon in September. During the mid-afternoon of September, the entraining case, while still too dry, had a smaller error than the control run. In general, at WLEF, the drying associated with the additional entrainment was not necessary and produced too dry of conditions. Compared to the observations, the September monthly mean diurnal cycle of temperature in the entraining case was too warm. During this month, the control case's temperature was similar to that observed. However, the simulated temperature was improved in July and August at the tower when entrainment was included. Overshooting thermals produced warmer and drier conditions, although with mixed results when compared to the observations.

Figure 3.3 presents the modifications of additional entrainment on net ecosystem exchange (NEE) (a-c) and CO₂ concentration (d-f) at 30 m at the WLEF tower during the summer of 1999. Too much uptake occurred in the morning and late afternoon of both cases, a common problem in SiB (Baker et al., 2003). The entraining case was warmer in the early morning, allowing plant stomata to open earlier and begin carbon assimilation. The warmer and drier conditions at midday forced the stomata to become smaller in the entraining case, reducing carbon uptake in order to minimize water loss. In August, the

control case produced a better estimate of NEE, but in July and September, the additional entrainment produced better results. These changes produced only small differences in the CO₂ concentration.

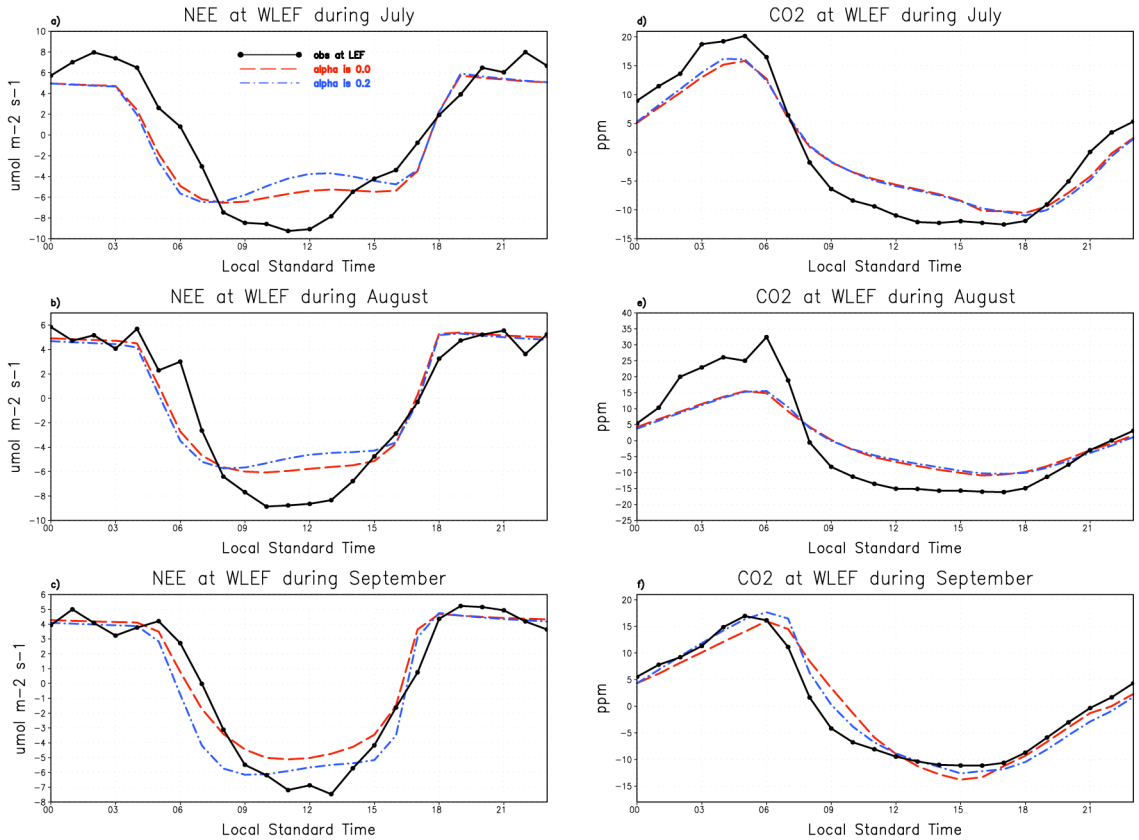


Figure 3.3 Monthly mean diurnal cycle at WLEF of net ecosystem exchange ($\mu\text{mol m}^{-2} \text{s}^{-1}$) during (a) July, (b) August, and (c) September and of CO₂ concentration perturbations (ppmv) during (d) July, (e) August, and (f) September at 30 m.

Figure 3.4 illustrates the differences in sensible (a-c) and latent (d-f) heat fluxes. The variations in the heat fluxes between the control and entraining cases illustrate the interactions between the PBL, the physiological responses, and the large-scale weather. As gradients in temperature and water vapor mixing ratio increase between the canopy air space (CAS) and the PBL, the sensible and latent heat fluxes increase respectively. The warming and drying of the atmosphere can close or open plant stomata in an evolved response to limit water loss. Closing the stomata limits transpiration, thus shifting the

Bowen ratio in favor of sensible heat flux. The decreased latent heat flux reduces PBL water vapor mixing ratio while the increased sensible heat flux increases PBL temperature. In addition, closing the stomata reduces carbon assimilation, increasing NEE and the CO₂ concentration. Cloud cover and thunderstorm evolution are tied to PBL temperature and moisture (Stull, 1988) and so the large-scale weather is also modified. Reduced cloud cover, associated with a drier PBL, allows more solar radiation to reach the ground, increasing the surface energy budget and amending sensible and latent heat fluxes. As the surface heat budget changes, so also does the entrainment heat flux at the top of the PBL through the proportionality between them. All of these processes are interconnected and produce feedbacks.

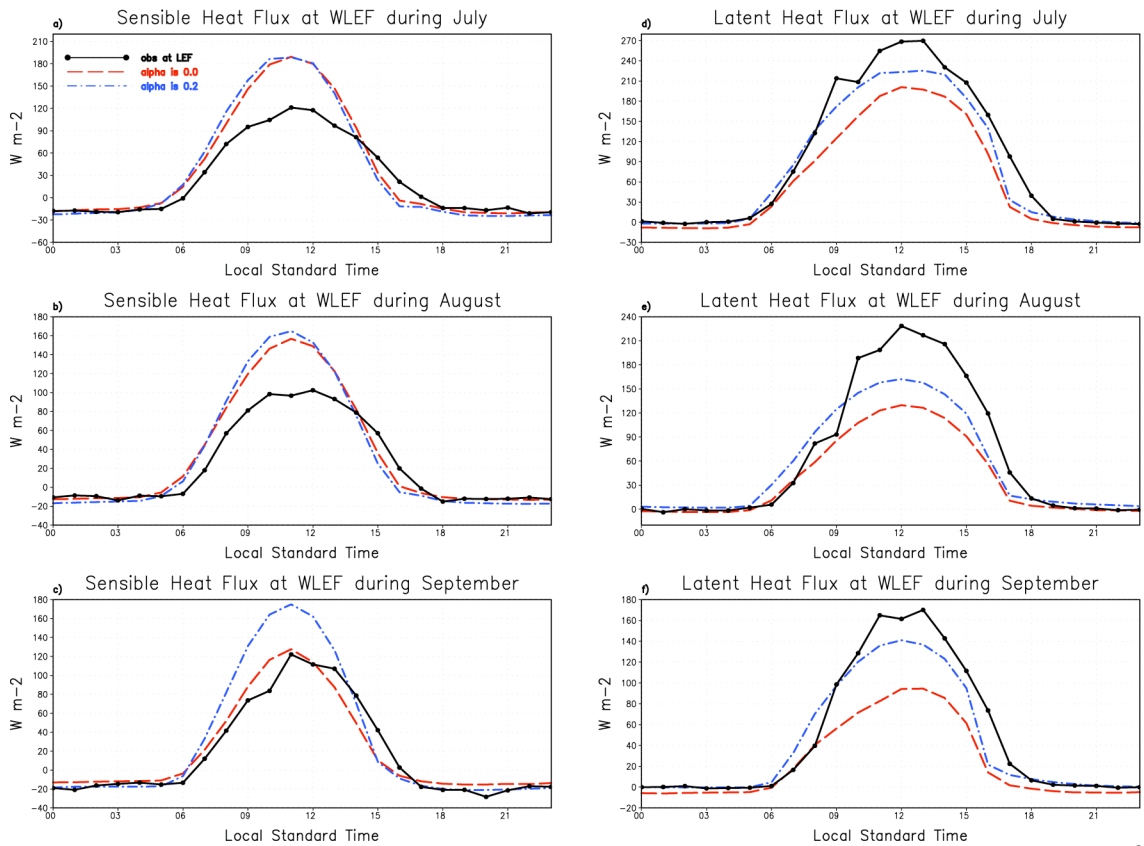


Figure 3.4 Monthly mean diurnal cycle at WLEF of sensible heat flux (W m^{-2}) during (a) July, (b) August, and (c) September and of latent heat flux (W m^{-2}) during (d) July, (e) August, and (f) September at 30 m.

The sensible heat flux of the control case was similar to that observed in September and too great in July and August. The additional entrainment produced larger sensible heat fluxes and so was less similar to the observations. However, entrainment from overshooting thermals improved estimates of latent heat flux during all three months considered. The latent heat flux of the control case was too little and the additional entrainment increased this flux.

3.5.2) Tower results

Since the sensible and latent heat fluxes indicate many of the variations associated with entrainment from overshooting thermals, comparisons of these two variables are provided across several different towers.

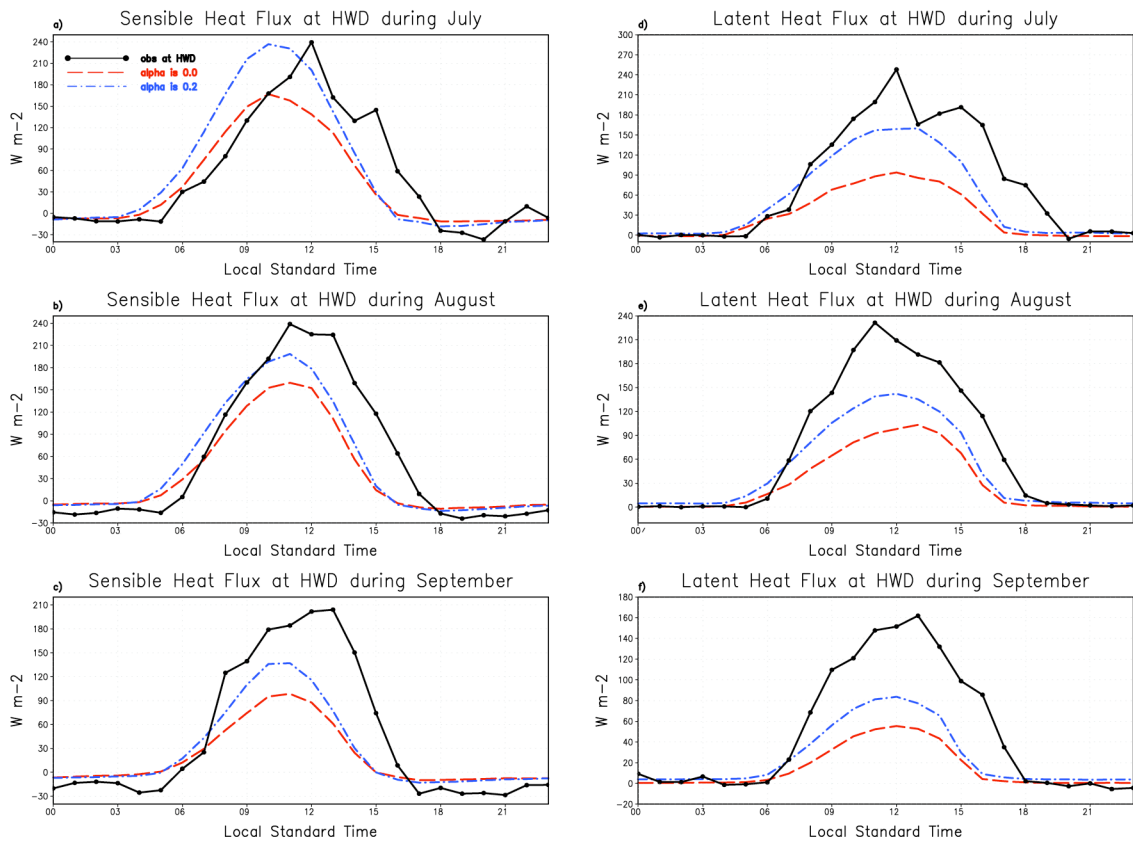


Figure 3.5 Monthly mean diurnal cycle at Howland Forest of sensible heat flux ($W m^{-2}$) during (a) July, (b) August, and (c) September and of latent heat flux ($W m^{-2}$) during (d) July, (e) August, and (f) September.

Comparisons of monthly mean diurnal cycles of sensible and latent heat fluxes at Howland forest to model simulations are made in Figure 3.5. The average of both sensible and latent heat fluxes during each month are better simulated by the entraining case. Entrainment produced slightly too much sensible heat flux in July, but it was closer to the observed flux than the control case. The entraining case produced too little sensible heat flux in August and September, but it was larger than the control case. The latent heat flux was too low during all three months in the control case. Entrainment increased the latent heat flux to better match the observations, but was still too low as well.

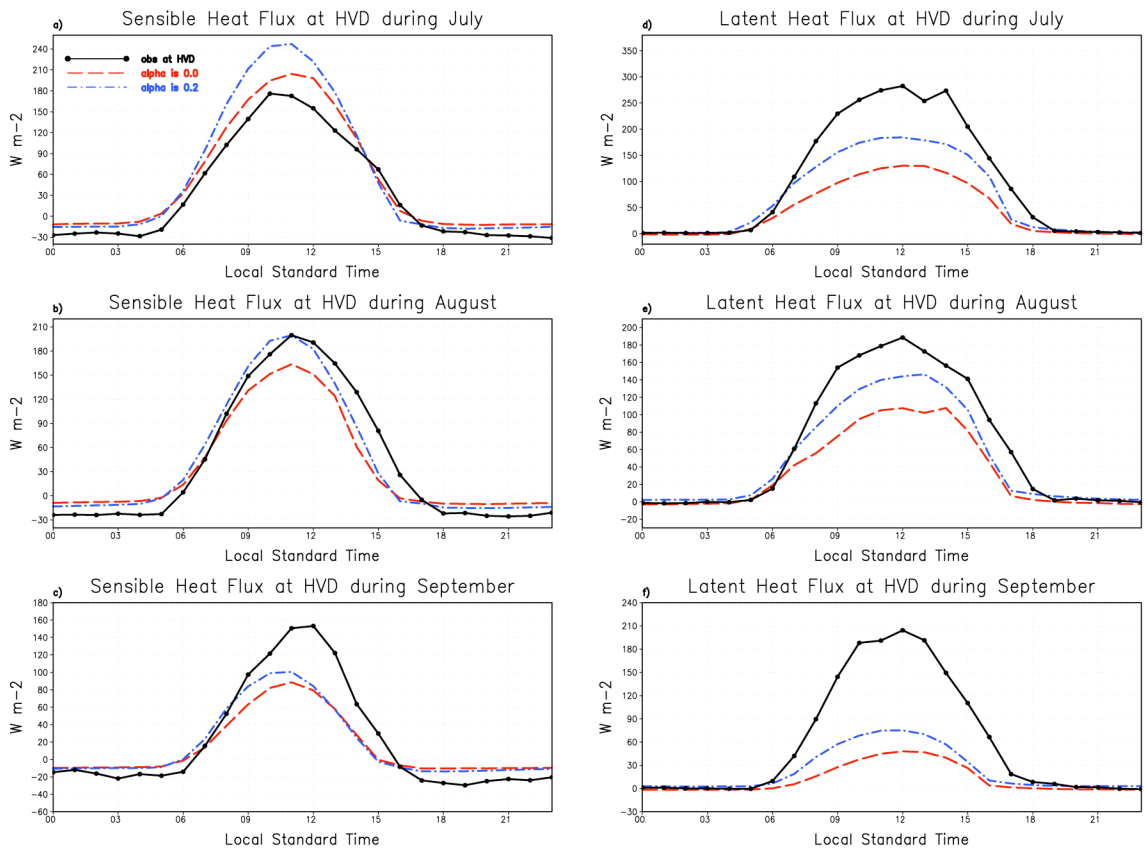


Figure 3.6 Monthly mean diurnal cycle at Harvard Forest of sensible heat flux ($W m^{-2}$) during (a) July, (b) August, and (c) September and of latent heat flux ($W m^{-2}$) during (d) July, (e) August, and (f) September.

The sensible and latent heat fluxes at Harvard Forest are shown in Figure 3.6. In July, the control sensible heat flux was too large and the additional entrainment produced an even larger flux. In August and September, the control case's sensible heat flux was too small and the entrainment produced a better representation. In August, the maximum sensible heat flux in the entraining case was similar to that observed. In September, the entraining case's sensible heat flux was still too low and could benefit from increased entrainment. The latent heat flux was too low in both the control and entraining cases for all three months. Although the additional entrainment improves the result, increased PBL top entrainment might produce a better result.

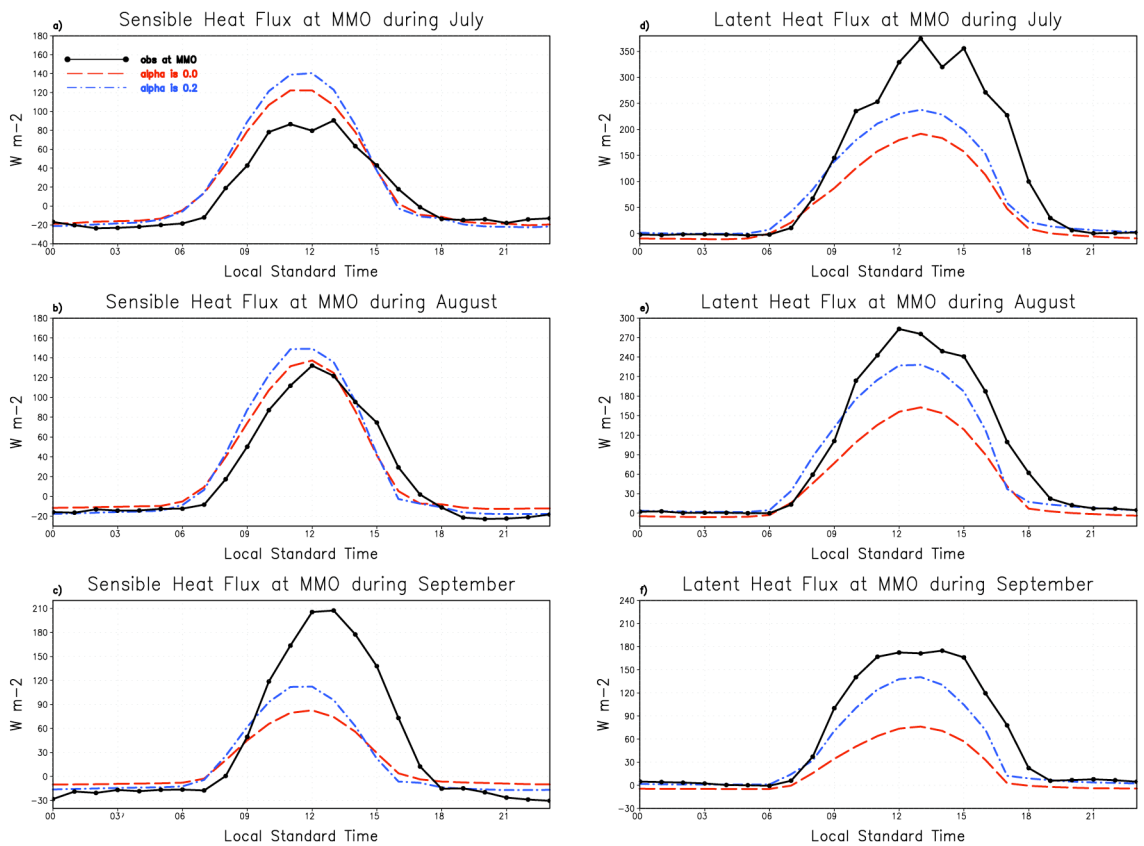


Figure 3.7 Monthly mean diurnal cycle at Morgan-Monroe of sensible heat flux ($W m^{-2}$) during (a) July, (b) August, and (c) September and of latent heat flux ($W m^{-2}$) during (d) July, (e) August, and (f) September.

Figure 3.7 compares monthly mean diurnal cycle of sensible and latent heat fluxes at Morgan-Monroe. In July and August, the sensible heat flux was too large in the control case. Adding entrainment increased the simulated sensible heat flux, producing a result less similar to the observations. In September, the sensible heat flux was over 100 W m^{-2} too low in the control case and entrainment helped improve the model estimate. Latent heat flux was consistently too low (by 100 W m^{-2} or greater) in the control case for all three months. Although the entraining case was also too low, it better represented the maximum flux present in the observations.

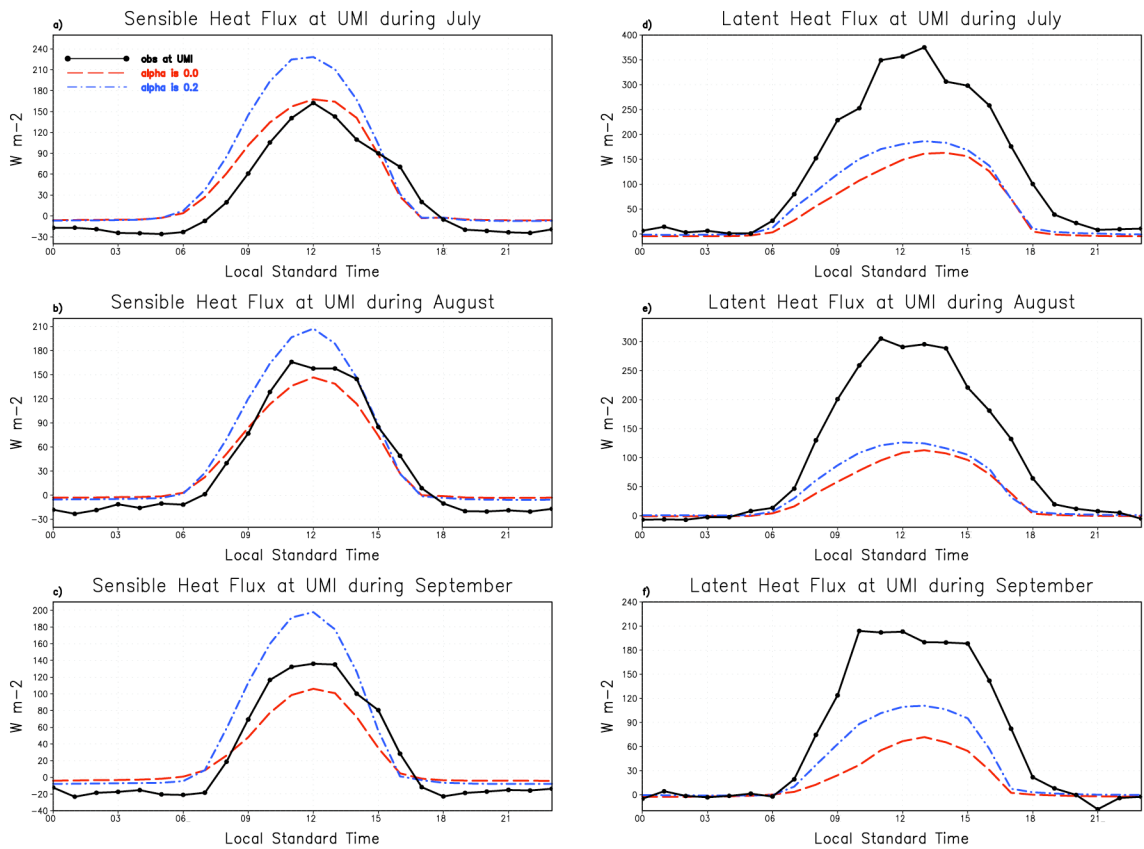


Figure 3.8 Monthly mean diurnal cycle at University of Michigan Biological Station of sensible heat flux (W m^{-2}) during (a) July, (b) August, and (c) September and of latent heat flux (W m^{-2}) during (d) July, (e) August, and (f) September.

At the University of Michigan Biological Station site (Figure 3.8), the results are similar to those at WLEF. The sensible heat flux became worse in the entraining case

while the model representations of latent heat flux were improved by the additional entrainment. In July, the control sensible heat flux was similar to that observed while it was a little low in August and September. PBL top entrainment with a proportionality constant of 0.2 degraded the results. However, the latent heat flux results indicate that a higher proportionality constant could produce better results since the control and entraining latent heat fluxes were too low during all three months.

Variations in the results across different towers indicate some of the diversity amongst the towers. Observations at the towers are representative of the different vegetation types, latitudes, and the weather experienced at each site. These findings indicate a need to use different proportionality constants dependent upon land surface type and time of year in order to minimize model error. A single value of α is not adequate to capture all the variation present in a regional model.

3.5.3) *National results*

Comparisons to observations at specific locations are instructive in explaining the range of different responses between the entraining and control cases. This section takes a broader approach and discusses the effects of overshooting thermals across the domain.

Figure 3.9 is a map of the differences in PBL depth between the entraining and control cases. This and the following figures show the time mean effects of entrainment from overshooting thermals averaged over the months of July, August, and September. When entrainment was included, the average PBL was 66.8 m deeper for an increase in depth of about 10.8%. The largest increases of around 300 to 400 m occurred over the dry Rocky Mountain region where the Bowen ratio was largest. Entrainment is proportional to the surface heat flux where

$$H = Q_H + \frac{0.61c_p\theta Q_E}{L}. \quad (2)$$

H represents the total heat flux, Q_H the sensible heat flux, Q_E the latent heat flux, c_p the specific heat at constant pressure, and L the latent heat of vaporization. Therefore, for a given amount of radiation, the larger the Bowen ratio (Q_H large compared to Q_E) the larger the heat flux and by extension the entrainment flux and the influence on the PBL depth. Locations where there is a lot of moisture, such as over the Southeast with the Gulf of Mexico as a nearby source, have a larger proportion of the energy budget contributing to latent heat flux and had a smaller difference in PBL depth between the entraining and control cases.

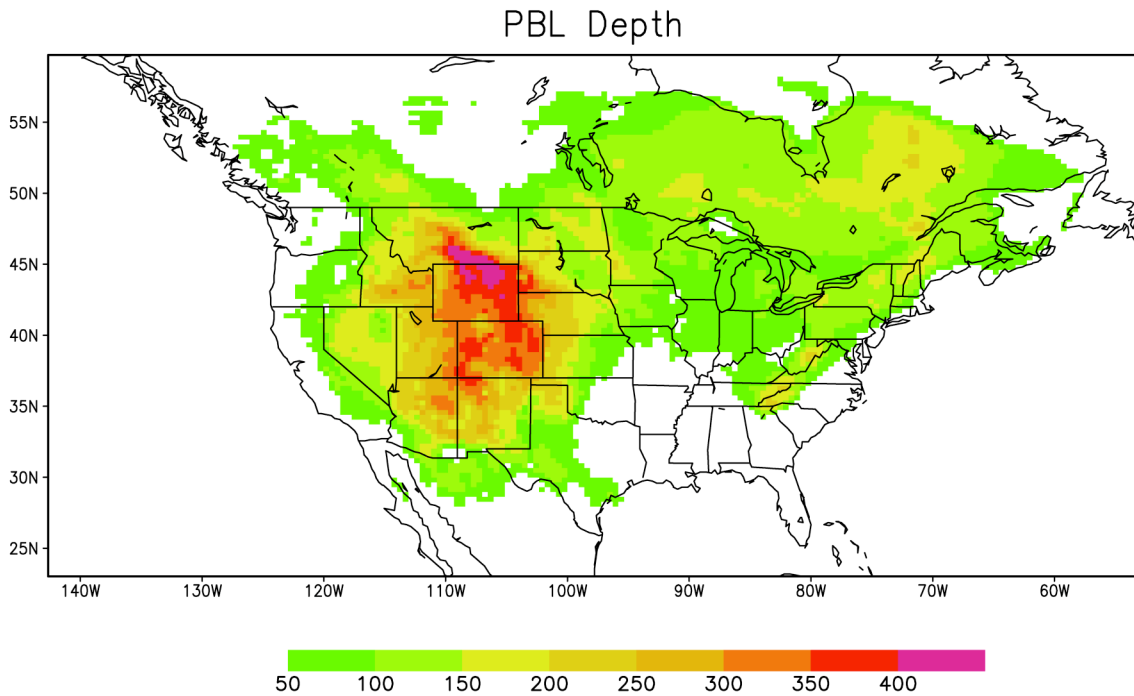


Figure 3.9 Effect of entrainment from overshooting thermals (entraining case minus control case) on PBL depth (m) in the time mean from July through September.

Figure 3.10a shows a map of the difference in water vapor mixing ratio between the two cases. There was a decrease in the mixing ratio everywhere in the domain for an average decrease of over 18% (1.5 g kg^{-1}). The largest decrease was just downstream of

the Rocky Mountains from North Dakota south into northern Texas. This region is also just downstream of the greatest change in PBL depth where the entrainment had its greatest impact. When the air left the region of greatest impact, it characterized the accumulated effect of the strongest entrainment across the Rocky Mountains. Large decreases in mixing ratio were also present in the Midwest from Illinois into Ohio and Michigan and along the Mexican border with Arizona and New Mexico. Smaller decreases were present in central Colorado and the Carolinas.

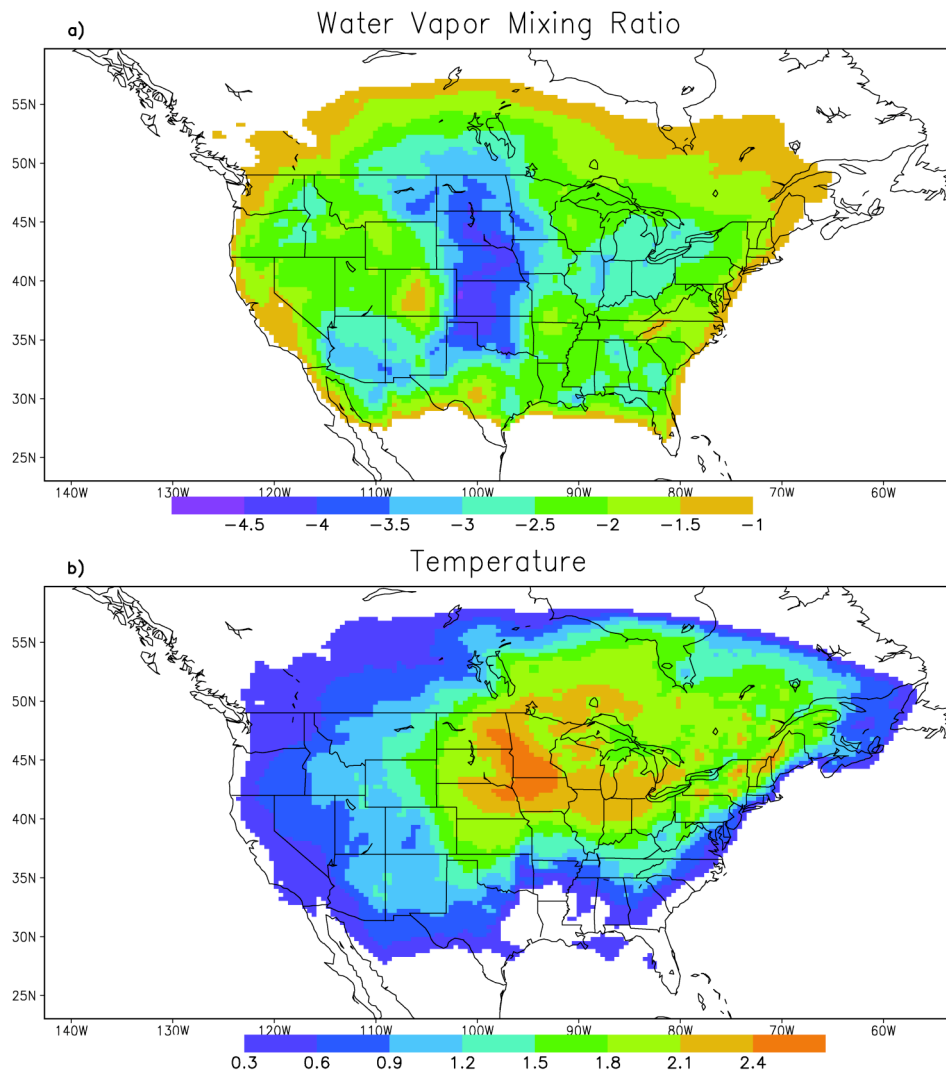


Figure 3.10 Effect of entrainment from overshooting thermals (entraining case minus control case) on (a) water vapor mixing ratio (g kg^{-1}) and (b) temperature (K) at 30 m in the time mean from July through September.

Figure 3.10b shows the map of average change in temperature due to entrainment. Temperature increased everywhere with an average increase of 4.3% (0.7°C). The greatest increases occurred in the eastern sections of the Dakotas, Nebraska, and Minnesota down into Iowa. Entrainment affected the water vapor mixing ratio more strongly than temperature.

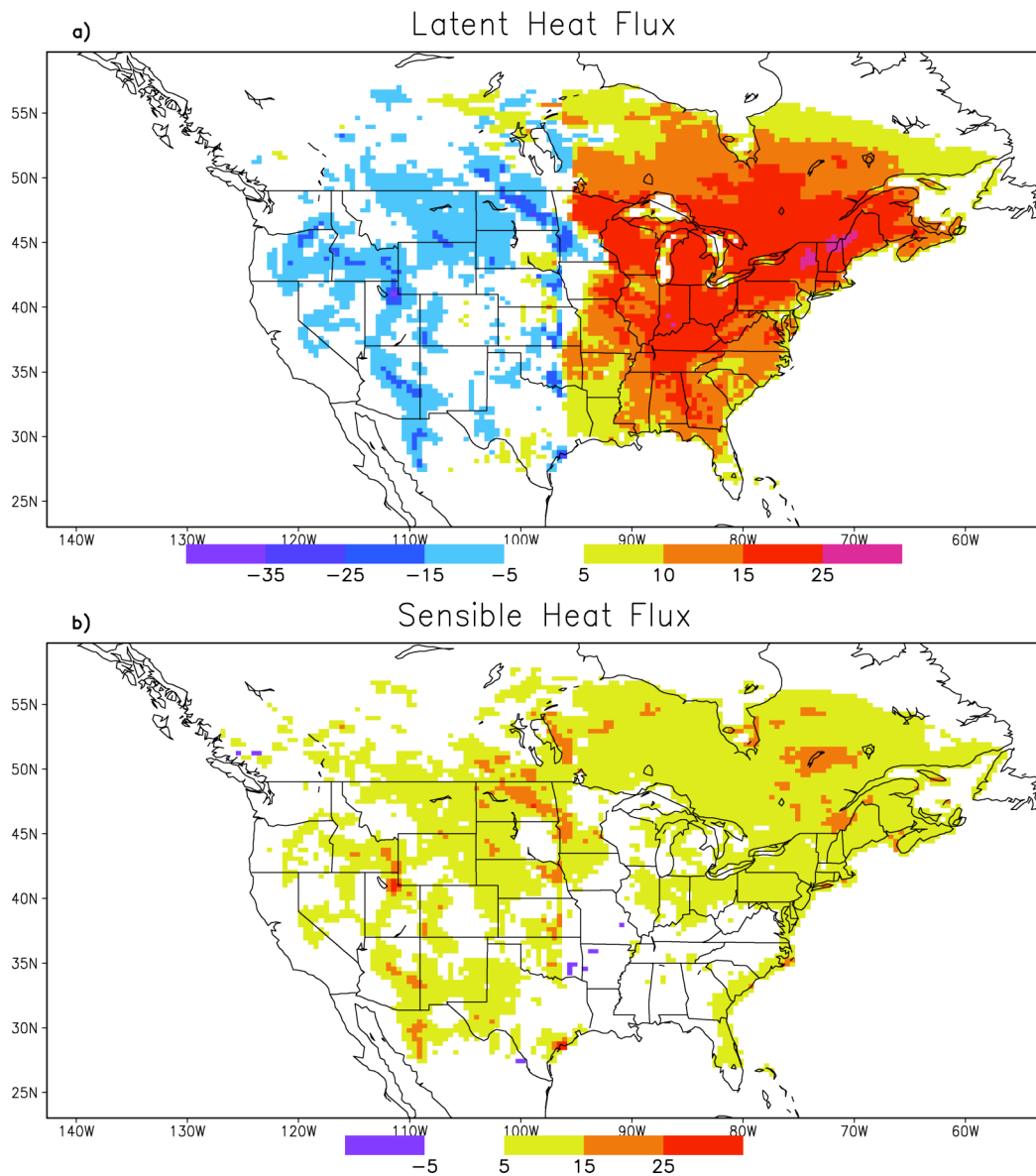


Figure 3.11 Effect of entrainment from overshooting thermals (entraining case minus control case) on (a) latent heat flux (W m^{-2}) and (b) sensible heat flux (W m^{-2}) in the time mean from July through September.

Both water vapor mixing ratio and temperature are measured with a high spatial and temporal resolution. Since they are affected by entrainment, they can be used to evaluate and improve estimates of the tunable parameter α . This suggests the utility of data assimilation for cases when boundary layer depth measurements are not available and can supplement PBL depth measurements when they do exist.

Figure 3.11a is a map of the time mean difference in latent heat flux from the CAS to the boundary layer. On average, the latent heat flux was increased by just over 12% (12.7 W), mostly in the eastern half of the United States. The eastern U.S. experienced a drought through much of summer 1999. It was also downwind of the region of greatest entrainment impact and had existed in the model domain the longest due to the prevailing westerlies. Therefore, the eastern half of the United States experienced the greatest accumulation of entrainment modification. In addition, the eastern U.S., in general, retains more moisture than the semiarid West that is available to be transported into the boundary layer and so a drier boundary layer can induce a greater flux of water vapor from the CAS because the plants and soil have more stored water to release.

Figure 3.11b is a map of the differences in sensible heat flux between the CAS and the boundary layer for the entraining and control cases. Sensible heat flux, on average, increased by almost 4 W in the time period of July through September. A drier, deeper PBL resulted in fewer clouds and so more solar radiation reached the ground. This allowed both the sensible and latent heat fluxes to increase. The stronger heat flux produced a stronger entrainment because of the proportionality between entrainment and

surface heat fluxes. This effect is only relevant when there are variations in cloud cover between the control and entraining cases.

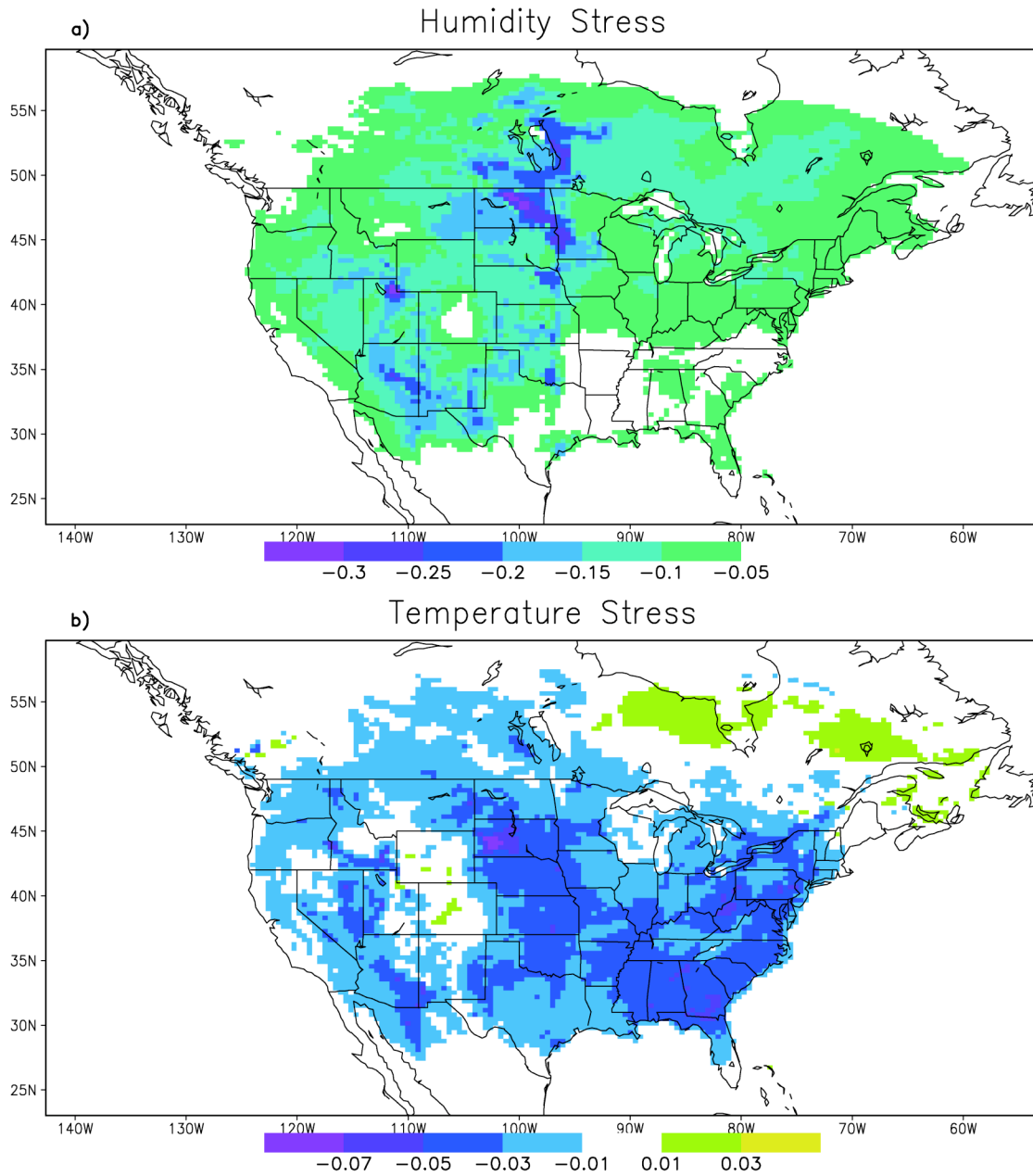


Figure 3.12 Effect of entrainment from overshooting thermals (entraining case minus control case) on (a) humidity stress and (b) temperature stress in the time mean from July through September.

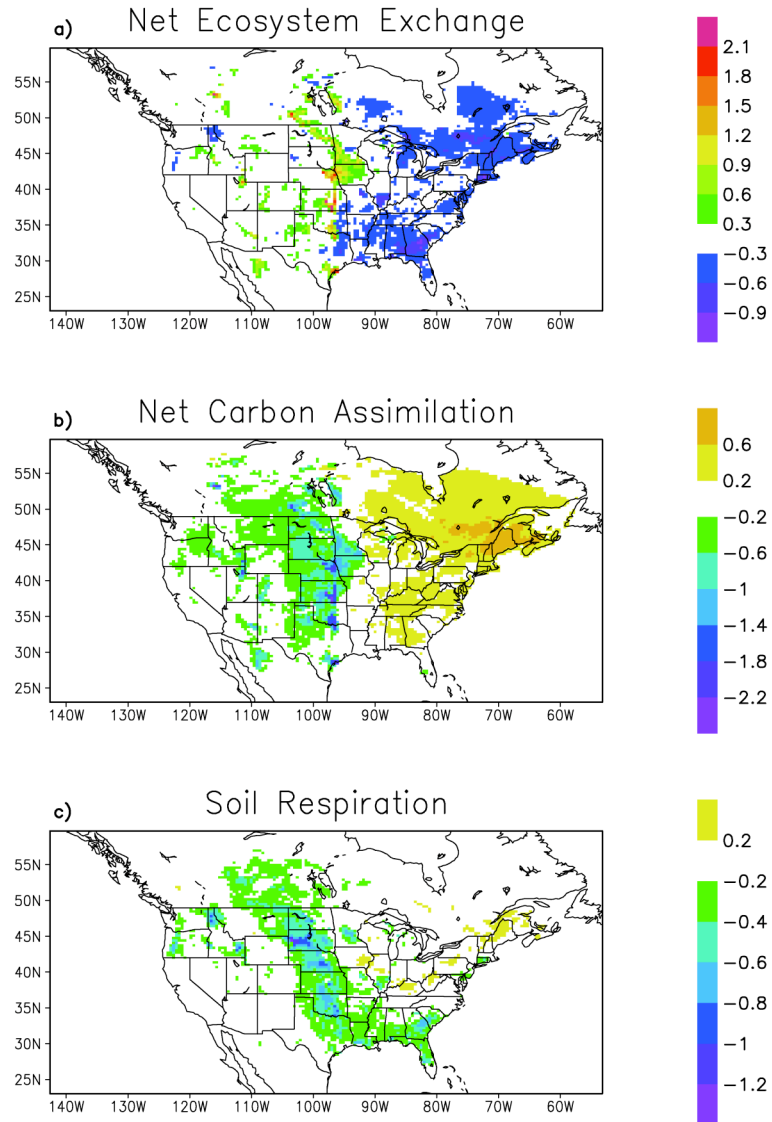


Figure 3.13 Effect of entrainment from overshooting thermals (entraining case minus control case) on (a) net ecosystem exchange ($\mu\text{mol m}^{-2} \text{s}^{-1}$), (b) carbon assimilation ($\mu\text{mol m}^{-2} \text{s}^{-1}$), and (c) soil respiration ($\mu\text{mol m}^{-2} \text{s}^{-1}$) in the time mean from July through September.

Figure 3.12a shows the physiological stress on vegetation due to low humidity. Stomata close to restrict water vapor loss when the leaf surface dries (Bonan et al., 2002; Ball et al., 1987; Collatz et al., 1991). This is expressed in the model as a decreased stress parameter. Stomatal closing results in decreased transpiration, reducing latent heat flux and increasing sensible heat flux. This acts to reduce the boundary layer humidity

and increase its temperature. Since a smaller stomatal opening produces decreased carbon assimilation, this parameter also indicates CO₂ concentration changes. When the additional entrainment of overshooting thermals is considered, the humidity parameter is decreased 10%, indicating diminished stomatal openings.

The effect of entraining thermals on physiological stress due to departures from a moderate temperature is illustrated in Figure 3.12b. This parameter has the same effect on stomatal openings as the humidity parameter. While warmer temperatures were present everywhere as was shown in Figure 3.10b, the temperature stress is not as straightforward. In regions where the summer temperature was warm, warmer temperatures due to entrainment produced smaller stomatal openings. However, in relatively cool locations such as northern latitudes and at high altitude, warmer temperatures were more moderate for the plants and stomata were opened wider. In regions of Canada and along the Rocky Mountains, warmer temperatures were actually beneficial to the plants. The average change in temperature stress resulting from the additional entrainment was about 2%, reducing stomatal openings slightly.

The width of the stomatal opening controls the amount of carbon that the vegetation is able to assimilate and modifies the NEE (Figure 3.13). NEE (Figure 3.13a) is decreased from the Mississippi River eastwards and in Southeastern Canada. NEE is increased to the west. Most of these changes are due to changes in carbon assimilation (Figure 3.13b). Assimilation was increased in the eastern half of the domain, mostly due to decreased cloud cover. The drying effect of overshooting thermals accumulated as air masses traversed the United States, producing drier conditions to the east. Fewer clouds permit more solar radiation to penetrate to the surface, allowing more photosynthesis by

the surface vegetation. Decreased carbon assimilation along the Great Plains was a result of warmer and drier conditions producing a closing of plant stomata. Reduced soil respiration (Figure 3.13c) through the Great Plains and along the Gulf of Mexico was a result of slightly reduced soil moisture. Enhanced soil respiration in the Ohio valley and New England was due to warmer soil temperatures.

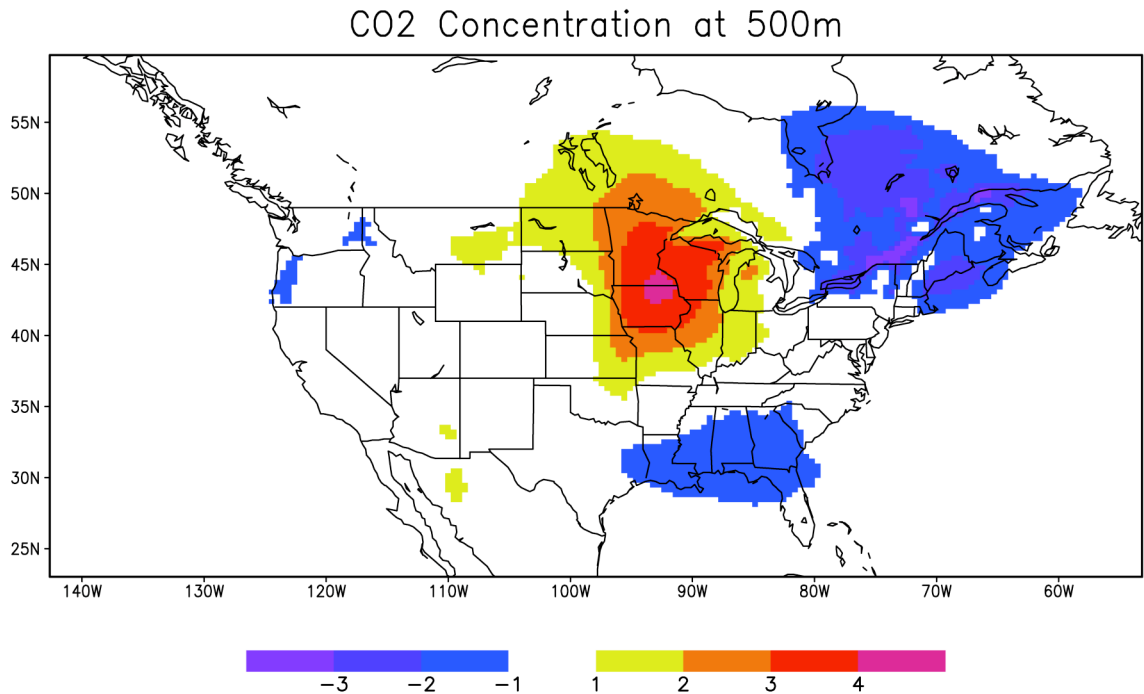


Figure 3.14 Effect of entrainment from overshooting thermals (entraining case minus control case) on CO₂ concentration at 500 m in the time mean from July through September.

Figure 3.14 illustrates the differences in CO₂ concentration at 500 m caused by PBL top entrainment. Lower concentrations are present in southeastern Canada and New England. Lower temperature stress (Figure 3.12b) created greater carbon assimilation (Figure 3.13b) in this region. Higher CO₂ concentrations centered on the upper Midwest were a result of reduced assimilation and a deeper PBL. The combination of a weak PBL depth response, greater carbon assimilation from increased solar radiation, and weaker soil respiration due to decreased soil moisture lead to lower CO₂ concentrations over the

states along the Gulf of Mexico, including Louisiana, Alabama, and Florida. On average, there was no change in CO₂ concentration, but the gradients of CO₂ were largely impacted by entrainment. There was a 7 ppmv gradient from the eastern Minnesota/Iowa border to the border of New York and Canada that is due just to entrainment. Estimates of sources and sinks of carbon are strongly dependent on CO₂ gradients, which are, in turn, dependent upon entrainment and PBL depth. Therefore, an error in PBL depth will lead to errors in source/sink estimates.

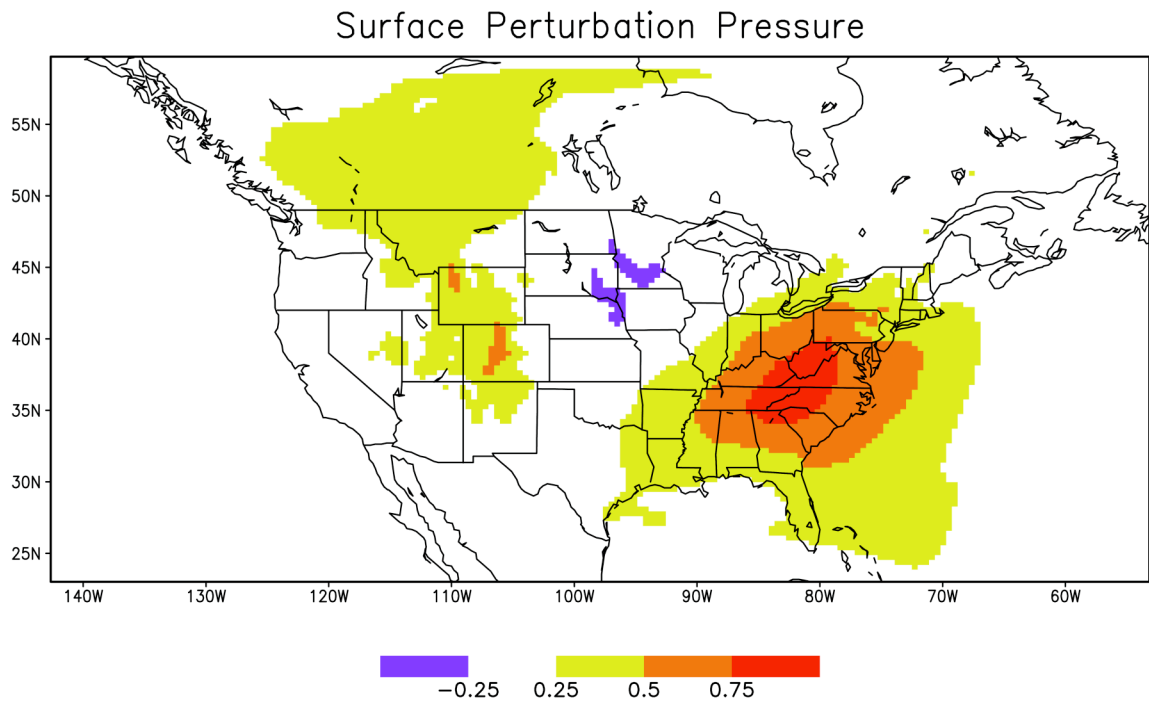


Figure 3.15 Effect of entrainment from overshooting thermals (entraining case minus control case) on surface perturbation pressure (hPa) in the time mean from July through September.

Overshooting thermals, although small, can produce changes in PBL depth, sensible and latent heat fluxes, temperature, and CO₂ concentration. These modifications combine to produce large-scale changes in the weather and climate. Figure 3.15 shows the time mean impact of overshooting thermals on the surface perturbation pressure. Thermals produced slightly higher pressure over Virginia, the Carolinas, and Tennessee.

Lower pressure was present over South Dakota and Minnesota. Variations in pressure indicated variations in every meteorological variable including wind velocity, frontal locations, and precipitation.

3.6) Conclusions

An entrainment parameterization was added to SiB-RAMS to include the effects of overshooting thermals. The parameterization warms and dries the boundary layer while cooling and moistening the inversion layer through a downward heat flux at the PBL top. The inclusion of entrainment effects increased the model estimate of the PBL depth in a simulation representing the weather conditions of late summer 1999.

The monthly mean diurnal cycle of PBL depth in July, August, and September at the WLEF tower in northern Wisconsin was simulated better when entrainment was included. This depth is important for CO₂ studies as an error in PBL depth relates linearly to errors in CO₂ concentration. Surface carbon fluxes are diluted by the volume of the PBL and so a deeper PBL means a given amount of carbon assimilation reduces the CO₂ concentration less than it would have otherwise. It was seen in Figure 3.14 that this could impact horizontal gradients of CO₂ and produce a model-observation mismatch even when the simulated fluxes are correct. Since most CO₂ concentration measurements are made near the surface and depend on the depth of the PBL and source/sink estimates of carbon depend on the carbon concentrations, correcting the PBL depth should also improve the source/sink estimates.

In addition to increasing the PBL depth, overshooting thermals and their associated entrainment impact temperature and water vapor mixing ratios. Temperature and water vapor are measured with a high spatial and temporal resolution. They can then

be used to evaluate the parameterization when PBL depth measurements are not available. High concentrations of temperature and water vapor measurements enable data assimilation of these observations to improve estimates of the tunable parameter α , thus improving estimates of entrainment, PBL depth, CO₂ concentrations, and source/sink estimates.

Overshooting thermals produce a complex interaction of PBL processes. The warmer and drier conditions at the leaf surface alter the stomatal openings, modifying the Bowen ratio and cloud cover. Closing of the stomata produces decreased carbon assimilation which, when combined with the dilution effect of a deeper PBL, produces higher CO₂ concentrations. Decreased cloud cover results in greater net radiation at the surface and a greater surface heat flux. Given that the heat flux at the top of the PBL is proportional to that at the surface, the entrainment heat flux is also increased. The small-scale impacts of overshooting thermals eventually sum to form variations in the large-scale weather.

REFERENCES

- Andres, R.J., G. Marland, I. Fung, and E. Matthews, 1996: A $1^{\circ}\times 1^{\circ}$ distribution of carbon dioxide emissions from fossil fuel consumption and cement manufacture, 1950-1990. *Global Biogeochemical Cycles*, **10**, 419-429.
- Angevine, W.M., R.J. Doviak, and Z. Sorbjan, 1994a: Remote sensing of vertical velocity variance and surface heat flux in a convective boundary layer. *J. Appl. Meteor.*, **33**, 977-983.
- Angevine, W.M., W.L. Ecklund, D.A. Carter, K.S. Gage, and K.P. Moran, 1994b: Improved radio-acoustic sounding techniques. *J. Atmos. Ocean. Technol.*, **11**, 42-49.
- Angevine, W.M., A.B. White, and S.K. Avery, 1994c: Boundary-layer depth and entrainment zone characterization with a boundary-layer profiler. *Bound. -Layer Meteor.*, **68**, 375-385.
- Ayotte, K.W., P.P. Sullivan, A. Andr n, S.C. Doney, A.A.M. Holtslag, W.G. Large, J.C. McWilliams, C.-H. Moeng, M.J. Otte, J.J. Tribbia, and J.C. Wyngaard, 1996: An evaluation of neutral and convective planetary boundary layer parameterizations relative to large eddy simulation. *Bound. Layer Meteor.*, **79**, 131-175.
- Baker, I., A.S. Denning, N. Hanan, et al., 2003: Simulated and observed fluxes of sensible and latent heat and CO₂ at the WLEF-TV tower using SiB2.5. *Global Change Biology*, **9**, 1262-1277.
- Baker, I.T., A.S. Denning, L. Prihodko, K. Schaefer, J.A. Berry, G.J. Collatz, N.S. Suits, R. St ckli, A. Philpott, and O. Leonard, 2007: Global net ecosystem exchange (NEE) of CO₂, Oak Ridge Natl. Lab., U.S. Dep. of Energy, Oak Ridge, Tenn. (Available at <http://www.daac.ornl.gov>)
- Bakwin, P.S., P.P. Tans, D.F. Hurst, and C. Zhao, 1998: Measurements of carbon dioxide on very tall towers: Results of the NOAA/CMDL program. *Tellus*, **50B**, 401-415.
- Baldocchi, D. et al., 2001: FLUXNET: A new tool to study the temporal and spatial variability of ecosystem-scale carbon dioxide, water vapor, and energy flux densities. *Bull. Am. Meteorol. Soc.*, **82**, 2415-2434.
- Ball, J.T., I.E. Woodrow, and J.A. Berry, 1987: A model predicting stomatal conductance and its contribution to the control of photosynthesis under different environmental conditions. *Progress in Photosynthesis Research*, ed. J. Biggens, 221-224.

- Barford, C.C., et al., 2001: Factors controlling long- and short-term sequestration of atmospheric CO₂ in a mid-latitude forest. *Science*, **294**, 1688-1691.
- Berger, B.W., K.J. Davis, P.S. Bakwin, et al., 2001: Long-term carbon dioxide fluxes from a very tall tower in a northern forest: Flux measurement methodology. *J. Atmos. Ocean. Technol.*, **18**, 529-542.
- Betts, A.K., 1973: Non-precipitating cumulus convection and its parameterization. *Quart. J. Roy. Meteor. Soc.*, **99**, 178-196.
- Bonan, G.B., S. Lewis, L. Kergoat, and K.W. Oleson, 2002: Landscapes as patches of plant functional types: An integrating concept for climate and ecosystem models. *Global Biogeochemical Cycles*, **16**, 5.1-5.23.
- Carson, D.J., 1973: The development of a dry inversion-capped convectively unstable boundary layer. *Quart. J. Roy. Meteor. Soc.*, **100**, 450-467.
- Collatz, G.J., J.T. Ball, C. Grivet, and J.A. Berry, 1991: Physiological and environmental regulation of stomatal conductance, photosynthesis and transpiration: A model that includes a laminar boundary layer. *Agric. For. Meteorol.*, **54**, 107-136.
- Corbin, K.D., A.S. Denning, L. Lu, J.-W. Wang, I.T. Baker, 2008: Possible representation errors in inversions of satellite CO₂ retrieval. *J. Geophys. Res.*, **113**, D02301.
- Davis, K.J., P.S. Bakwin, C. Yi, B.W. Berger, C. Zhao, R.M. Teclaw, and J.G. Isebrands, 2003: The annual cycles of CO₂ and H₂O exchange over a northern mixed forest as observed from a very tall tower. *Global Change Biology*, **9**, 1278-1293.
- Davis, K.J., D.H. Lenschow, S.P. Oncley, C. Kiemle, G. Ehret, A. Giez, and J. Mann, 1997: Role of entrainment in surface-atmosphere interactions over the boreal forest. *J. Geophys. Res.*, **102**, D24.
- Deardorff, J.W., 1974: Three-dimensional numerical study of the height and mean structure of a heated planetary boundary layer. *Boundary-Layer Meteorol.*, **7**, 81-106.
- Denning, A.S., I.Y. Fung, and D.A. Randall, 1995: Latitudinal gradient of atmospheric CO₂ due to seasonal exchange with land biota. *Nature*, **376**, 240-243.
- Denning, A.S., J.G. Collatz, C. Zhang, D.A. Randall, J.A. Berry, P.J. Sellers, G.D. Colello, and D.A. Dazlich, 1996a: Simulations of terrestrial carbon metabolism and atmospheric CO₂ in a general circulation model. Part 1: Surface carbon fluxes. *Tellus*, **48B**, 521-542.

- Denning, A.S., D.A. Randall, G.J. Collatz, and P.J. Sellers, 1996b: Simulations of terrestrial carbon metabolism and atmospheric CO₂ in a general circulation model. Part 2: Spatial and temporal variations of atmospheric CO₂. *Tellus*, **48B**, 543-567.
- Denning, A.S., T. Takahashi, and P. Friedlingstein, 1999: Can a strong atmospheric CO₂ rectifier effect be reconciled with a “reasonable carbon budget? *Tellus*, **51B**, 249-253.
- Denning, A.S., M. Nicholls, L. Prihodko, I. Baker, P.-L. Vidale, K. Davis, and P. Bakwin, 2003: Simulated variations in atmospheric CO₂ over a Wisconsin forest using a coupled ecosystem-atmosphere model. *Global Change Biology*, **9**, 1241-1250.
- Denning, A.S., N. Zhang, C. Yi, M. Branson, K. Davis, J. Kleist, P. Bakwin, 2008: Evaluation of modeled atmospheric boundary layer depth at the WLEF tower. *Agric. and Forest Meteorol.*, **148**, 206-215.
- Ecklund, W.L., D.A. Carter, and B.B. Balsley, 1988: A UHF wind profiler for the boundary layer: Brief description and initial results. *J. Atmos. Ocean. Technol.*, **5**, 432-441.
- Freitas, S.R., K. Longo, M. Silva Dias, P. Silva Dias, R. Chatfield, Á. Fazenda, and L.F. Rognrigues, 2006: The coupled aerosol and tracer transport model to the Brazilian developments on the Regional Atmospheric Modeling System: Validation using direct and remote sensing observations. International Conference on Southern Hemisphere Meteorology and Oceanography (ICSHMO), 8., 101-107. CD-ROM. ISBN 85-17-00023-4.
- Gerbig, C., J.C. Lin, S.C. Wofsy, B.C. Daube, A.E. Andrews, B.B. Stephens, P.S. Bakwin, and C.A. Grainger, 2003: Toward constraining regional-scale fluxes of CO₂ with atmospheric observations over a continent: 1. Observed spatial variability from airborne platforms. *J. Geophys. Res.*, **108**, D00301.
- Grell, G.A., 1993: Prognostic evaluation of assumptions used by cumulus parameterizations. *Mon. Wea. Rev.*, **121**, 764-787.
- Grell, G.A. and D. Devenyi, 2002: A generalized approach to parameterizing convection combining ensemble and data assimilation techniques. *Geophys. Res. Lett.*, **29**(14), 1693.
- Gurney, K.R. et al., 2002: Towards robust regional estimates of CO₂ sources and sinks using atmospheric transport models. *Nature*, **415**, 626-630.

- Gurney, K.R. et al., 2003: TransCom 3 CO₂ inversion intercomparison: 1. Annual mean control results and sensitivity to transport and prior flux information. *Tellus*, **55B**, 555-579.
- Hansen, M., R. DeFries, J.R.G. Townshend, and R. Sohlberg, 2000: Global land cover classification at 1km resolution using a decision tree classifier. *Int. J. of Remote Sensing*, **21**, 1331-1365.
- Harrington J.Y., 1997: The effects of radiative and microphysical processes on simulated warm and transition season Arctic stratus. PhD Diss., Atmospheric Science Paper No 637, Colorado Statue University, Department of Atmospheric Science, Fort Collins, CO 80523, 289 pp.
- Hollinger, D.Y., et al., 2004: Spatial and temporal variability in forest-atmosphere CO₂ exchange. *Global Change Biology*, **10**, 1689-1706.
- Kawa, S.R., D.J. Erickson III, S. Pawson, and Z. Zhu, 2004: Global CO₂ transport simulations using meteorological data from the NASA data assimilation system. *J. Geophys. Res.*, **109**, D183112.
- Klemp, J.B. and R.B. Wilhelmson, 1978: The simulation of three-dimensional convective storm dynamics. *J. Atmos. Sci.*, **35**, 1070-1096.
- Lin, S.J. and R.B. Rood, 1996: Multidimensional flux-form semi-Lagrangian transport schemes. *Mon. Weather Rev.*, **124**, 2046-2070.
- Marland, G., T.A. Boden, and R.J. Andres, 2005: Global, regional and national CO₂ emissions, in *Trends: A compendium of Data on Global Change*, Carbon Dioxide Inf. Anal. Cent., Oak Ridge Natl. Lab., U.S. Dep. of Energy, Oak Ridge, Tenn. (Available at http://cdiac.ornl.gov/trends/emis/em_cont.htm)
- McGrath-Spangler, E.L., A.S. Denning, K.D. Corbin, and I.T. Baker, 2008: Implementation of a boundary layer heat flux parameterization into the Regional Atmospheric Modeling System (RAMS). Submitted to ACPD MS# 2008-0252.
- Mellor, G.L. and T. Yamada, 1982: Development of a turbulence closure model for geophysical fluid problems. *Rev. Geophys.*, **20**, 851-875.
- Nicholls, M.E., A.S. Denning, L. Prihodko, P.-L. Vidale, I. Baker, K. Davis, and P. Bakwin, 2004: A multiple-scale simulation of variations in atmospheric carbon dioxide using a coupled-biosphere-atmospheric model. *J. Geophys. Res.*, **109**, D18117.
- NOAA/NCDC <<http://www.ncdc.noaa.gov/oa/climate/research/1999/perspectives.html>>

- Pielke, R.A., 1991: Overlooked scientific issues in assessing hypothesized greenhouse gas warming. *Environ. Software*, **6**, 100-107.
- Rayment, R. and C.J. Readings, 1974: A case study of the structure and energetics of an inversion. *Quart. J. Roy. Meteor. Soc.*, **100**, 221-233.
- Schmid, H.P., C.S.B. Grimmond, F. Cropley, B. Offerle, and H.-B. Su, 2000: Measurements of CO₂ and energy fluxes over a mixed hardwood forest in the mid-western United States. *Agric. and Forest Meteorol.*, **103**, 357-374.
- Schmid, H.P., H.-B. Su, C.S. Vogel, and P.S. Curtis, 2003: Ecosystem-atmosphere exchange of carbon dioxide over a mixed hardwood forest in northern lower Michigan. *J. Geophys. Res.*, **108(D14)**, 4417.
- Sellers, P.J., D.A. Randall, G.J. Collatz, J.A. Berry, C.B. Field, D.A. Dazlich, C. Zhang, G.D. Collelo, L. Bounoua, 1996a: A revised land surface parameterization (SiB2) for atmospheric GCMs, Part 1: Model formulation. *J. Climate*, **9**, 676-705.
- Sellers, P.J., Y. Mintz, Y.C. Sud, and A. Dalcher, 1986: A simple biosphere model (SiB) for use within general circulation models. *J. Atmos. Sci.*, **43**, 505-531.
- Sellers, P.J., S.O. Los, C.J. Tucker, C.O. Justice, D.A. Dazlich, G.J. Collatz, and D.A. Randall, 1996b: A revised land surface parameterization (SiB2) for Atmospheric GCMs. Part II: The generation of global fields of terrestrial biophysical parameters from satellite data. *J. Climate*, **9**, 706-737.
- Smagorinsky, J.S., 1963: General circulation experiments with the primitive equations. 1: The basic experiment. *Mon. Weather Rev.*, **91**, 99-164.
- Stull, R.B., 1976: The energetics of entrainment across a density interface. *J. Atmos. Sci.*, **33**, 1260-1267.
- Stull, R.B., 1988: *An introduction to boundary layer meteorology*. Kluwer Academic Publishers, Norwell, MA. 666 pp.
- Sullivan, P.P., C.-H. Moeng, B. Stevens, D.H. Lenschow, and S.D. Mayer, 1998: Structure of the entrainment zone capping the convective atmospheric boundary layer. *J. Atmos. Sci.*, **55**, 3042-3064.
- Takahashi, T., S.C. Sutherland, C. Sweeney, A. Poisson N. Metzl, B. Tilbrook, N. Bates, R. Wanninkhof, R.A. Feely, C. Sabine, J. Olafsson, and Nojiri, 2002: Global sea-air CO₂ flux based on climatological surface ocean pCO₂, and seasonal, biological, and temperature effects. *Deep-Sea Research Part II*, **49**, 1601-1622.

- Walko, R.L., C.J. Tremback, J. Panetta, S. Freitas, and A.L. Fazenda, 2002: RAMS Regional Atmospheric Modeling System version 5.0 model input namelist parameters. 8 Dec 2006 <http://www.cptec.inpe.br/brams/input_namelist.shtml>
- Wang, J.-W., A.S. Denning, L. Lu, I.T. Baker, K.D. Corbin, and K.J. Davis, 2007: Observations and simulations of synoptic, regional, and local variations in atmospheric CO₂. *J. Geophys. Res.*, **112**, D04108.
- White, A.B., C.W. Fairall, and D.W. Thompson, 1991: Radar observations of humidity variability in and above the marine atmospheric boundary layer. *J. Atmos. Ocean. Technol.*, **8**, 639-658.
- Willis, G.E. and J.W. Deardorff, 1974: A laboratory model of the unstable planetary boundary layer. *J. Atmos. Sci.*, **31**, 1297-1307.
- Wofsy, S.C., et al., 1993: Net exchange of CO₂ in a mid-latitude forest. *Science*, **260**, 1314-1317.
- Yi, C., K.J. Davis, B.W. Berger, and P.S. Bakwin, 2001: Long-term observations of the dynamics of the continental planetary boundary layer. *J. Atmos. Sci.*, **58**, 1288-1299.
- Yi, C., K.J. Davis, P.S. Bakwin, A.S. Denning, N. Zhang, A. Desai, J.C. Lin, and C. Gerbig, 2004: Observed covariance between ecosystem carbon exchange and atmospheric boundary layer dynamics at a site in northern Wisconsin. *J. Geophys. Res.*, **109**, D08302.
- Zhang, N., 2002: Observations and simulations of the planetary boundary layer at a tall tower in northern Wisconsin. Master's thesis, Colorado State University, Department of Atmospheric Science, Fort Collins, CO 80523, 71 pp.
- Zupanski, D., A.S. Denning, M. Uliasz, M. Zupanski, A.E. Schuh, P.J. Rayner, W. Peters, and K. Corbin, 2007: Carbon flux bias estimation employing Maximum Likelihood Ensemble Filter (MLEF). *J. Geophys. Res.*, **112**, D17107.

Chapter 4

Conclusions and Future Work

4.1) Conclusions

Overshooting thermals and their associated entrainment are essential to carbon budget studies. However, thermals are too small to be resolved by most mesoscale models and so are often neglected. They mix free tropospheric and boundary layer air and in so doing, they warm and dry the boundary layer through entrainment of free tropospheric air and cool and moisten the overlying inversion, producing conditions that require less energy input to grow the PBL. Mass is also injected into the boundary layer, growing it directly. A deeper PBL dilutes the effect of surface carbon fluxes, inducing smaller diurnal amplitudes of CO₂ concentration.

In addition, the altered atmospheric conditions modify the vegetative response. The vegetation shifts the Bowen ratio in response to warmer and drier conditions, reinforcing the initial perturbation if the response involves a closing of plant stomata. This is done as an optimal response of the physiology to environmental conditions at the leaf surface. This optimal response also alters the assimilation of carbon, adjusting carbon fluxes into and out of the biosphere.

Most observations of CO₂ concentration are taken within the boundary layer and are influenced by the depth of the PBL. In atmospheric inversion studies, downstream CO₂ concentrations are compared to observations and used to optimize prior upstream

sources and sinks (Gerbig et al., 2003; Zupanski et al., 2007). An error in the estimated flux scales linearly with errors in PBL depth.

In order to improve PBL estimates, a parameterization of the effects of overshooting thermals was included in the ecosystem-atmosphere model SiB-RAMS. The parameterization includes a tunable parameter, α , that is equal to the negative of the ratio of the entrainment heat flux at the top of the PBL to the surface heat flux. It induces a warmer, drier boundary layer and affects CO₂ concentration, the radiative budget, and other meteorological variables by mixing characteristics of the PBL and the overlying inversion at the interface between them. In an idealized study, as α increased, the temperature, water vapor mixing ratio, PBL depth, and CO₂ concentration changed almost linearly. As α adjusted from zero to a value of 0.2, the concentration of CO₂ changed by nearly 5 ppmv.

A second experiment was performed to investigate the interactions among the large-scale weather, the PBL, and land surface of late summer 1999. The monthly mean diurnal cycle of PBL depth at the WLEF site in northern Wisconsin was more accurately simulated for the months of July, August, and September by the inclusion of the entrainment parameterization and the model domain averaged increase in PBL depth was almost 11%.

Entrainment from overshooting thermals produced a warmer, drier, and deeper PBL by mixing free tropospheric air down into this layer. The modified atmospheric conditions induced a closing of plant stomata, reducing latent heat flux, increasing sensible heat flux, and reducing carbon assimilation. Increased sensible heat flux acted to warm the PBL further. The drier conditions produced a reduction in cloud cover,

allowing more solar radiation to reach the surface and modifying the surface energy budget. An increase in the surface energy budget, in turn, increased entrainment at the PBL top due to the proportionality between the two heat fluxes. The modified PBL processes altered the large-scale weather and horizontal gradients of CO₂ concentration. Since CO₂ concentration gradients are essential to source/sink estimation, this has large implications for carbon budget studies, such as when inverse modeling is employed. Inverse modeling techniques compare model CO₂ concentrations to those observed and adjust the model surface carbon fluxes in order to minimize differences. Thus, model errors due to an inaccurate PBL depth can lead to unnecessary surface flux modifications. Although small, overshooting thermals are responsible for meteorological and ecophysiological properties on a scale comparable to synoptic scale weather patterns.

4.2) Future Work

Temperature and water vapor mixing ratio are measured frequently in time and with a high spatial resolution. Since these variables are modified by entrainment, they can be used to evaluate the strength of the parameterization and α . They can also be used to supplement the lower concentration of PBL depth measurements such as from satellite observations in data assimilation techniques.

Future work will focus on incorporating the maximum likelihood ensemble filter (MLEF) data assimilation technique (Zupanski, 2005) into the SiB-RAMS model in order to better estimate α and thus improve model PBL depth estimates.

REFERENCES

- Gerbig, C., J.C. Lin, S.C. Wofsy, B.C. Daube, A.E. Andrews, B.B. Stephens, P.S. Bakwin, and C.A. Grainger, 2003: Toward constraining regional-scale fluxes of CO₂ with atmospheric observations over a continent: 2. Analysis of COBRA data using a receptor-oriented framework. *J. Geophys. Res.*, **108**, D003770.
- Zupanski, M., 2005: Maximum likelihood ensemble filter: Theoretical aspects. *Mon. Weather Rev.*, **133**, 1710-1726.
- Zupanski, D., A.S. Denning, M. Uliasz, M. Zupanski, A.E. Schuh, P.J. Rayner, W. Peters, and K.D. Corbin, 2007: Carbon flux bias estimation employing Maximum Likelihood Ensemble Filter (MLEF). *J. Geophys. Res.*, **112**, D17107.